77250

DETERMINATION OF MOTOR PARAMETERS IN TWO PHASE PERMANENT-MAGNET VARIABLE-RELUCTANCE MOTOR BY FINITE ELEMENTS AND DYNAMIC SIMULATION OF MOTOR AND DRIVE PERFORMANCE ANALYSIS

77250

A Thesis Submitted to the
Graduate School of Natural and Applied Sciences of
Dokuz Eylül University
In Partial Fulfillment of the Requirements for
the Doctor of Philosophy in Electrical and Electronics Engineering

by
Hacer ÖZTURA

June, 1998
İZMİR

PhD THESIS EXAMINATION RESULTS FORM

We certify that we have read this thesis and that in our opinion it is fully adequate, in scope and in quality, as a thesis for the degree of Doctor of Philosophy.

Associate Prof. Dr. Eyüp Akpınar
(Advisor)

....
(Committee Member)

....
(Committee Member)

Approved by the
Graduate School of Natural and Applied Sciences

Prof. Dr. Cahit Helvacı
Director

ACKNOWLEDGEMENTS

I would like to express to my gratitude to my supervisor, Assoc. Prof. Dr. Eyüp AKPINAR, for his continuos helps and encouragement at every stage of this Ph.D. thesis. I am also grateful to him for letting me share his professional knowledge and experience.

I would also like to thank my husband İbrahim, my son Özgü, and my daughter Öykü for their patience during this study.

ABSTRACT

In this study, the dynamic analysis of the two phase, permanent magnet variable reluctance motor and its drive circuit has been made for the first time. The motor parameters which are required for the dynamic analysis have been obtained by using finite element method.

The motor used in this study has been designed and the magnetic field analysis has been carried out by using the finite element method ; the static torque of motor and torque-speed characteristics for the different current values have been obtained. In this study, dimensions of a motor has been chosen such that the motor can develop 100W output power at its rated conditions.

The motor parameters are the back emf induced in the stator windings and also the winding's inductance and resistance. Of these parameters back emf and windings inductance have been calculated through the application of finite element method. The stator winding resistance has been computed analytically.

The excitation logic of phases has been obtained with the help of static torques calculated by using the finite element method.

The model of the motor and drive in state space form has been derived by using the generalized machine theory for dynamic simulation and these equations have been solved through 4th order Runga Kutta by using the FORTRAN programming language. The stator current has been kept in the limited range with the application of 'Hysteresis Current Control'. Proportional Integral (PI) speed controller has been employed in the closed loop system.

ÖZET

Bu çalışmada iki fazlı sabit mıknatıslı değişken relüktanslı motorun ve sürücü devresinin dinamik analizleri ilk defa yapılmıştır. Dinamik analiz için gerekli olan motor parametreleri sonlu elemanlar yöntemi kullanılarak elde edilmiştir.

Bu çalışmada kullanılan motor tasarlanmıştır ve manyetik alan analizleri sonlu elemanlar yöntemi kullanılarak yapılmıştır; motorun statik torkları ve tork-hız karakteristiği farklı akım değerleri için elde edilmiştir. Bu çalışmada motor boyutları düşünülen koşullarda 100 W çıkış gücü üretebilecek bir motor olarak seçilmiştir.

Motor parametreleri, stator sargılarında indüklenen back emf, sargı endüktansı ve direncidir. Bu parametrelerden back emf ve sargı endüktansı sonlu elemanlar yöntemiyle hesaplanmıştır. Stator sargı direnci ise analitik olarak elde edilmiştir.

Fazları uyarma mantığı sonlu elemanlar yardımıyla çıkarılan statik tork eğrilerinden elde edilmiştir.

Dinamik simülasyonlar için motor ve sürücü devresinin durum denklem modeli, genelleştirilmiş makine teorisi kullanılarak çıkarılmış ve bu denklemler Fortran programlama dili kullanılarak 4. dereceden Runga Kutta ile çözdürülmüştür. Simulasyonlarda "Hyteresis current control" kullanılarak stator akımı sınırlanan bölgede tutulmuştur. Oransal Integral (PI) hız kontrolu kapalı çevrim sisteminde kullanılmıştır.

CONTENTS

Page

Contents..........III

List of Figures..........VII

List of Tables..........XI

Chapter One

INTRODUCTION

General..........1

Chapter Two

FINITE ELEMENT METHOD ANALYSIS

2.1 Introduction..........10

2.2 The Properties of Finite Element Analysis..........12

2.3 Applications to Electrical Machinery and Devices..........14

2.4 ANSYS Program..........16

2.5 Magnetic Field Analysis in the Package Program..........17

  2.5.1 Static Magnetic Analysis..........18

    2.5.1.1 Scalar Magnetic Potential Method..........18

2.5.1.2 Vector Magnetic Potential Method....18
2.5.2 Harmonic Magnetic (AC) Analysis....19
2.5.3 Transient Magnetic Analysis....20

Chapter Three

THE ANALYSIS OF PERMANENT MAGNET VARIABLE RELUCTANCE MOTOR WITH FINITE ELEMENT

3.1 Introduction 22
3.2 The Machine Geometry and Dimensions 23
  3.2.1The Geometry of Machine 23
  3.2.2 The Design of the Machine Dimensions 24
    3.2.2.1 Radial Thickness of the Magnet 25
    3.2.2.2 Rotor Speed 26
    3.2.2.3 Armature Core Length 27
    3.2.2.4 Diameter of Stator Core 28
    3.2.2.5 Length of The Air Gap 28
    3.2.2.6 Stator Current Density 29
    3.2.2.7 Stator Back Core Width 29
3.3 Calculation of the Magnetic Field by the Two-Dimension Finite Element Method 31
  3.3.1 Magnetic field Distributions 33
  3.3.2 Boundary Conditions....35
3.4 The No-Load and On-Load Magnetic Field Distrubition 35
3.5 Torque Calculation 40
  3.5.1 Maxwell Stress Tensor Method 41
  3.5.2 Coenergy Derivation Method 42
  3.5.3 Calculated Torque Values 43
    3.5.3.1 The Static Torque 43
    3.5.3.2 The Reluctance Torque 48

3.6 Computation of Machine Parameters 49

3.6.1 Armature Induced Emf Waveform 49

3.6.2 Armature Winding Inductance 53

3.6.2.1 Calculation of Inductances as Removing Permanent Magnet 54

3.6.2.2 Calculation of Inductances with Energy and Current Perturbation..............61

3.6.3 Armature Winding Resistance 67

Chapter Four

SIMULATION OF THE PERMANENT MAGNET VARIABLE RELUCTANCE MOTOR DRIVE

4.1 Modeling of the Motor 71

4.1.1 The Electromagnetic Torque 76

4.2 Drive Circuit 79

4.3 Closed Loop Controllers 85

4.4 Detection of Rotor Position 89

4.5 The Simulation Program 90

4.6 The Results of the Simulation 93

4.6.1 The Results of Open Loop System 94

4.6.2 The Results of Closed Loop System 101

4.6.3 Computation Of The Machine Efficiency 110

4.6.4 The Closed Loop Analysis While The Inductances Are Constant 112

4.6.5 Load Disturbances 121

4.6.5.1 Applying Positive Step Change on Load Torque 122

4.6.5.2 Applying Negative Step Change on Load Torque 126

4.6.5.3 Step Change on Reference Speed 130

Chapter Five
CONCLUTION

5.1 General 134
5.2 Furtherwork 136

REFERENCES

References 137

APPENDICES

Appendix A 146

LIST OF FIGURES

Page

Figure 2.1 The structure of the variable reluctance permanent magnet motor ..11
Figure 2.2 The element 12
Figure 3.1 Motor geometry 25
Figure 3.2 The B-H curve of rotor and stator steel 26
Figure 3.3 mmf axis of stator phases with respect to phase current 27
Figure 3.4 The dimensions of the motor 30
Figure 3.5 The mesh structure of the motor 33
Figure 3.6-a) Flux line graphic at no load 37
Figure 3.6-b) Flux line graphic at on load when phase A is excited...................37
Figure 3.7 Flux density graphic at no load 38
Figure 3.8 Flux density graphic at on load 39
Figure 3.9 The integration path for torque calculation 43
Figure 3.10 The direction of phase A current 44
Figure 3.11 The torque graphic when A phase is N pole 44
Figure 3.12 The distribution of the rotor and stator poles 45
Figure 3.13 The direction of phase B current 45
Figure 3.14 The torque graphic when phase B is N pole 46
Figure 3.15 The static torque developed by machine 46
Figure 3.16 The torque graphic when the phase A is S pole 47
Figure 3.17 The torque graphic when phase B is S pole 47
Figure 3.18 The static torque graphic 48
Figure 3.19 The reluctance torque 49

Figure 3.20 The nodes placed on border line between main pole and coil area.....50
Figure 3.21 The MVP difference of phase A 51
Figure 3.22 The MVP difference of phase B 51
Figure 3.23 Computed back emf for phase A 52
Figure 3.24 Computed back emf for phase B 53
Figure 3.25 Graphical interpretation of energy and coenergy 56
Figure 3.26 Self inductance of phase A 58
Figure 3.27 Self inductance of phase B 58
Figure 3.28 Self inductance of phase A' 59
Figure 3.29 Self inductance of phase B' 59
Figure 3.30 Mutual inductance between phase A and phase B 60
Figure 3.31 Mutual inductance between A and A' 60
Figure 3.32 Mutual inductance between B and B'..61
Figure 3.33 Perturbation of excitation current...65
Figure 3.34 Self inductance of phase A with two different method.......................66
Figure 3.35 Self inductance of phase B with two different method.......................66
Figure 3.36 The cross section of the motor geometry...68
Figure 4.1 The complete drive circuit 70
Figure 4.2 Five winding PM machine model 72
Figure 4.3 The chopper drive circuit 80
Figure 4.4 Chopper drive current waveform and transistor switching time 82
Figure 4.5 Closed loop control of drive circuit 86
Figure 4.6 Hysteresis current control 88
Figure 4.7 The flowchart of simulation program 93
Figure 4.8-a) The rotor speed (I=2.5 A & TL=0.15 Ntm) 95
Figure 4.8-b) The extended rotor speed (I=2.5 A & TL=0.15 Ntm) 96
Figure 4.8-c) The electromagnetic torque at standstill(I=2.5 A & TL=0.15 Ntm)...96
Figure 4.8-d) The electromagnetic torque at steady state(I=2.5 A & TL=0.15 Ntm) 98
Figure 4.8-e) The phase currents at standstill (I=2.5 A & TL=0.15 Ntm) 98
Figure 4.8-f) The phase currents at standstill (I=2.5 A & TL=0.15 Ntm) 99

Figure 4.8-g) The phase currents at steady state (I=2.5 A & TL=0.15 Ntm) 100
Figure 4.9 Electromagnetic torque versus angular rotor speed 101
Figure 4.10-a) The angular speed graphic of closed loop.......................................102
Figure 4.10-b) The electromagnetic torque of closed loop....................................103
Figure 4.10-c) The phase currents of closed loop..104
Figure 4.10-d) The input power of closed loop..105
Figure 4.10-e) The output power of closed loop..106
Figure 4.11-a) The extended angular speed graphic..106
Figure 4.11-b) The extended electromagnetic torque graphic 107
Figure 4.11-c) The extended phase currents graphic..108
Figure 4.11-d) The extended input power graphic..109
Figure 4.11-e) The extended output power graphic...109
Figure 4.11-f) The extended terminal voltages graphic..110
Figure 4.12 The efficiency graphic...112
Figure 4.13-a) The angular speed for L=constant 116
Figure 4.13-b) The extended angular speed for L=constant 116
Figure 4.13-c) The electromagnetic torque for L=constant....................................117
Figure 4.13-d) The extended electromagnetic torque for L=constant.....................117
Figure 4.13-e) The phase currents for L=constant..118
Figure 4.13-f) The extended phase currents for L=constant...................................118
Figure 4.13-g) The extended terminal voltages for L=constant..............................119
Figure 4.13-h) The input power for L=constant...119
Figure 4.13-i) The extended input power for L=constant.......................................120
Figure 4.13-j) The output power for L=constant..120
Figure 4.13-k) The extended output power for L=constant....................................121
Figure 4.14-a) The rotor speed...122
Figure 4.14-b) The extended rotor speed...123
Figure 4.14-c) The electromagnetic torque..124
Figure 4.14-d) The extended electromagnetic torque...124
Figure 4.14-e) The phase currents..125
Figure 4.14-f) The extended phase currents 125

Figure 4.15-a) The rotor speed..126
Figure 4.15-b) The extended rotor speed...127
Figure 4.15-c) The electromagnetic torque...128
Figure 4.15-d) The extended electromagnetic torque...128
Figure 4.15-e) The phase currents..129
Figure 4.15-f) The extended phase currents 129
Figure 4.16-a) The rotor speed..130
Figure 4.16-b) The extended rotor speed...131
Figure 4.16-c) The electromagnetic torque...131
Figure 4.16-d) The extended electromagnetic torque...132
Figure 4.16-e) The phase currents..133
Figure 4.16-f) The extended phase currents 133

LIST OF TABLES

Page

Table 3.1 The magnetic and physical properties of NdFeB type permanent magnet....24

Table 3.2 The color code of flux density graphic at no load 38

Table 3.3 The color code of flux density graphic at on load....40

YK

CHAPTER 1

INTRODUCTION

According to a recent study, around 55 % of the electric energy generated is consumed by electric motor-driven systems. By wisely selecting the electric motors and semiconductor devices they drive, a considerable amount of energy can be saved. The electric motor is a device that converts electrical energy to mechanical energy. The power loss, which is the difference between the electrical input power and mechanical output power should be minimized. The winding on the rotor is one of the sink for power loss. This winding is replaced by permanent magnet materials if the field current is not a key control parameter. Modern motors are designed and analyzed by using digital computers in order to maximize the efficiency during the operation. Therefore, the modeling of the machine and formulation of the problems are most critical part for doing research and studying of electrical machines in addition to be expertise on material that would be used to construct a machine.

The electrical machines take many forms and are known by many names - dc, synchronous, induction, hysteresis, permanent magnet, variable reluctance etc. Although these machines appear to be quite dissimilar and require a variety of analytical techniques, the physical principles governing their behavior are quite similar.

For a long time DC motors were preferred for the applications requiring a precise control of the speed, high starting torque, and fast acceleration. DC motor has a complex structure due to the presence of the commutator and rotor winding. Cost of dc motor are also high compared to the AC motors at the same power rating.

Besides dc motor's main inconvenients, in relation with the brush weakening and speed limitation have reduced their efficiency.

The desire to overcome the problems encountered by the dc motors has directed research to the control of induction motor as a variable speed drive. Variable frequency variable voltage inverters have been introduced as a speed controller of induction motors. Later pulse width modulated inverters have been developed. This type of inverter uses fewer IGBT or IGCT as a switching elements. The inverter-induction motor pair has already been a serious commercial alternative to the dc drive systems.

Academic and industrial research over the past 15-20 years has introduced a third alternative to the competition between dc and ac drives. This new alternative is the variable reluctance motor.[K. J. Strnat 1991] This motor has a very simple and robust construction. The rotor does not have a winding of any type. The stator windings are concentrated windings. The constructional features of VRM's are very simple compared to induction motors and especially to dc motors.

The variable reluctance motor (VRM) provide certain performance advantages. These advantages include simple and robust motor, good efficiency, excellent reliability, high-speed capability and good thermal characteristics. However, these machines also have their own disadvantages, such as relatively high torque ripple and current commutation difficulties during high speed operation.

The driver configuration is also rather simple. Each phase of this motor can be excited by unidirectional currents. As a result of this only single power switch is required per phase. The most important disadvantage of the drive is that a feedback is required from the rotor position.

After the recent developments in permanent magnet materials, brushless DC permanent magnet motor (PM BLDCM) and permanent magnet variable reluctance motors (PM VRM) has became very popular [K. J. Strnat 1991].

Permanent magnets have been used in electrical machinery for over 100 years, but because of recent dramatic improvements in their properties and availability, their application in electro-mechanical devices is now rapidly growing.

The use of permanent magnets provide important advantages in electrical machiniery application. Chief among these are that they do not require rotating winding and eliminate the need for mechanical commutators or slip rings on the rotor. Thus lower rotor losses, smaller rotor, less inertia, higher rotor speeds possibility, reduced machine length, reduced electromagnetic interference , and no arcing are obtained. In addition since armature is located on the stator, larger surface area, improved heat transfer, more copper area, and reduced copper losses are observed. These characteristics are very desirable in high speed performance applications. The price paid for these performance advantages includes increased system complexity and cost [Nehl W. T. & Demerdash N. A. O. 1992, p 86-108].

In very small machines, permanent magnet excitation almost always results in a lower manufacturing cost. The efficiency of permanent magnet machine is generally higher than of wound-field machine because of the elimination of the field electrical loss. Also, where field control is not required, the use of permanent magnet excitation simplifies the contraction of the machine and eliminates two electrical terminal and their associated wiring. In addition consequent advantages are included: a higher torque for a given frame size, improved efficiency, better dynamic response and reduced weight and volume.

There are two problems and risks of using permanent magnet excitation. First, the field magnet can be demagnetized by armature reaction mmf or by overheating of magnet, causing the machine to become inoperate. Second, the flux density which permanent magnets can operate results in air-gap flux densities that are much lower than those in wound- field machines.

Therefore, PM motors are started largely to use everywhere small size, high reliability, precise speed control and fast response are required. Because of these unquestionable advantages of PM motors, they represent the kernel of many special purpose drives and servomechanisms, computer peripherals.

The electrical machines may exhibit various magnetic materials (Alnico, Ferrite, SmCo, or NdFeB) having different direction of magnetization, two or three phases, concentrated or distributed winding, various shapes of magnetic circuits, nonuniform gaps, auxiliary salient poles which have no winding, auxiliary magnet, internal inside-field type rotor or external outside-field type rotors.

All these aspects highly affect not only the performances, but also the prices of the motor, as well as their reliability, production and processing ability and effectiveness. Three type motors which are 3 phase 6 poles and outside-field type, 2 phase 4 poles and inside-field, and 2 phase 4 poles nonuniform airgap and outside-filed, are examined and compared in literature [M.Rizzo & A.Savani & J. Trowski 1992], [M.Rizzo & A.Savani & J. Trowski & S. Wiak 1994]. The permanent magnet motors with constant and variable airgap are investigated in literature [M. Rizzo 1992]. In this, radial and tangential component of flux densities are computed by using two dimensional (2-D) finite element method. At the other published work [M.Rizzo & A.Savani & J. Trowski 1991], the static torque graphics of four different types motor as inside or outside field and 2 or 3 phase are calculated by using Maxwell Stress Tensor method and the influence of number of poles and inside or outside field structure on the torque of small DC motors is investigated. The paper [J. Trowski & K. Komeza & A. Pelikant & S. Wiak & M. Rizzo &A. Savani 1992] represents results of joint works of authors on background of review of recent literature on DC permanent magnet normal and brushless (BLDC) dc , stepper, variable, and switched reluctance motors. Torque-speed graphics of these motors are also obtained and all parameters are shown to have a crucial influence on the performance of motors. A numerical method to compute the flux distribution in the machine is used in [M. Marinescu & N. Marinescu 1992] for PM excitation consisting of segments magnetized non radially with different directions of magnetization and the advantages of the new excitation are investigated for a small torque fluctuations and extremely low armature reaction. At [O. Craiu & N. Dan & E.A. Badea 1995], the computation of the torques variation with respect to angular position is calculated for ferrite type PM DC motor while magnetic saturation and temperature's effect is considered.

The other important topic in this subject is design and optimization. The design and optimization of small PM motor is presented in [A. Miraoui & L.D. Fang & & K. Li & S.Charbonnier 1992]. The weight optimization is done in addition to the increase of average torque. In literature [X. Dexin & B. Baodong & Y.Yingying & W. Fengxiang 1995], the method for the shape optimization in the non-linear magnetic devices is presented. The simulated annealing algorithm combined with the complex strategy is used. In [K.R. Davey 1995], the optimal design of a magnet assembly to maximize the average magnetic field in the airgap is carried out.

The constant torque and therefore constant velocity produced by the motor is one of the most important requirements for the user. So the great part of research are focused to torque, torque ripple, and reduction of reluctance and cogging torque. At [L. Petkovska & M. Cundey 1992], [M. Marinescu & N. Marinescu 1988], and [N. Sadowski & Y. Lefevre & M.L. Mazenc & J. Cros 1992], the no load and on load torque of various type permanent magnet motor are calculated by using one of the different torque calculation methods or several of them. Than the results are compared to measurements and each other. Similarly, the torque calculations for switched reluctance motor without PM are made at literature [M.Moallem & C.M. Ong 1990] by using 2D and 3D modeling for finite element method (FEM). At [V. Gangla & J.D.L.Ree 1991], the analytical formulas to evaluate the electromechanical forces and torques involved in brushless surface mounted permanent magnet machines from design parameters is developed. The accuracy of the model was verified by using FEM.

In general for PM motors, torque pulsation is an important origin of vibration, acoustic noise and speed fluctuations. At literature [S.M. Hwang & D. K. Lieu 1995], the effect of magnet pole shaping and magnet arc length on the torque ripple and on the output torque are discussed by using FEM. At the other published work [S. Clenet & Y. Lefevre &N. Sadowski & S. Astier & M.L. Mazenc 1993], to control output torque and to compensate torque ripple, the supply waveshape is examined. In other word, the current equation can be written as a function of cogging torque. Similar study is made at literature [J.Y. Hung & Z. Ding 1993], [R. Carlson & M.L. Mazenc & J. C.S. Fagundes 1992] using on analytic approach.

The reluctance torque is often a principal source of vibration and control difficulty in motors, especially at low speed and loads. The reduction of reluctance torque in PM motors is analyzed at literature [S.Hwang & D.K. Lieu 1994]. Finally, the reluctance torque is calculated by using Maxwell Stress Tensor and 2D modeling for FEM. Then, the reluctance torque is reduced by using two different methods which are rotor pole skewing and stator pole notching.

The main parts of electromagnetic torque ripple is originated from the cogging torque. The reduction of cogging torque has examined at [B. Accermann & J.H.H. Janssen & R. Sottek & R.I. Van 1992], [T. Ishikawa & G.R. Slemon 1993], and [T. Li & G. Slemon 1988]. In [B. Accermann & J.H.H. Janssen & R. Sottek & R.I. Van 1992], the reduction can be obtained by adjusting the width of the magnet pole or the slots. The results are obtained by analytically and compared with FEM. By appropriate choice the tooth plus slot dimension, the cogging torque has been reduced to about %1 of rated torque at [T. Li & G. Slemon 1988]. Furthermore, [T.

Ishikawa & G.R. Slemon 1993] shows the ripple torque can be reduced by shifting the pole pairs by half a slot pitch and by choosing the value of magnet width.

Since the PM's are the most expensive part of the motor, it is obvious that the optimization of the motor cost will be oriented towards reducing the volume of the magnet while the produced torque will not be decreased. For this purpose, torque optimization is presented by changing the PM dimensions at [L. Petkovska & M. Cundev & G.Cvetkovski 1995].

For two types PM - BLDC motor, the effects of overload on parameters and performance are investigated at [N.A. Demerdash & T.A. Nyamusa 1985], [M.A. Alhamadi & N.A. Demerdash 1994]. In this study, the effects of overload on demagnetization of the PM and on other machine parameters such as armature inductances and induced back emf are investigated by using FEM, then the dynamic performance of such motors under overload conditions is simulated. At [N.A. Demerdash & M.A. Alhamadi 1996], the analysis of parameters and performance of PM - BLDC motors and drives are reviewed and summarized. The armature induced emf and armature winding inductances are calculated by using 3D-FE formulation. After parameter calculation, the performance simulation of PM - BLDC motor drive is presented. This simulations are based on a state-space motor-conditioner network model. At [T.W. Nehl & N.A. Demerdash 1992], state space models are developed for rotating machines using abc frame lumped parameter network model.

Some of papers are interested in different techniques for parameter estimation. For instance, [N.A. Demerdash & T.M. Hijazi & A.A. Arkadan 1988], [O.Craiu & C. Raduti & N.Dan 1995], [T.W. Nehl & F.A. Fouad & N.A. Demerdash 1982] calculates the induced voltage in windings of the electrical machines, as space - time function. At [N.A. Demerdash & F.A. Fouad & T.W. Nehl 1982], a method which is based on perturbation of the energy stored in the magnetic field, is used in calculating winding inductances in ferrite type PM electrical machine. Results of calculation of winding inductances are in very good agreement with corresponding measured values.

At [M. Wing & J.F. Gieras 1992], the steady state performance of small commutator PM DC motors are presented. The numeric, analytic, and experimental results are compared. The results show that finite element technique has a better accuracy over the analytic method. A dynamic model for simulation of the radially oriented PM synchronous machines and drive circuit is presented at [T.W. Nehl & F.A. Fouad & N.A. Demerdash & E. A. Maslowski 1982]. This modeling approach combines use of the 2D FEM for solving nonlinear magnetostatic field problems and associated machine parameter determination with a nonlinear network model based on generalized network graph theory concepts. The measured and calculated voltage and current waveforms are obtained excellent agreement.

The factors affecting motor performance are the other research area. At [T.W. Nehl & N.A. Demerdash & F.A. Fouad 1985], the impact of emfs, inductances, and commutation angle on BLDCM are examined. Literature [M.A. Alhamadi & N.A. Demerdahs 1991] investigates effects of skewed PM mounting on the performance of BLDCM drive. This skewing of PM is effective in reducting the harmonic contents in both the induced emfs in the armature and torque profiles.

The aim of this thesis is the dynamic simulation and prediction of the performance of the permanent magnet variable reluctance motor and its drive circuit in which parameters inductances and emfs, are obtained entirely from finite element field analysis of the magnetic circuit. A dynamic model for simulation of this motor and the associated drive is developed here as the first time. The approach of the thesis combines use of the two dimensional finite element method for determination of machine parameters with a dynamic model based on state space form. The advantage of the approach is that the geometry changes on the overall system can be assessed without the construction of costly prototypes.

The parameter calculation methods by using finite element and dynamic simulation by using state space form, which were used on PM-BLDC motors in [T.W. Nehl & F.A. Fouad & N.A. Demerdash & E. A. Maslowski 1982], [N.A. Demerdash & T.A.

Nyamusa 1985], [M.A. Alhamadi & N.A. Demerdash 1994], [N.A. Demerdash & M.A. Alhamadi 1996] are applied on a PM-VRM in this study. The nonlinear model of the machine is combined with the drive circuit and closed loop controllers.

The other parts of the study have been organized as follows:

Chapter 2 describes the finite element method and the package program used in this study. The equation for the purpose of obtaining the magnetic field distribution of the machine is derived.

Chapter 3 is the analysis of permanent magnet variable reluctance motor with finite element method. The magnetic field analysis has been described by giving dimensions of the machine and the specifications of the material. The back emf induced in the stator winding and the inductance values of these windings have been calculated here as well as the static torque of the motor. In this chapter the inductances have been computed by using two different techniques i.e, energy perturbation technique which is experimantally verified in [T. W. Nehl, F. A. Fouad & N. A. O. Demerdash 1982] and co-energy technique . Discussion on these two techniques is given.

Chapter 4 is dedicated to the dynamic simulations of the motor and its drive circuitry. The motor has been modeled together with the driver circuit and the equations of the current, speed, and electromagnetic torque, which are to be obtained in the state space form as a result of non-linear modeling approach used here. The equations have been worked out through the FORTRAN programming language applying the 4 th order Runga Kutta. Furthermore, simulations have been made for the entire system by including current and speed controllers to the program.

In the 5 th and last chapter, the results have been interpreted and the contributions made to the literature are discussed. At the end, the furtherwork suggests the topics related to this study that can be performed by researchers.

CHAPTER TWO

FINITE ELEMENT METHOD ANALYSIS

2.1 Introduction

The electrical and magnetic systems can be described by the ordinary and partial differential equations. There are two basic different solution methods of differential equations. One of them is exact solution method (or analytical method) and the other is approximate solution method (or numerical method). The finite element method which is used in this study is one of the numerical solution methods. This method is one of the powerful numerical techniques used for solving differential equations having the initial and boundary-values in geometrically complicated regions.

In this study, the finite element method is applied to the magnetic field analysis of the permanent magnet variable reluctance motor (PM VRM). The rotor and stator structure of this machine is shown in figure 2.1.

Although the finite element method is often the easiest to use, it is not necessarily the best method for every physical problem. Because the entire domain in some cases has simple geometry and the boundary conditions are well defined, other approximate methods or even analytical methods might produce faster and more accurate results.

The name of finite element summarizes the basic concept of the method: the transformation of an engineering system with an infinite number of unknowns (the response at very location in a system) to one that has a finite number of unknowns related to each other by elements of finite size. The unknowns, called degrees of freedom (dof), represent the responses to applied input. [Ansys PC magnetics reference manual 1991]

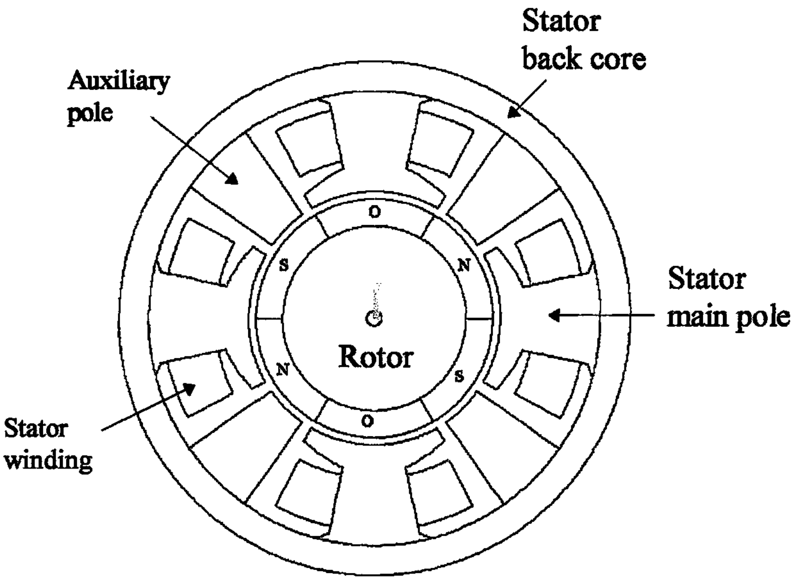

Figure 2.1. The structure of the permanent magnet variable reluctance motor

The element is the critical part of the finite element method (FEM). It interconnects degrees of freedom, establishes how they act together, and determines how they respond to applied input.

Every element has one or more nodes that lie along its boundary. Nodes are the coordinate locations where other elements can be connected and also at which the degrees of freedom and actions are located. Information is passed from element to element only at common (shared) nodes.

Too manyfold are the sources of errors. These include inadequate modeling, discretization errors, wrong definition of boundary conditions, error in input data, inaccurate determination of material parameters, etc. The handling of problems, interfaces and insufficient iterations are other reasons for inaccurate results which are not always transparent to user.

2.2 The Properties of Finite Element Analysis

In this study, both the triangular and rectangular elements are used. These elements, as shown in figure 2.2-a and figure 2.2-b, have four nodes that would carry upto four degrees of freedoms. In this study, each element carries one dof that is the magnetic vector potential, A_z.

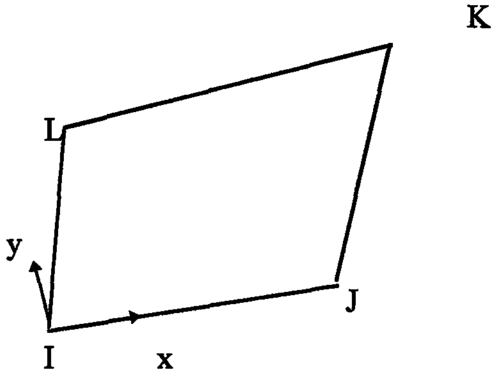

(a) Rectangular elements

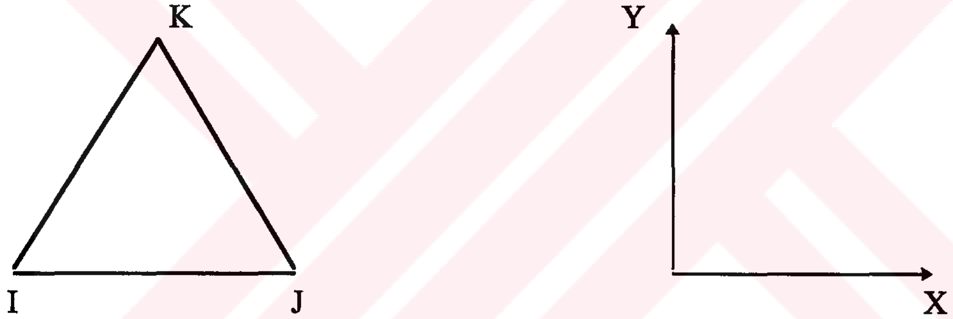

(b) Triangular elements

(c) Global Coordinate system

Figure 2.2 The element

Each element has own element coordinate system. X-Y is the global coordinate system as shown in figure 2.2-c and x-y is the element coordinate system as shown figure 2.2-a. This coordinate variables can be properly defined in the rectangular and polar coordinate systems. This element coordinate system is very important, specially, if there is a rotating part having the permanent magnets and, the location and polarization of them are the source of the magnetic field distribution in the stationary and moving magnetic materials. The polarization of permanent magnet is described by using this coordinate system. The x-axis of the element is set to be in parallel to the line between I and J representing orientation of the magnet from the south to north. The permanent magnet material should be described with its coercive force in the FEM in addition to the exact location of the magnet.

A permanent magnet can be represented by the equivalent MMF created by the current density of $\overline{J}_m$. Hence the current density, $\overline{J}_m$ is related to the coercive force vector of the permanent magnet, $\overline{H}_c$, as given below [S. Chen & K. J. Binns & Z. Liu & D. W. Shimmin 1992], [O. Craiu & N. Dan & E. A. Badea 1995];

$$\overline{J}_m = Curl(\overline{H}_c) \tag{2.1}$$

In this study, the meshing of motor geometry and number of iterations are chosen properly, in order to avoid the error on the calculation [M. Moallem & C. M. Ong 1990]. Since the stored energy in the air-gap is crucial for the estimation of machine performance, the air-gap discritization meshing must become dense. At least three layer elements are recommended in the air-gap [Ansys Magnetics User's Guide 1993]. In this study, four layer elements are chosen in the air-gap.

The finite element method, used here, has two load steps. The first step is to find an approximate solution by using 5 iterations. Then the results of first step is accepted as an input to the second load step . The converged solution is obtained from the second and last load step with 20 iteration.

The current density (A/m^2 for MKS) is kept constant in the elements. That represents the effect of the MMF created by the stator currents. The direction of the current is perpendicular to the global coordinate system created by X-Y shown in figure 2.2-c. This perpendicular axis is named Z direction. The positive polarity of the current is defined in the direction of +Z.

2.3 Applications to Electrical Machinery And Devices

The finite element method is used to analyze the magnetic field distribution in the permanent magnet variable reluctance machines. The non-linear relation between the flux density and flux intensity requires the numerical techniques to be used for the magnetic field analysis.

A general formulation of the electromagnetic field problem in a permanent magnet variable reluctance machine can be given by Maxwell's equation as; [H. P. Neff 1991]

$$Curl\overline{H} = \overline{J} + \frac{\partial\overline{D}}{\partial t} \qquad (2.2)$$

where $\overline{H}$ [A/m] is the magnetic field intensity , $\overline{J}$ [A/m^2] is the current density, and $\overline{D}$ [C/m^2] is the electric flux density. The time derivative of electrical flux density is named displacement current density.

The following assumptions which are widely used for the analysis of the electrical machines using the finite element technique, are accepted in this study [S. L . Ho & W. N. Fu & H. C. Wang 1995].

1. The displacement currents are neglected.
2. The end effects are neglected.
3. The vector potential has an axial component only in Z direction, while the magnetic field is situated in planes normal to the machine axis.
4. There are no leakage fluxes on the outer surface of stator core.

Since the displacement currents are neglected, the equation (2.2) can be rewritten;

$$Curl\overline{H} = \overline{J} \qquad (2.3)$$

The relation between magnetic field intensity $\overline{H}$ and magnetic flux density $\overline{B}$ is given below when permanent magnets are considered;

$$\overline{B} = \mu_o(\mu_r\overline{H} + \overline{M}_o) \qquad (2.4)$$

where μ_o is the relative permeability of air, μ_r is the relative permeability of the material, and $\overline{M}_o$ [A/m] is the remanent intrinsic magnetization vector of the permanent magnet. The magnetic field intensity is obtained from equation (2.4);

$$\overline{H} = \frac{1}{\mu_o\mu_r}\overline{B} - \frac{1}{\mu_r}\overline{M}_o \qquad (2.5)$$

where μ, which is equal to $(\mu_o.\mu_r)$, and μ_0 are equal to $(1/\nu)$ and $(1/\nu_0)$ respectively.

$$\overline{H} = \nu\overline{B} - \frac{\nu}{\nu_o}\overline{M}_o \qquad (2.6)$$

The magnetic flux density can be calculated by using magnetic vector potential $\overline{A}$.

$$\overline{B} = Curl\overline{A} \qquad (2.7)$$

If the equation (2.6) and (2.7) are substituted into equation (2.3);

$$Curl\left(\nu Curl\overline{A}\right) - Curl\left(\frac{\nu}{\nu_o}\overline{M}_o\right) = \overline{J} \qquad (2.8)$$

The equation (2.8) represents the general vector Poisson equation for the static magnetic field (x and y) components of $\overline{A}$ and $\overline{J}$ are zero in the case of 2D application in the FEM. Because it is assumed that the vector potential has an axial component only, while the magnetic field is situated in planes normal to the machine axis. Therefore $\overline{A}$ and $\overline{J}$ can be expressed in terms of their components as given below;

$$\overline{A}=\begin{bmatrix} A_x \\ A_y \\ A_z \end{bmatrix}=\begin{bmatrix} 0 \\ 0 \\ A_z \end{bmatrix} \quad , \quad \overline{J}=\begin{bmatrix} J_x \\ J_y \\ J_z \end{bmatrix}=\begin{bmatrix} 0 \\ 0 \\ J_z \end{bmatrix} \qquad (2.9)$$

By solving the equation (2.8) of the magnetic vector potential at each nodal point in the regions, A_z can be calculated [M. V. K. Chari & G: Bedrosion & J. D' Angelo & A Konrad 1993], [S. L . Ho & W. N. Fu & H. C. Wong 1995], [H. Kardestuncer & D.H. Norrie 1987].

2.4 ANSYS Program

The ANSYS package program was introduced by Swanson Analysis System Incorporated (SASI), in 1970. The ANSYS program is a general-purpose finite element analysis program.

There are about 850 commands in the program, each of them is designed for a specific function. These commands are the primary tools which are used to communicate with the package program. The easiest way to communicate with the program is via the menu system. The program menu is organized into a tree structure with logical groupings of related topics. There are three main groupings which can be thought of as three different trees. They are: "Main Commands", "Utility Commands", and "Reference". The details of these trees are out of the scope of this writing.

The program is organized into two basic levels. They are begin level and processor (or routine) level. The begin level acts as a gateway into and out of the ANSYS program. It is also used for certain global program controls such as defining the job-name, clearing the database, and making copies of binary files. At the processor level, several processors routines are available, each serving a specific purpose. These are PREP7 (general preprocessing), SOLUTION (loading and solving), POST1 (general postprocessing), and AUX15 (file translation from a CAD) etc [Ansys User manual Procedure 1992].

The static magnetic analysis can be done either using the 2D or 3D computational technique at the package program. These two types of analysis have several advantages and disadvantages over each other. In 2D analysis, only the cross-section of motor is considered. The axial length of motor is not used in the finite element analysis. Therefore, the effects of the end point of phase winding, namely 'end effects', is omitted. If the 3D analysis is used, the axial length of motor is also considered and the end effect is included in the finite element computation. But element and node numbers of 3D modeling increases too much. This means that the storing capacity of computer and computation time of the analysis increase enormously when it is compared with 2D method. Since the skewing is not considered here, the flux distribution along the axial axis is uniform. The assumptions that are made in the previous section (2.3) and non-skewing enable the use of 2D method.

2.5 Magnetic Field Analysis in the Package Program

Typical quantities of interest in a magnetic analysis are flux density, field intensity, torque, inductance, eddy currents, power loss, and flux leakage. The magnetic field is created as a results of existing an electric current, a permanent magnet, or an applied external field. The ANSYS program uses Maxwell's equations for the magnetic field analysis. The primary unknown (degrees of freedom) calculated in this program is the magnetic potential. The other magnetic field quantities are then estimated from the magnetic potentials. Three types of magnetic analysis are possible [Ansys User manual Procedure 1992]:

1. Static magnetic analysis
2. Harmonic magnetic analysis
3. Transient magnetic analysis

2.5.1 Static Magnetic Analysis

The flux created by the permanent magnets and the stator currents is stationary in time at the specific rotor position, therefore, there is no any time dependent variable. The static magnetic analysis that is used in this study, calculates the magnetic field distribution in the permanent magnet variable reluctance motor given in figure 2.1.

This analysis consists of the scalar and vectoral magnetic potential methods which are described below.

2.5.1.1 Scalar Magnetic Potential Method

The scalar magnetic potential methods are used in the case of implementation of 3D method. Within the scalar potential formulation, three different methods are available. These are:

1. Reduced Scalar Potential
2. Difference Scalar Potential
3. Generalized Scalar Potential

2.5.1.2 Vector Magnetic Potential Method

The vector potential method is implemented for both 2D and 3D analysis of the electromagnetic field. There are two different methods available within the vector potential formulation. These are given below;

1. Constrained Magnetic Vector Potential
2. Unconstrained Magnetic Vector Potential

In this work, the vector magnetic potential method is chosen because the other techniques require 3D modeling. The constrained magnetic vector potential method has been selected here since the meshing of the air gap depends on two nodes located on the same coordinates. One of these nodes refers to the stationary part (i.e stator) as the other is rotating with rotor. A constraint is defined between these two nodes at every step of the rotation.

2.5.2 Harmonic Magnetic (AC) Analysis

The harmonic magnetic analysis is a technique used to calculate the effects of alternating current (AC) source or an imposed alternating external field in electromagnetic devices. The eddy currents, skin effects, power loss due to eddy currents, stored magnetic energy, magnetic forces induced by eddy currents, and inductance are estimated. The typical applications cover the analysis of the transformers, ac motors, and almost any electromagnetic device that works with AC.

The harmonic analysis is a linear analysis. Therefore, non linearities such as B-H curves will be ignored. The electric and magnetic field are coupled. Variation of the field with respect to time is assumed to be sinusoidal with the same frequency. Eddy currents may be significant and heavily influence the field structure in the model. Material properties may be temperature dependent.

Since the entire field must vary sinusoidally, this would prevent permanent magnets or effects of saturation from being simulated using the harmonic analysis. Permanent magnets supply a constant flux to the system. Saturation of the material indicates that as the field intensity increases, the flux density in material would not be able to follow the same sinusoidal behavior.

If the saturated regions are significant, then a nonlinear transient analysis will be required. If the multiple frequencies or permanent magnets are required and the materials are linear, a linear transient analysis required.

The harmonic analysis have some advantages as;

- require single step analysis,
- minimizes disc storage,
- can address multiple currents with different phase shape shifts.

On the other hand, there are some disadvantages;

- ignores saturation effects
- applied currents or imposed fields are for single frequency

2.5.3 Transient Magnetic Analysis

Transient magnetic analysis is a technique used to calculate time-varying electric and magnetic fields, such as those due to surges in electric current or pulsed external fields. Examples of quantities of interest are eddy currents, power loss due to eddy currents, and magnetic forces induced by eddy currents. The transient analysis may be linear or nonlinear.

If the physical problem have leads which can not be characterized as being static nor harmonic, a transient analysis can be performed.

The electric and magnetic fields are coupled. Variation of the field with respect to time is arbitrary. The material properties may be nonlinear and linear material properties may be temperature dependent. The permanent magnets can be included in the analysis. The eddy currents can be simulated in the current carrying conductors and are assumed to have a significant effect on the calculation of the field. The transient analysis can not simulate the hysteresis effects on the material. The displacement currents and their coupling to the magnetic field are also ignored.

In the transient analysis, a numerical evaluation is used to determine the change of the degrees of freedom as a function of time. Program may be saving more data and need more disk space. It require more time steps and more iterations, because of severe current rate of change.

CHAPTER THREE

THE ANALYSIS OF PERMANENT MAGNET VARIABLE RELUCTANCE MOTOR WITH FINITE ELEMENT METHOD

3.1 Introduction

The permanent magnet variable reluctance motor which is electronically controlled and commutated, has been recently developed as a micro motor after the widely use of semiconductor devices and permanent magnet materials. These motors can be used in many motion control and servo systems.

After the widely use of power electronics technology, the reliable, robust and energy efficient electrical machines have been designed and investigated for industrial applications. The prediction of the machine performance in detail is necessary to design and specify the constraints on the machine dimensions. The computer simulation of this machine can be used to compare the performance with the conventional type of machines, and it helps to investigate if it can be preferred in the industrial application or not.

The detailed computer simulation program, that will be presented in the next chapter, requires the prediction of the parameters of the machine. One effective algorithm, that is preferred here, is the finite element technique to predict these parameters. These parameters are induced electromotive force induced in the stator windings, mutual and self inductances.

In this chapter, the application of the 2D finite element technique to the solution of the magnetic field distributed in the permanent magnet variable reluctance motor will be presented. Also the static torque characteristic of the machine is obtained from the finite element solution in order to estimate the control logic of drive circuit and to observe the pulsation of the torque developed by the machine.

3.2 The Machine Geometry and Dimensions

3.2.1 The Geometry of Machine

A two phase, permanent magnet variable reluctance motor is used in this study. This machine has a variable reluctance between stator and rotor. The stator has four main poles and four auxiliary poles as it is shown in figure 3.1. The armature windings are wound around the main poles. These concentrated windings are connected to the drive circuit. The rotor has four poles created by using the permanent magnets. Each permanent magnet part on the rotor occupies 60 mechanical degrees measured over the circle around the air-gap. Two out of four poles are magnetized S-pole and the others are magnetized as N pole. The interpolar sections which is the area between the permanent magnet poles are occupied by air or non magnetic material. The non magnetic material is represented by O. The permanent magnet material that is used in this machine, is the Neodymium Iron Boron (NdFeB) type with the flux density (B_r) of 0.8T and the flux intensity (H_c) of 557.32 kA/m with radial magnetization. The radial thickness l_m of the permanent magnet material is 3.6mm. The rest of the properties of NdFeB magnets are listed in table 3.1 [K. J. Strnat 1991], [T. J. Sokira & W. Jaffe 1990], [T. J. E. Miller 1989].

The core of stator and rotor is made of laminated steel. The magnetization curve of this core is given in figure 3.2[United States Steel 1980]. The relative permeability of the stator core is assumed to be sufficiently large that the leakage flux out of the core can be neglected. This assumption was used to specify the boundary conditions mentioned in section 3.3.2.

Table 3.1 The magnetic and physical properties of NdFeB type permanent magnet.

Magnetic characteristics		
Quantity	**Unit**	**NdFeB Magnets**
Energy Product $(B.H)_{max}$	$k.J/m^3$	52.0
Residual Induction B_r	T	0.8
Coercive Force H_c	kA/m	557.324
Intrinsic Coercivity H_{cl}	kA/m	1 433.121
Recoil Permeability μ_r	H/m	1.1423
Temperature coefficient of B_r to 100°C	% / °C	-0.10
Temperature coefficient of H_{cl} to 100°C	% / °C	-0.50
Maximum Operating Temperature	°C	180
Physical Properties		
Curie Temperature	°C	335
Electrical Resistivity	μΩcm	143
Density	g/cm^3	7.6
Thermal Conductivity	W/(cm. °C)	0.07

3.2.2 The Design Of The Machine Dimensions

800 rad/sec.

In this study, 50 Volt, 2 Amper, and 900 rad/sec motor has been designed and analyzed. The initial dimensions of the machine are obtained by using the equations given below. The finite element analysis has been performed to examine the flux density values of magnetic circuit. The stator pole shoes, main pole and auxiliary pole, the number of stator windings, inner diameter of the stator core, outer diameter of the stator core, the effective area required for the windings, the arc of the stator pole shoes and the width of auxiliary poles have been estimated under the constraint on current and flux densities. According to the result of field analysis performed by FEM, the motor dimensions are set.

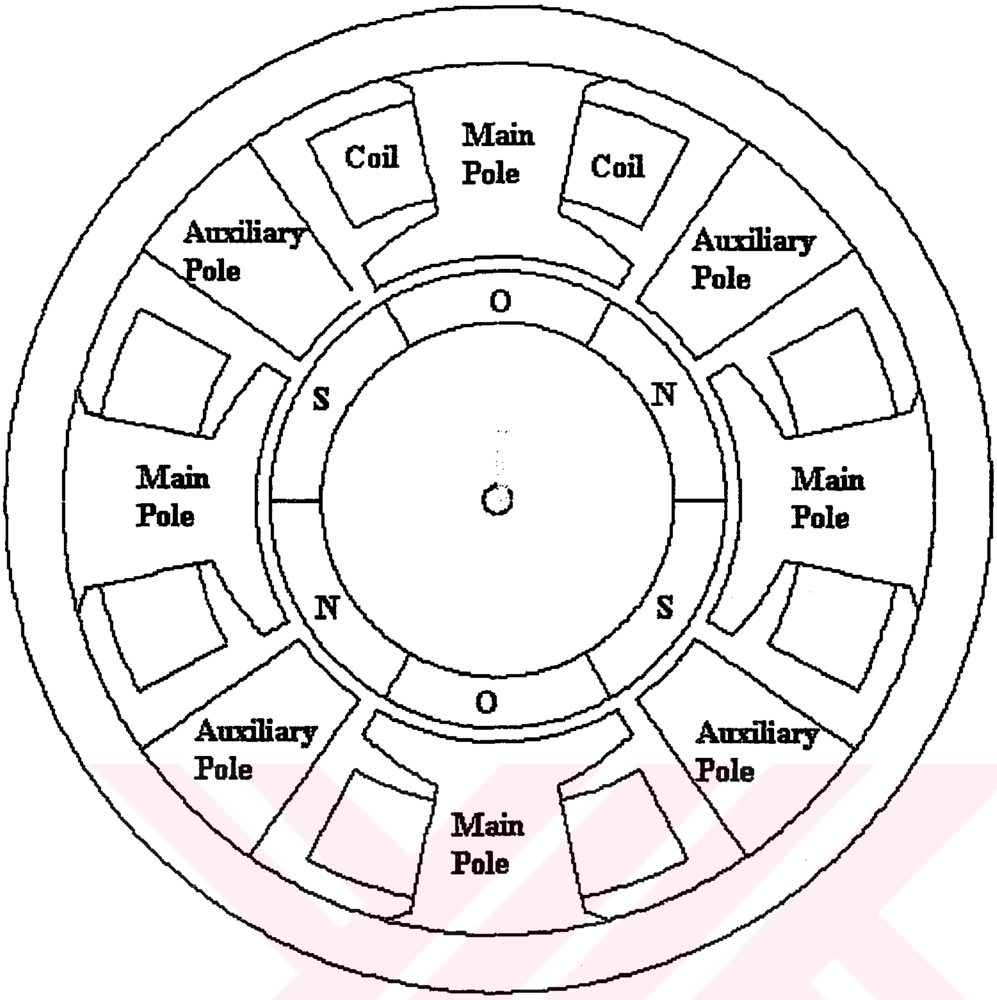
Main
Pole
Coil
Coil
Auxiliary
Pole
Auxiliary
Pole
O
S
N
Main
Pole
Main
Pole
N
S
O
Auxiliary
Pole
Auxiliary
Pole
Main
Pole

Figure 3.1 Motor geometry

3.2.2.1 Radial Thickness of the Magnet

The air gap flux density B_g above NdFeB magnets can be related to the magnet's residual flux density B_r, the relative permeability μ_r, and the dimensions [G. R. Slemon 1994, p 1123-1138], [G. R. Slemon & X. Liu 1992], [G. R. Slemon 1994, p134-140], [G. R. Slemon 1991].

$$B_g = \frac{l_m'}{g_e + l_m'} . B_r \tag{3.1}$$

where $l_m' = (l_m / \mu_r)$, and g_e is the effective air gap length. The value g_e is typically about 1.05 g for permanent magnet machines. l_m is the magnet length and g is the actual air gap length. For the NdFeB, the radial thickness l_m of the magnet to achieve this flux density is then given by choice of the dimension ratio,

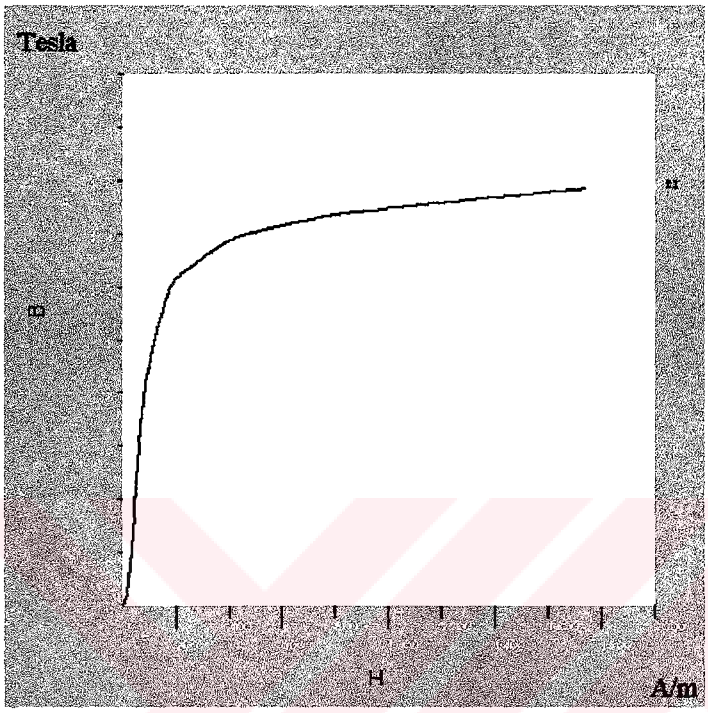

Figure 3.2 The B-H curve of rotor and stator steel

$$\frac{l_m}{g_e} \approx 2.5 - 6.5 \qquad (3.2)$$

3.2.2.2 Rotor Speed

Figure 3.3 shows the magnetic axis of the mmf in space. When the current is given to the winding of phase A the axis of the mmf is aligned to the main pole of this phase. When the current is turned off from phase A and applied to phase B, the mmf will form on the main pole of phase B from now on. This change in the magnetic field axis will take place at 90 mechanical degrees apart. Since the magnets of the rotor will tend to follow the poles of magnetic field, the rotor will run. When the motor has no load, the rotor speed will be almost equal to the speed of the magnetic field. Therefore, the speed of the rotor can be defined as the speed of the magnetic field. The speed of the magnetic field created by stator currents will be $w=\pi / (2.\Delta t)$ where Δt is the half of the switching period.

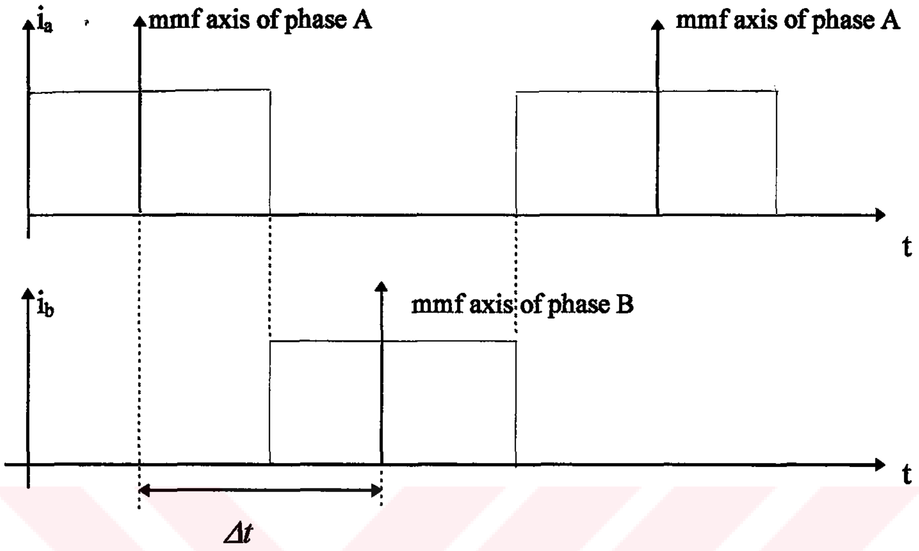

Figure 3.3 mmf axis of stator phases with respect to phase currents

3.2.2.3 Armature Core Length

The length of the stator can be related to the induced voltage in the windings on the main pole as follows;

$$emf = -N.A.\frac{dB}{dt} = -N.l.d.\frac{dB}{dt} \qquad (3.3)$$

where N is the number of the turn and ϕ is the flux of the stator pole. Flux is the multiplication of the flux density B and cross sectional area of main pole, A. In addition, area is composed of stator length l and main pole width d. The change of the flux density with respect to rotor position and rotor position with respect to time is substituted in equation (3.3);

$$emf = -N.l.d.\frac{dB}{d\theta}.\frac{d\theta}{dt} \qquad (3.4)$$

The last term of the right hand side of equation (3.4) is the speed of the magnetic field (*w*). The other derivative can be written as proportion of a small changes. Hence,

$$emf = -N.l.d.w.\frac{\Delta B}{\Delta\theta} \qquad (3.5)$$

[A. Kusko & S. M. Peeran 1987] shows graphically that flux density in the coil is changing linearly from its positive maximum to the negative minimum, and this change is approximately 2B_r and takes place during 120 degrees of rotor angle. Therefore, equation (3.4) provides a solution to the stator length. If the armature terminal voltage is prespecified.

3.2.2.4 Diameter of Stator Core

The basic shape of the motor is related to the ratio of rotor length to rotor radius. This choice may be based on several criteria. One might be the shape giving the minimum loss in the stator winding. It can be shown that this occurs for

$$\frac{l}{r} \approx \frac{10}{p} \qquad (3.6)$$

where *r* is length from origin to the middle point of the air gap and *p* is pole number. After the determination of *l*, *r* is chosen by means of equation (3.6).

3.2.2.5 Length of The Air Gap

The minimum value for the actual air gap is set by mechanical considerations and is given as ;

$$g = 0.2 + 0.003\sqrt{r.l} \qquad \text{mm} \qquad (3.7)$$

where l is the stator length. This stator length is already calculated at rated armature voltage by using equation (3.5).

3.2.2.6 Stator Current Density

The stator diameter is also related to current density in the stator winding. This current density is determined by the winding current and number of turn. With a stator winding current I, number of turn N, and utilization factor k , coil area A_c is calculated from the equation below.

$$2.5 \leq \frac{N.I}{A_c.k} \leq 10 \qquad \text{A/mm}^2 \qquad (3.8)$$

where utilization factor is chosen about 0.5.

3.2.2.7 Stator Back Core Width

The stator back core thickness l_b in figure 3.4 can be chosen to give appropriate value of maximum back core flux density B_y. Using the constraint on the back core flux density B_y, air gap flux density B_g and diameter of stator core, the stator back core width can be approximately estimated from the equation given as follows;

$$l_b = \frac{B_g.\pi.r}{6.B_y} \qquad (3.9)$$

The motor axial length, stator core diameter, r ,the air-gap, the number of turn per pole, and thickness of the magnet are chosen as l =50 mm, r =16.5 mm, g =1 mm, l_m =3.6 mm, and N= 96 respectively. The constraints on the stator current density and flux density are chosen as 5 Amps.t/mm^2 and 1.5 Tesla respectively.[M. Ermis &

H.B.Ertan & E. Akpınar & F. Ülgüt 1992] The other machine dimensions are obtained by using the field analysis of FEM given in next section. The stator and rotor dimensions shown in the figure 3.4 are as follows; The unit of the lengths are mm and angles are degree.

θ_c(°)	θ_a(°)	θ_p(°)	θ_m(°)	r_i mm	l_{ps} mm	l_b mm	l_c mm	r_r mm	r_m mm	r_s mm
12	20	24	60	1	2	4	7	12.4	16	34.5

The optimum design has been kept out of scope of this thesis.

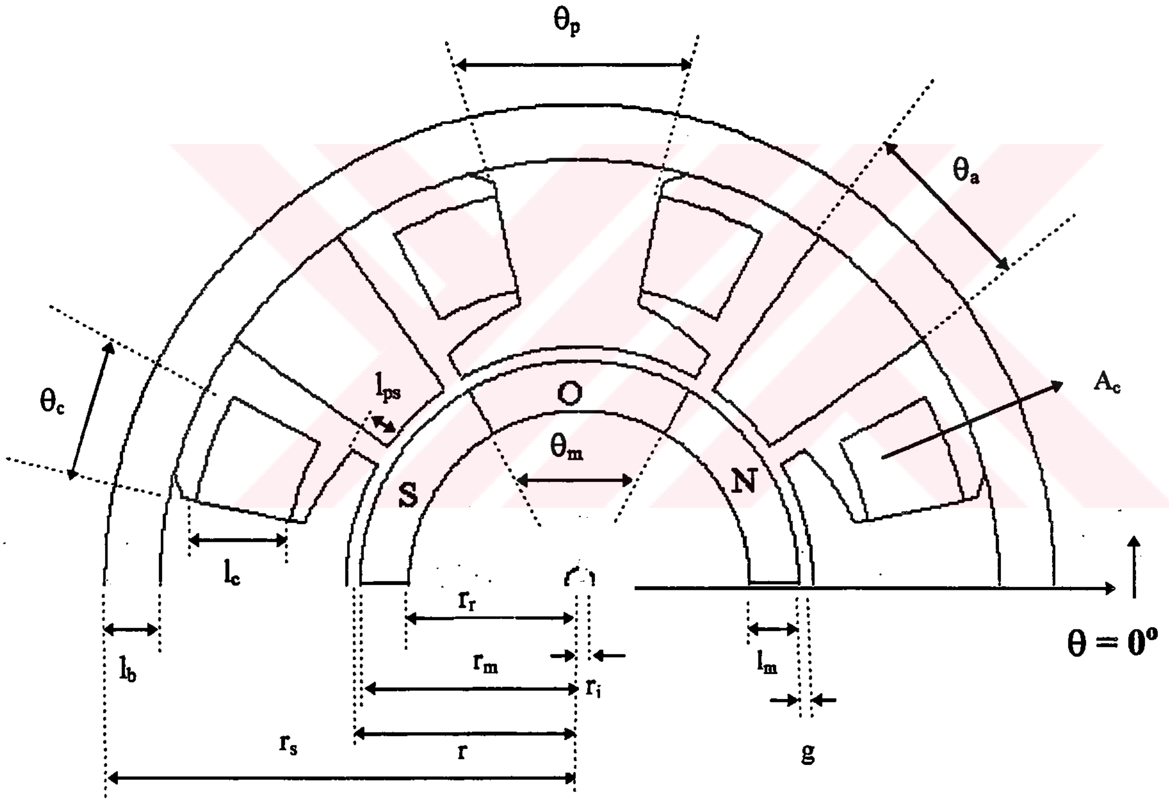

θ_p
θ_a
A_c
θ_c
l_{ps}
O
θ_m
S
N
l_c
l_b
r_r
r_m
r_i
r_s
r
l_m
g
$\theta = 0°$

Figure 3.4 The dimensions of the motor

3.3 Calculation of the Magnetic Field by the two-dimensional Finite Element Method

In the magnetic field analysis, one objective is to carry out a two dimensional finite element analysis in order to find the magnetic field distribution in the machine. The mesh modeling of the motor is seen in Figure 3.5.

The assumptions made in the study are given as follows:

1. Permanent magnets are isotropic, and have a linear demagnetization characteristics.
2. Eddy currents are ignored. → AC 'de olur.
3. The end effects are neglected. → 2D olduğundan .
4. The vector potential has an axial component only.
5. There are no leakage fluxes on the outer surface of stator core.
6. The displacement current is ignored. AC'de olur.

Since the air gap between the stator and rotor is not constant, the reluctance varies due to the change of the rotor position. Therefore the flux distribution in the machine and the torque developed by the machine are a function of the rotor position. The inductances due to various windings are also a function of the rotor position. This is the reason why the magnetic field analysis in this study has been carried out from 0 degrees to 360° of rotor position by the step length of 2 degrees.

In order to implement the two dimensional finite element solutions, the machine geometry is discretized into small first order triangular and rectangular elements. The selection of the triangular or rectangular element is depending on the structure. There are 9542 nodes and 9110 elements in finite element grids of the permanent magnet variable reluctance machine used here.

The finer mesh can provide the more accurate of the results. A finite element model which is too coarse will produce poor analysis results, it is also too large to run on a given computer. Therefore, this is wasteful of computer resources. Ideally, the mesh density should vary across the model, coarse in region where the solution results are expected to vary less and finer where the results are expected to have step gradients. It is important and difficult problem to predict which areas require a finer mesh and how fine those regions should be.

The solution of this problem is a combination of experience, guesswork, and confirmation (trial and error). The most important of which is confirmation. Some of the techniques might be employed to resolve this question include:

1. Compare the results of a preliminary analysis with independently derived experimental or known accurate analytical results. Refine the mesh in regions where the discrepancy between known and calculated results is too great.
2. Perform an initial analysis using what seems to be a 'reasonable' mesh. Reanalyze the problem using twice as many elements in critical regions, and compare the two solutions. If the two meshes give nearly the same results, then the mesh is probably adequate. If the two meshes yield substantially different results, then further mesh refinement might be required.

In this study, the second trial and error method mentioned above is used, because of lack experimental results.

In figure 3.5, blue color represents the air-gap region. purple color represents rotor and stator steel. The coil area is given by black and non magnetic material is given red. Finally, green and pink represent S and N pole magnets.

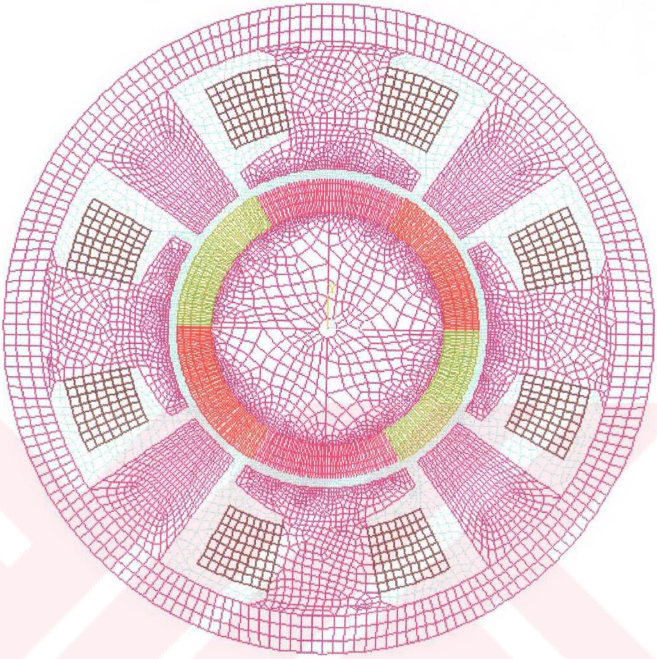

Figure 3.5 The mesh structure of the motor

3.3.1Magnetic Field Distribution

The solution of two dimension nonlinear magnetostatic problems is obtained from where the field sources are current densities or permanent magnets. The computation is employed to predict the flux distribution in a permanent magnet variable reluctance motors both at rated load and no-load operating conditions.

The magnetostatic field problem expressed by using Maxwell's equations is given below after rearranging the equation (2.8):

$$Curl\left(\nu Curl\left(\overline{A}\right)\right) - Curl\left(\frac{\nu}{\nu_o}\overline{M}_o\right) = \overline{J} \qquad (3.10)$$

The coercive force vector $\overline{H}_c$ is related to the remanent intrinsic magnetization vector $\overline{M}_o$ [Ansys Theoretical Manual 1991];

$$\mu\overline{H}_c = \mu_o\overline{M}_o \qquad (3.11)$$

The equation (3.11) can be rearranged;

$$\nu_o\overline{H}_c = \nu\overline{M}_o \qquad (3.12)$$

This equation is substituted into the equation (3.10)

$$Curl(\nu Curl(\overline{A})) - Curl(\overline{H}_c) = \overline{J} \qquad (3.13)$$

The effect of the permanent magnet is simulated as current density;

$$\overline{J}_m = Curl(\overline{H}_c) \qquad (3.14)$$

Therefore the mathematical model of a PM motor can be expressed by the equation given below; [S. Chen & K. J. Binns & Z. Liu & D. W. Shimmin 1992], [M. A. Rahman & P. Zhou 1991], [M. Wing & J. F. Gieras 1992], [O. Craiu & N. Dan & E. A. Badea 1995], [M. Rizzo 1992], [V. Gangla & J. D. La Ree 1991]

$$Curl(\nu Culr(\overline{A})) = \overline{J} + \overline{J}_m \qquad (3.15)$$

$\overline{J}$ is the armature current density and $\overline{J}_m$ is the equivalent current density corresponding to the coercive force of the permanent magnet.

The package program ANSYS, based on the concept of Newton-Raphson method, performs a numerical solution of equation (3.15), and the output data is the value of the magnetic vector potential in every node of the discreatized domain.

3.3.2 Boundary Conditions

The boundary condition is a general term that involves the constraints throughout the model. The boundary conditions can specify the boundary of the model or it can be applied to nodes and elements in the model. In this study, the full geometry of the machine is described in the finite element program since the electromagnetic torque is necessary to be calculated. Dirichlet homogeneous boundary conditions, which are defined as a value of unknown parameter (dof) at the boundries, are chosen as zero for magnetic potential at the center of the rotor and outer part of the stator back core.

Two nodes are defined at the same location on the path circulating at center of the air gap between stator and rotor pole faces. For instance, the node 1051 and node 1385 are located on same point. This is required because the rotation of the rotor is described according to the specification of the position between two independent parts. One of them is stationary and the other is moving. Therefore these two nodes must be communicated during the period of solution, and the constraint equation is defined between these nodes. Otherwise, for every position of the rotor, the air gap should be described with a new geometry and the nodes should be defined again.

3.4 The No-Load and On-Load Magnetic Field Distributions

The equation (3.15) is used for the analysis of no-load conditions. If $\bar{J}$ is defined as zero, it corresponds to no-load case. $\bar{J}$ can be defined for any armature current corresponding to a particular load .

The analysis of permanent magnet variable reluctance motor has been done in no-load and rated load conditions. In the no-load simulation, there is no current at stator winding. However the simulation results of the on-load are obtained under rated current of 2 amperes. Some parameters of the machine such as torques, self, and mutual inductances are calculated under load conditions. The induced back emf and reluctance torque are calculated from no-load.

After the equation (3.15) is solved and nodal values of magnetic vector potentials are obtained, the flux lines which are drawn for both cases are given in figure 3.6. The flux lines are created by drawing the lines between the nodes having the same magnetic vector potentials. The different values of vector potential are indicated with different colors on the figures.

The most significant difference between the Figure 3.6-a and Figure 3.6-b is the flux distribution in the main pole corresponding to phase A . In no load condition there is a symmetry. The flux enters the pole shoes from one end and goes through it until it goes out of the other end, thus completing the loop. In load condition, the flux which enters the pole shoes of the phase A forms a closed loop by going through the main pole, the back core and the auxiliary pole.

The flux density distribution in the motor at no load is shown in figure 3.7. The magnitude of flux density is given with color codes. The direction of flux is given with the direction of the vector. The maximum value of flux density is 1.31 T at the boundary of N and S type magnets during no-load case.

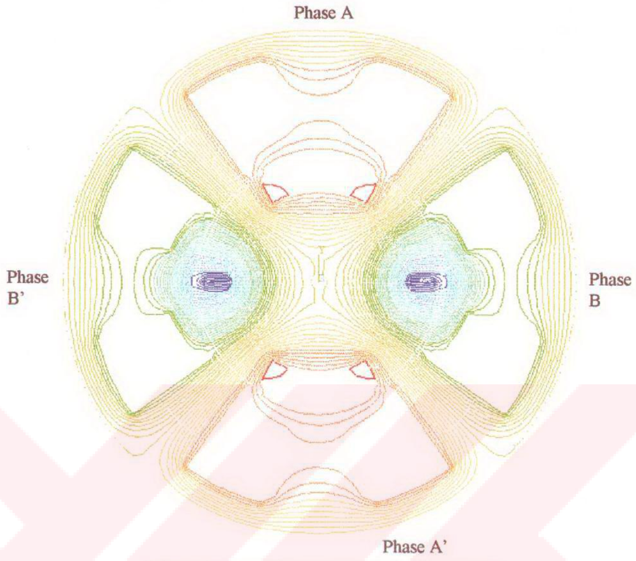
Phase A
Phase B'
Phase B
Phase A'

Figure 3.6-a) Flux line graphic at no load

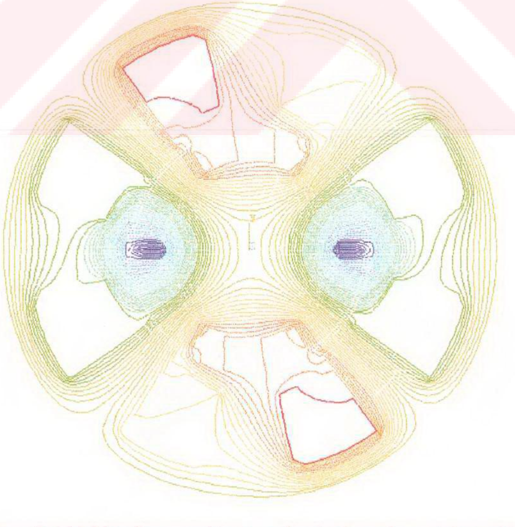

Figure 3.6-b) Flux line graphic at on load when phase A is excited

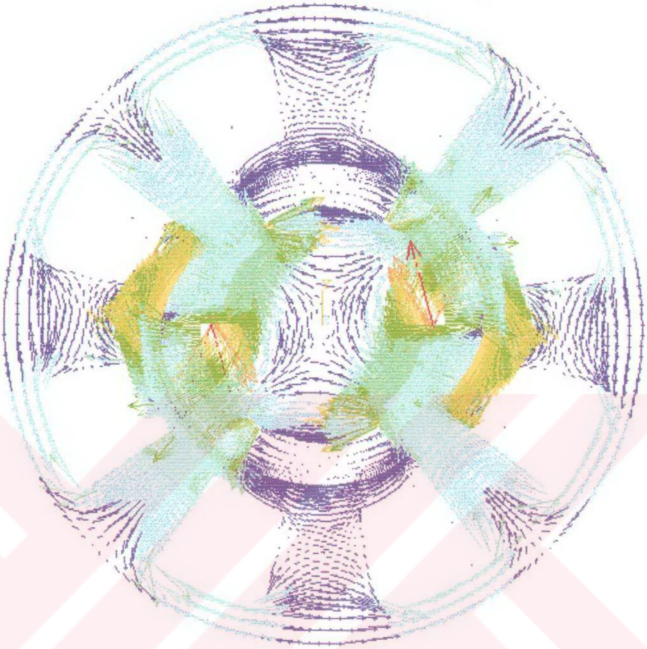

Figure 3.7 Flux density graphic at no load

This numerical values of flux densities corresponding to color codes are given in table 3.2.

Table 3.2 color code of flux density graphic at no load

Color code	Numerical value (T)
Dark Blue	0.701E-4
Light Blue	0.163925
Very Light Blue	0.32778
Light Green	0.491635
Dark Green	0.655491

Light Yellow	0.819346
Dark Yellow	0.983201
Orange	1.147
Red	1.311

The flux density distribution of the motor under load is given in figure 3.8. The numerical values of the flux densities corresponding to color codes under load condition are given in table 3.3. The symmetry of flux density take places after 180 degrees in either case as it is clearly observed from figure 3.7 and figure 3.8.

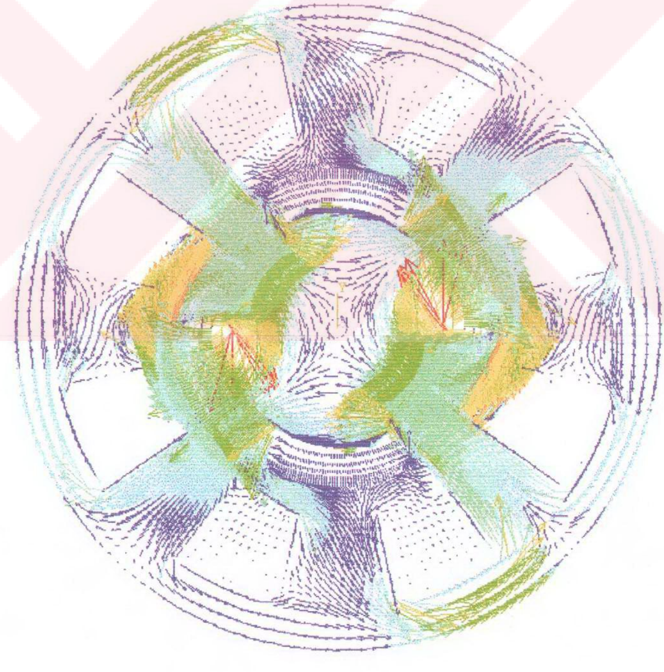

Figure 3.8 Flux density graphic at on load

Table 3.3 color code of flux density graphic at on load

Color code	Numerical value (T)
Dark Blue	0.795E-4
Light Blue	0.150549
Very Light Blue	0.301019
Light Green	0.451489
Dark Green	0.601959
Light Yellow	0.752429
Dark Yellow	0.902899
Orange	1.053
Red	1.204

3.5 Torque Calculation

The static torque as a function of rotor position is obtained by using the FEM. This calculation has been carried out after the discreatization of air gap in four layers of elements and subdividing these layers into two parts (each part has two layers). The elements, which belong to the rotor, are containing the inner part of the air gap and they are rotated with the rotor. The element in two layer, that belong to the stator, are kept stationary with the stator core. The rotating elements are called as 'moving band'. The constraint equations mentioned in section 3.3.2 are deleted before starting the rotation. Then the stator and rotor are observed as two independent sections. The mass rotor is rotated with the two layers of element in the air gap 2 degrees in every step. At this location of the rotor, the constraint equations linking the nodes in the stator zone and rotor zone are defined again. Finally the torque calculation is performed under these constraints.

The electromagnetic torque can be calculated by using one of the following methods:

- Maxwell Stress Tensor Method
- Coenergy Derivation Method
- Coulumb's Virtual Work Method
- Arkkio's Method
- Flux-Current (magnetizing current) Method

[N. Sadowski & Y. Lefevre & M. L. Mazenc & J. Cros 1992], [J. Trowski K. Komeza & A. Pelikant & S. Wiak &M. Rizzo & A. Savani 1992], [L. Petkovska & M. Cundev & G. Cvetkovski 1995], [M. Marinescu & N. Marinescu 1988], [S. Salon & S. Bhatia & D. Burow 1997] show that the torque values obtained by these methods are very close if the rotation step is equal to the discretization step and a very fine mesh is done. In this study, Maxwell Stress Tensor method is chosen for the torque estimation under on-load conditions. Both Maxwell Stress Tensor and Coenergy Derivation Method, are used for the calculation of the reluctance torque. These two different methods were selected here because the torque computation takes less time in these two methods [L. Petkovska & M. Cundev & G. Cvetkovski 1995]. In addition, the package program used in this study contains the direct commands for using these two methods, however an extra dedicated subroutine can be necessary for the rest of the techniques given above. The detail of these method have been given in the following sections.

3.5.1 Maxwell Stress Tensor Method

Torque is computed from the force which is produced by the Maxwell Stress Tensor over a closed surface's placed in the air-gap enclosing the rotor. The expression for the force on the closed surface S is [M. Moallem & C. M. Ong 1990]

$$\bar{F} = \int_S \tau ds \qquad (3.16)$$

$\bar{\tau}$ Is given by the inner product of the Maxwell stress tensor and the normal $\bar{n}$ to the surface;

$$\bar{\tau} = \bar{n}\left[\overline{BB} - \frac{1}{2}\bar{B}^2\right]\frac{1}{\mu_0} \tag{3.17}$$

By substituting equation (3.17) into equation (3.16);

$$\bar{F} = \frac{1}{\mu_0}\int_S\left[\left(\bar{B}\bar{n}\right)\bar{B} - \frac{1}{2}\bar{B}^2\bar{n}\right]ds \tag{3.18}$$

and the torque can be computed as follows [ANSYS Magnetic user's guide 1993], [Ansys Electromagnetics 1992], [R. Plonsey & E.R. Collin 1961], [N. Sadowski & Y. Lefevre & M. L. Mazenc & J. Cros 1992];

$$\bar{T} = \bar{r}x\bar{F} = \int_S\left[\mu_0(\frac{\bar{B}}{\mu_0}\bar{n})(\bar{r}x\frac{\bar{B}}{\mu_0}) - \frac{\bar{B}^2}{2\mu_0}(\bar{r}x\bar{n})\right]ds \tag{3.19}$$

where $\bar{r}$ is the radius of the cylindrical surface of integration.

3.5.2 Coenergy Derivation Method

The force and torque can be derived from the co-energy of the system. The torque is calculated as a derivative of the magnetic co-energy with respect to the rotation angle θ by maintaining the current constant. That is, ∂W is magnetic coenergy change at a virtual change of rotor position $\partial\theta$ [N. Sadowski & Y. Lefevre & M. L. Mazenc & J. Cros 1992].

$$T = L\left.\frac{\partial W}{\partial\theta}\right|_{i=\mathrm{constant}} \tag{3.20}$$

where L is the rotor length. In the numerical modeling, this derivation is approximated by the difference between two successive calculations.

$$T = L\frac{\left(W_{\theta+\delta} - W_{\theta}\right)}{\delta} \qquad (3.21)$$

where δ represents the displacement.

3.5.3 Calculated Torque Values

3.5.3.1 The Static Torque

The Maxwell Stress Tensor method is used to predict the electromagnetic torque in this work. In the package program, the equation that is used to compute torque was given in equation (3.19). The path which is chosen at the integration is shown in figure 3.9. [Ansys Electromagnetics 1992] The integration path is drawn in the air gap along the center line between the stator and rotor. Then the static torque is calculated at nodes which are located on the path using by the equation (3.19).

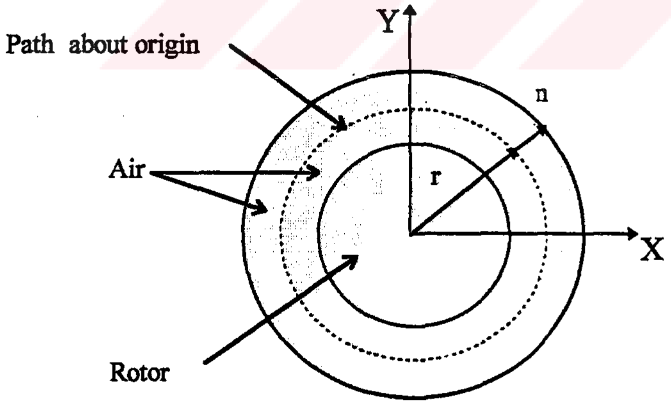

Figure 3.9 The integration path for torque calculation

The static torque is calculated by using each phase winding energized. 2 Amps of dc armature current is applied to phase A as shown in figure 3. 10. The phase B is left open. The static torque at each rotor step is calculated and the result is plotted and given in figure 3.11.

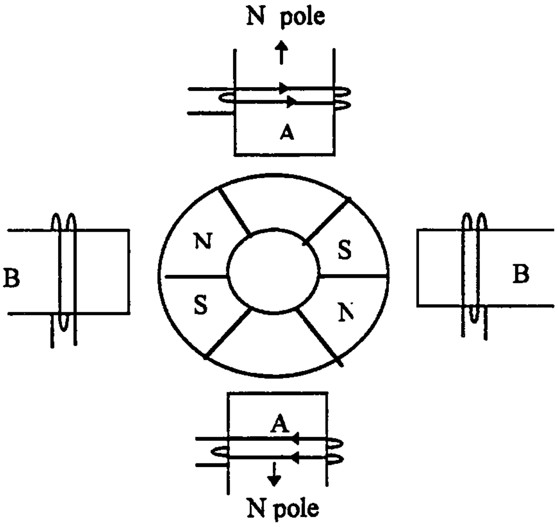

Figure 3.10 The direction of phase A current

The main poles of stator and permanent magnets of rotor are given in figure 3.12 as a distributed form on the axis of space angle. On the stator, each pole occupies 60 degrees of space sperated and between these from each other by 30 degrees of air gap. On the rotor side, the permanent magnets are located over 120 degrees of space sepeared from each other by 60 degrees of air gap. It is obvious ,that the period of air gap reluctance is 180 degrees and hence the symmetry of static torque is created after180 degrees of rotation.

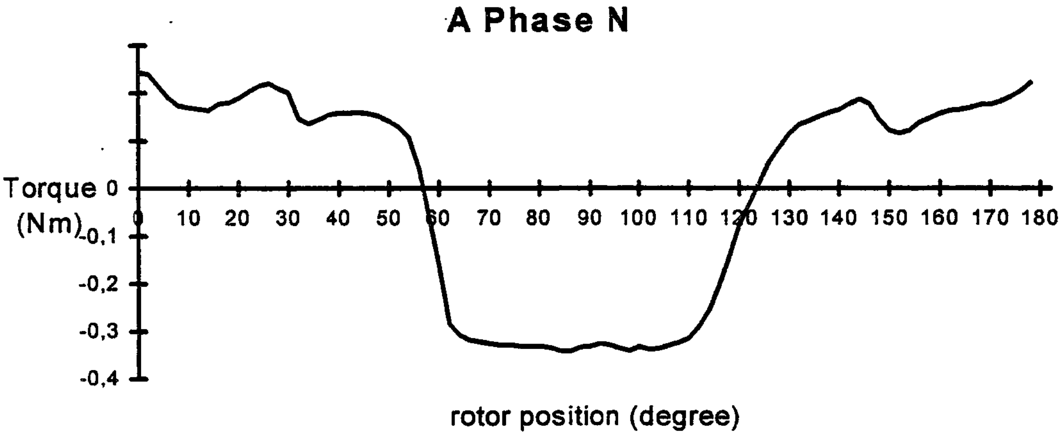

Figure 3.11 The torque graphic when A phase is N pole

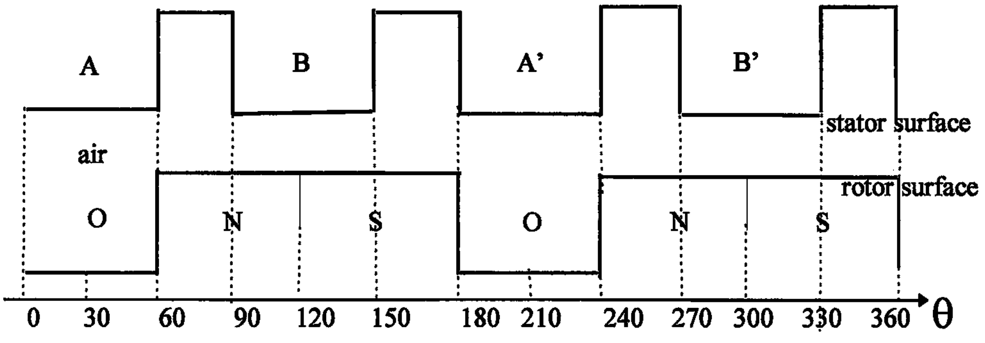
A
B
A'
B'
stator surface
air
rotor surface
O
N
S
O
N
S
0
30
60
90
120
150
180
210
240
270
300
330
360
θ

Figure 3.12 The distribution of the rotor and stator poles

The algorithm used for phase A is repeated for phase B as shown in figure 3.13. The phase B is energized by 2 Amps of the dc current and phase A is left open-circuit. The static torque developed by the machine is depicted in figure 3.14. This graphic has a waveform a 90 degrees phase shift of the figure 3.11.

As it is clear from the figure 3.11 and figure 3.14, the static torque takes some negative values which may create the blocking torques as the rotor is rotating in one direction. Therefore these negative values of the torque are eliminated by disconnecting the related phase winding from the sources.

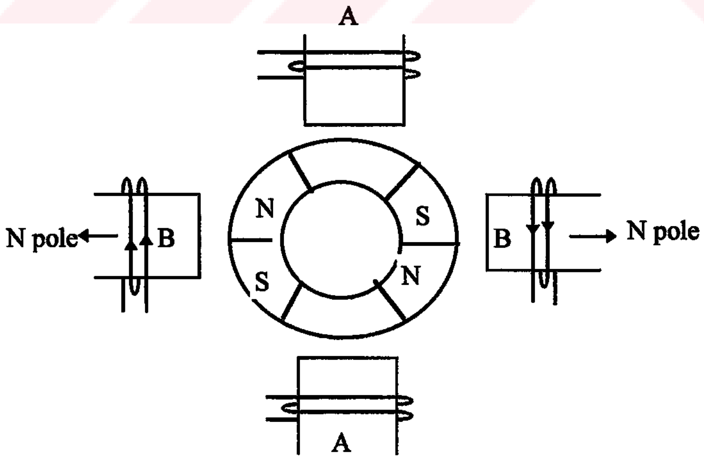
A
N pole
B
N
S
S
N
B
N pole
A

Figure 3.13 The direction of phase B current

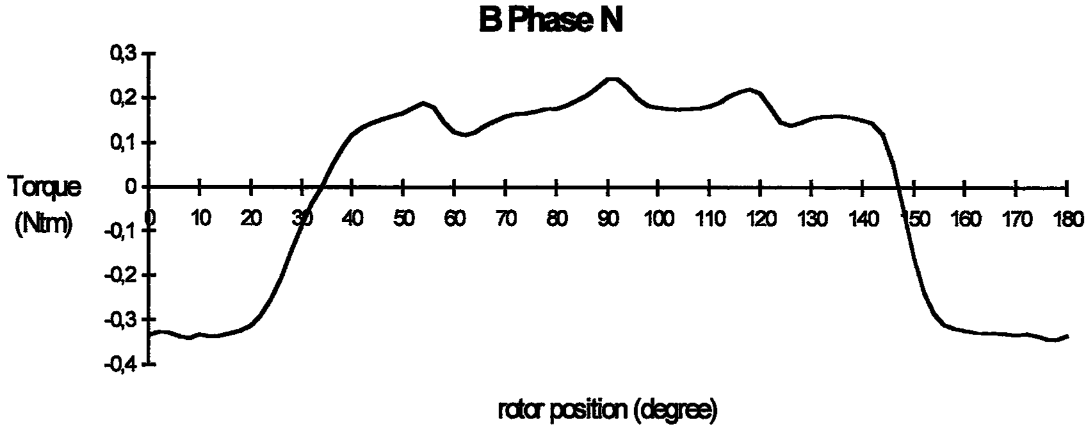

Figure 3.14 The torque graphic when phase B is N pole

The resultant torque-rotor position curve given in figure 3.15 is obtained from the combination of the positive torques developed by the phase A and phase B.

The average value of static torque in figure 3.15 is positive at every position of rotor. The possibility of developing the average static torque which could be more than that value presented in figure 3.15 has been investigated.

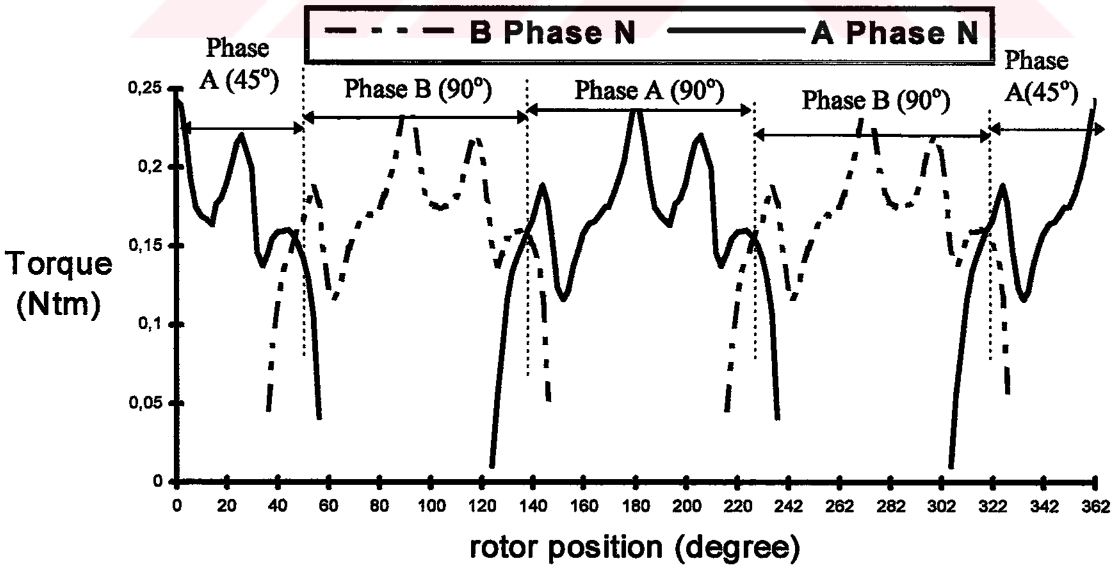

Figure 3.15 The static torque developed by machine

When the direction of the current in figure 3.10 and figure 3.13 is changed to opposite, the S pole is created. The torque graphics which are calculated in this condition are given in figure 3.16 and figure 3.17.

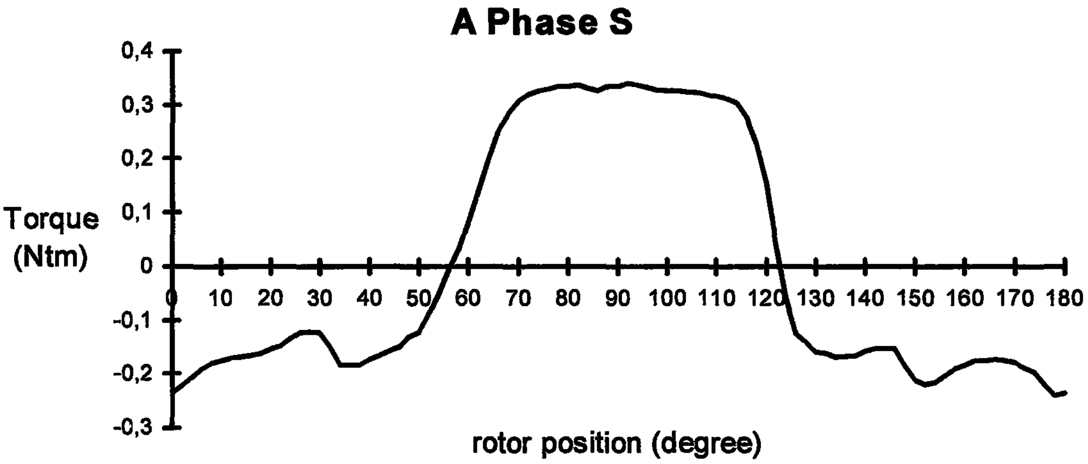

Figure 3.16 The torque graphic when the phase A is S pole

If the positive parts of both graphics are combined as it is presented in figure 3.18, it is observed that there is no any torque developed for some rotor positions. For instance, neither A nor B are excited between 30 and 60 degrees. Therefore, the phases will be exited during 90 degrees by the drive circuit such that the torque developed by the machine exhibits the envolope given in figure 3.15.

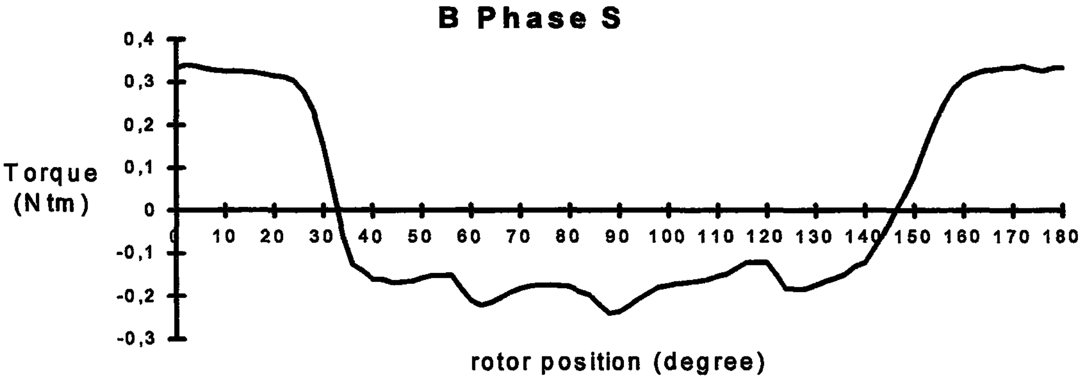

Figure 3.17 The torque graphic when phase B is S pole

Figure 3.17 The torque graphics when phase B is S pole

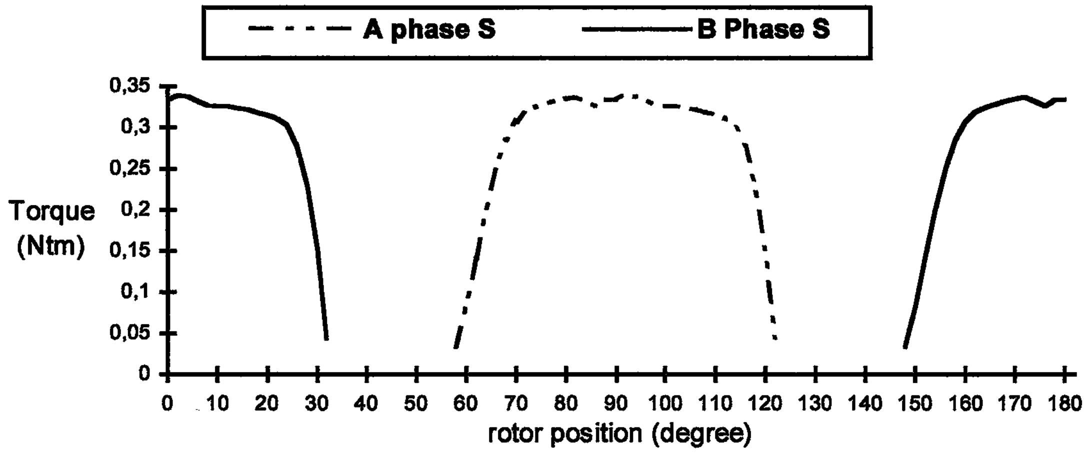

Figure 3.18 The static torque graphic

3.5.3.2 The Reluctance Torque

The torque developed by the machine, while the stator windings are disconnected from the source, has a zero average value over the period of 180 degrees. The effect of this torque can be observed during the transition periods even if its average value is zero. This effect is considered in the equation derived for the electromagnetic torque in the next chapter. In this section, the reluctance torque is calculated as a function of rotor position using the finite element technique. Both are Maxwell Stress Tensor Method and Coenergy Derivation Method are used. The peak value of reluctance torque is around 0.05Ntm which is 2 percent of the static torque. Since the period of the reluctance is 180 degrees, the reluctance torque has the same period. [S. Clenet & Y. Lefevre & N. Sadowski & S. Astier & M. J. Mazenc 1993], [M. Moallem & C. M. Ong 1990], [M. Wing & J. F. Gieras 1992], [L. Petkovska, M.Cundev & G. Cvetkovski 1995]

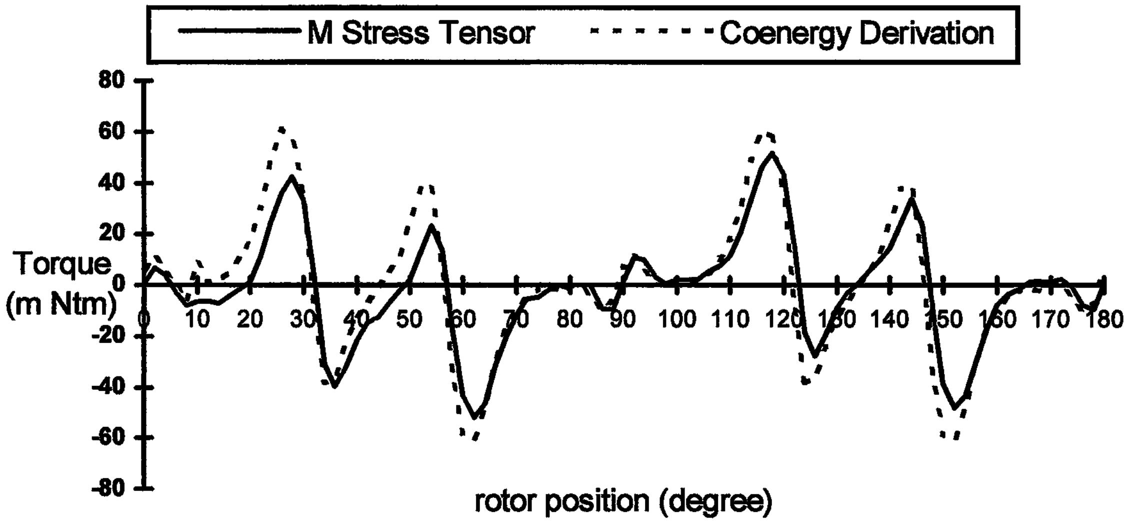

Figure 3. 19 The reluctance torque

3. 6 Computation of Machine Parameters

The aim of this part is to estimate the machine parameters that will be used in the non-linear model representing the permanent magnet variable reluctance motor and its drive circuitry. These parameters are the self and mutual inductances of the windings, induced back emf in the armature windings and the winding resistances. The latter one is predicted by using an analytical expression as the others are obtained from the finite element analysis. As it will be seen later, the induced emf waveforms are also necessary to complete the modeling. The detail of the estimation will be presented in following sections.

3.6.1 Armature Induced EMF Waveform

The field analysis in no-load case is used to calculate the back emfs in the stator windings. After the solution of equation (2.8) governing the magnetic vector potential distribution in the machine is obtained, the flux linkage is computed. The relation between the back emf in the coil and the flux linkage is given in equations (3.22) and (3.23).

$$e(\theta) = -N.\frac{d\phi}{dt} = -N.\frac{\partial\phi}{\partial\theta}.\frac{\partial\theta}{\partial t} = -N.\frac{\Delta\phi}{\Delta\theta}.w = -N.\frac{\left(\phi^{(k)} - \phi^{(k-1)}\right)}{\Delta\theta}.w \tag{3.22}$$

where Δθ is the displacement of the rotor from "k-1" to "k" position, N is the number of turn per pole, and w is the velocity of the moving rotor. In this calculation Δθ is to equal 2 degree. $\phi^{(k)}$ is the linkage magnetic flux computed as; [M. A. Alhamadi & N. A. Demerdash 1991], [T. W. Nehl & N. A. O. Demerdash 1992], [T. J. E. Miller & R. Rabinovici 1994]

$$\phi^{(k)} = \left(A_{n1}^{(k)} - A_{n2}^{(k)}\right).l \tag{3.23}$$

where A_{n1}, A_{n2} are the MVP on the n_1 , n_2 nodes. n_1 , n_2 which are shown in figure 3.20 are the numbers of the nodes placed on the slip surface which correspond to the axis of the coil and l is the length of the armature core. [O. Craiu & C. Raduti & N.Dan 1995]

The graphics of MVP difference between n_1 and n_2 nodes at the k-th step for phase A and B (that is flux linkage per length) are given in figure 3.21 and figure 3.22 respectively.

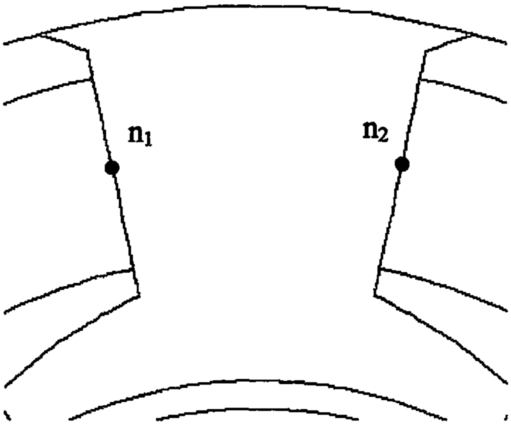

Figure 3.20 The nodes placed on border line between main pole and coil area

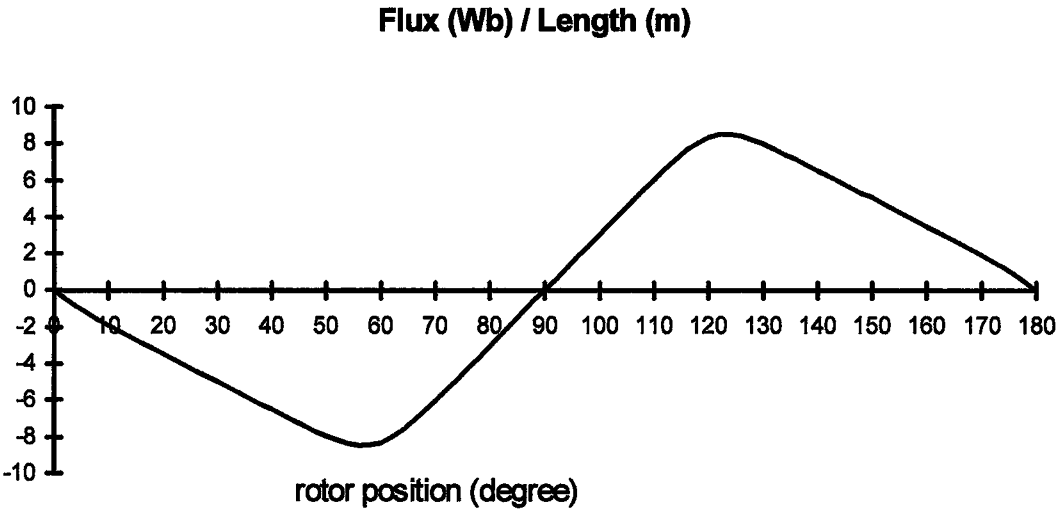

Figure 3.21 The MVP difference of phase A

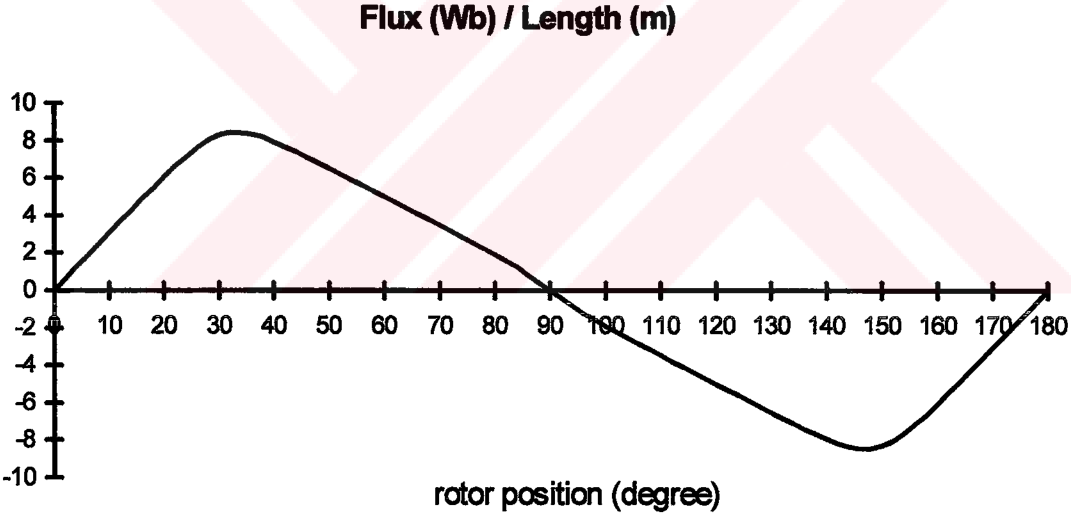

Figure 3.22 The MVP difference of phase B

The MVP difference of phase B has a phase shift of 90 degrees from the MVP difference of phase A. Although the zero-crossing point is at the 90 degrees, these graphics are not an exact sinusoidal waveform. The maximum value of MVP is taking place at 30 degrees instead of 45 degrees. The reason of this that the nonsymmetrical location of the permanent magnets on the rotor periphery [A. Kusko & S. M. Peeran 1987].

The induced coil voltages per angular speed for phase A and B are calculated by using the equation (3.22) and the distribution of MVPs. The results are plotted as a function of rotor position as being shown in figure 3.23 and figure 3.24.

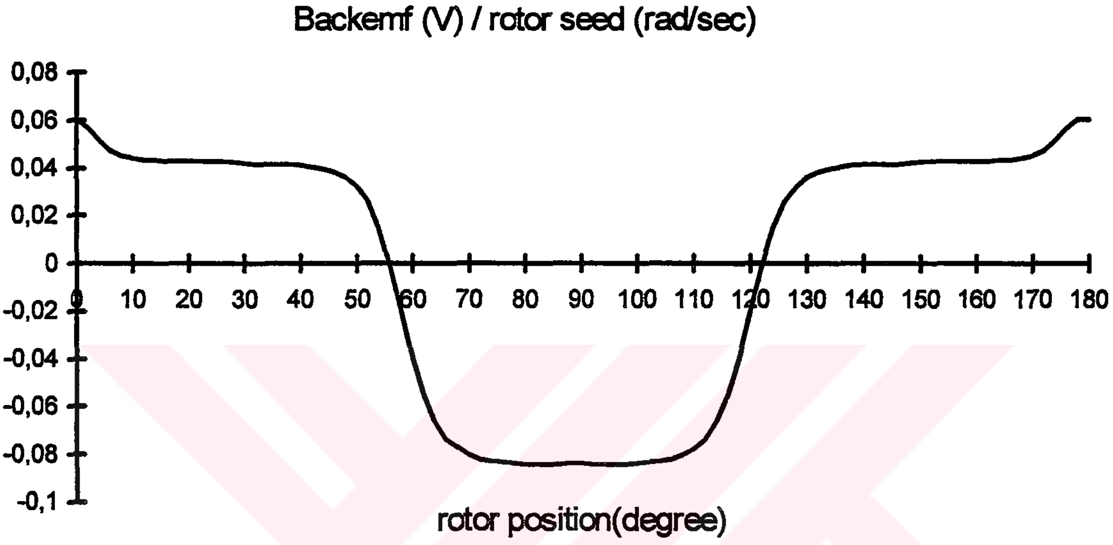

Figure 3.23 Computed back emf for phase A

The phase delay between the back emfs on phase A and phase B windings is 90 degrees. But the positive and negative peak values are not equal to each other, as it is expected from the observation made on the waveform of MVP. The reason of this that the positive and the negative slopes over the waveshapes of MVPs are not equal to each other. In other words, if the mvp graphic of phase A is considered, it has a negative slope between 0 and 60 degrees and positive slope between 60° and 120°. The negative slope is two times of the positive slope. Hence the positive level of back emf is half of the negative level as it can be observed from figure 3.23 and figure 3.24. The same observations can be concluded to phase B .

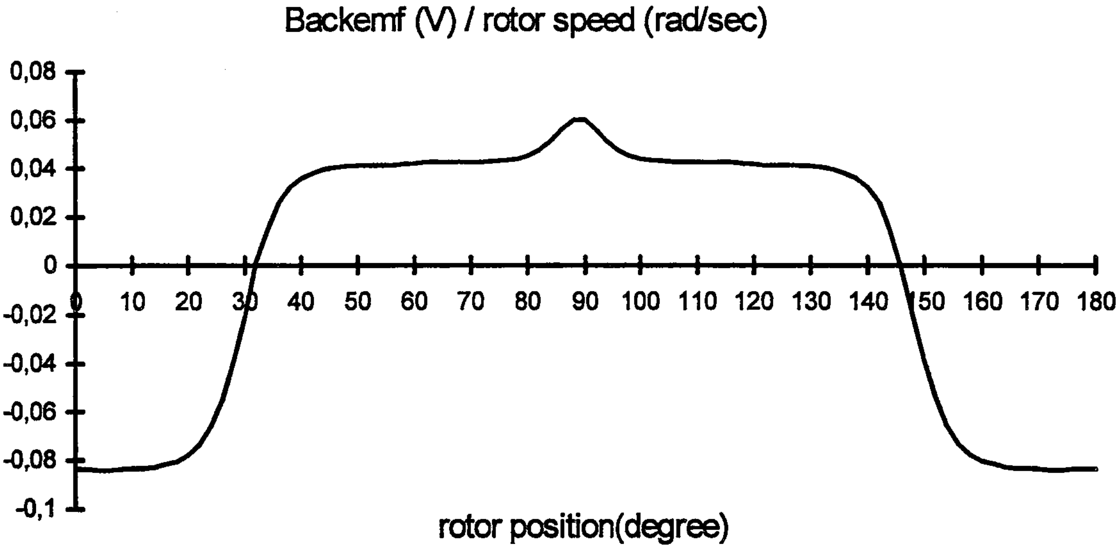

Figure 3.24 Computed back emf for phase B

3.6.2 Armature Winding Inductance

Two different methods are used to calculate the inductance in this study. Both methods are using the stored energy in the machine. In the first method, the coercive force of the magnet is removed, thus a permanent magnet is defined only with its relative permeability. In the other method, energy and current perturbation is applied to calculate the self inductances, while the permanent magnets are being preserved in the model. The current perturbation technique is varified experimentally [M. A. Alhamadi & N. A. O. Demerdash 1994]. These two different methods are explained in detail in the following sections.

3.6.2.1 Calculation of Inductances as Removing Permanent Magnet

The armature is considered as a four-winding system, which are magnetically coupled and electrically isolated, since there are four main poles having four concentrated windings.

The magnetic property of the permanent magnet is removed. The coercive force of magnet is not given, only the relative permeability is defined on the material. The rated load current is applied to phase A or B and the total stored energy in the motor is expressed in terms of current and flux linkages by using the following formulation.

$$W_T = \lambda_1 . i_1 + \lambda_2 . i_2 + \lambda_3 . i_3 + \lambda_4 . i_4 \qquad (3.24)$$

where i_1 and i_2 are coil currents. λ_1, λ_2, λ_3 and λ_4 are also flux linkages which belong to these coils. Flux linkage can be written in terms of current and inductance an given in equation (3.25) using the straight line representing the λ-i curve around the operating current.

$$\begin{aligned} \lambda_1 &= i_1 . L_{11} + i_2 . L_{12} + i_3 . L_{13} + i_4 . L_{14} \\ \lambda_2 &= i_1 . L_{21} + i_2 . L_{22} + i_3 . L_{23} + i_4 . L_{24} \\ \lambda_3 &= i_1 . L_{31} + i_2 . L_{32} + i_3 . L_{33} + i_4 . L_{34} \\ \lambda_4 &= i_1 . L_{41} + i_2 . L_{42} + i_3 . L_{43} + i_4 . L_{44} \end{aligned} \qquad (3.25)$$

where L_{11}, L_{22}, L_{33}, and L_{44} are the self and L_{12}, L_{13}, L_{14}, L_{21}, ..., L_{43} are the mutual inductances. If the equation (3.25) is substituted into equation (3.24) then the total energy can be written in terms of currents and inductances;

$$\begin{aligned} W_T = {} & i_1^2 . L_{11} + i_2^2 . L_{22} + i_3^2 . L_{33} + i_4^2 . L_{44} + 2.i_1.i_2.L_{12} + \\ & 2.i_1.i_3.L_{13} + 2.i_1.i_4.L_{14} + 2.i_2.i_3.L_{23} + 2.i_2.i_4.L_{24} + 2.i_3.i_4.L_{34} \end{aligned} \qquad (3.26)$$

The coenergy is equal to half of that total energy since λ-i curve is linearized around the operating point, so [Ansys Magnetics User's Guide 1993], [A. E. Fiztgerald, C. Kingsley, S. D. Umans 1992];

$$W=\frac{1}{2}\left(i_1^2.L_{11}+i_2^2.L_{22}+i_3^2.L_{33}+i_4^2.L_{44}\right)+i_1.i_2.L_{12}+$$

$$i_1.i_3.L_{13}+i_1.i_4.L_{14}+i_2.i_3.L_{23}+i_2.i_4.L_{24}+i_3.i_4.L_{34} \quad (3.27)$$

If the only phase A is energized by the current of i_1 Amps then the equation (3.27) yields (3.28)

$$W=\frac{1}{2}.i_1^2.L_{11} \quad (i_2=i_3=i_4=0) \qquad \text{and} \qquad L_{11}=\frac{2.W}{i_1^2}$$

$$(3.28)$$

$$W=\frac{1}{2}.i_3^2.L_{33} \quad (i_1=i_2=i_4=0) \qquad \text{and} \qquad L_{33}=\frac{2.W}{i_3^2}$$

From the equation (3.28), L_{11} and L_{33} can be estimated.

If the same logic is applied for the self inductance of the phase B, the following equalities can be written.

$$W=\frac{1}{2}.i_2^2.L_{22} \quad (i_1=i_3=i_4=0) \qquad \text{and} \qquad L_{22}=\frac{2.W}{i_2^2}$$

$$(3.29)$$

$$W=\frac{1}{2}.i_4^2.L_{44} \quad (i_1=i_2=i_3=0) \qquad \text{and} \qquad L_{44}=\frac{2.W}{i_4^2}$$

In equation (3.28) and (3.29), the coenergy is computed by FEM at the rated stator current applied to the winding. Therefore, the coenergy in equation (3.28) or (3.29) is the area under the linear curve in figure 3.25. The non-linear magnetization

magnetization curve is linearilized around the operating point, hence, the slope of this line is the inductance value in equations equation (3.28) and (3.29).

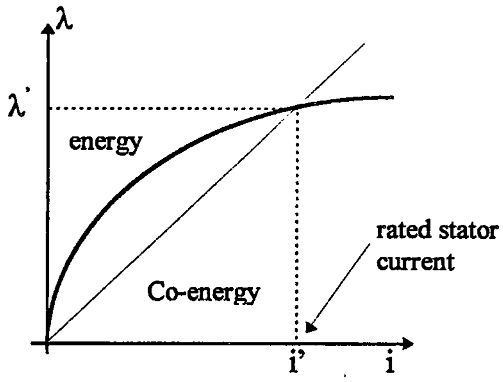

Figure 3.25 Graphical interpretation of energy and coenergy

In the computation of mutual inductance, the operation is done by two steps. In the first step, the phase A and B currents are applied in the same polarity ($i_1=i_2$) then the co-energy W_1 is obtained. In the second step, the phase A current is kept in the original polarity as the phase B current is applied in reverse polarity, the energy W_2 is obtained. Then,

$$W_1 = \frac{1}{2}.i_1^2.L_{11} + i_1.i_2.L_{12} + \frac{1}{2}.i_2^2.L_{22}$$

$$W_2 = \frac{1}{2}.i_1^2.L_{11} - i_1.i_2.L_{12} + \frac{1}{2}.i_2^2.L_{22} \tag{3.30}$$

If these energies are subtracted from each other, then the mutual inductance can be calculated as follows ;

$$W_1 - W_2 = 2.i_1.i_2.L_{12} \qquad (i_3=i_4=0 \text{ Amps}) \tag{3.31}$$

$$L_{12} = \frac{W_1 - W_2}{2.i_1.i_2} \tag{3.32}$$

In the same manner, the following equations can be obtained easily for the other windings inductances:

$$L_{13} = \frac{W_1 - W_2}{2.i_1.i_3}$$

$$L_{14} = \frac{W_1 - W_2}{2.i_1.i_4}$$

$$L_{23} = \frac{W_1 - W_2}{2.i_2.i_3} \qquad (3.33)$$

$$L_{24} = \frac{W_1 - W_2}{2.i_2.i_4}$$

$$L_{34} = \frac{W_1 - W_2}{2.i_3.i_4}$$

The variation of inductances as a function of rotor position are obtained using this method. The inductance value is calculated at a fixed rotor position. The inductances displayed in figure 3.26 - figure 3.29 are obtained using the data collected from 18 different rotor positions taking place from 0 to 180 degrees.

The values of L_{11} and L_{22} show fluctuation around the approximate average level of 5.42 mH. There is a phase delay of 90 degree between L_{11} and L_{22}. The value of L_{11} is minimum at 0 degree and maximum at 90 degree. Since the relative permeability of the permanent magnets is not equal to unity, the flux distribution takes different values, so do the inductances.

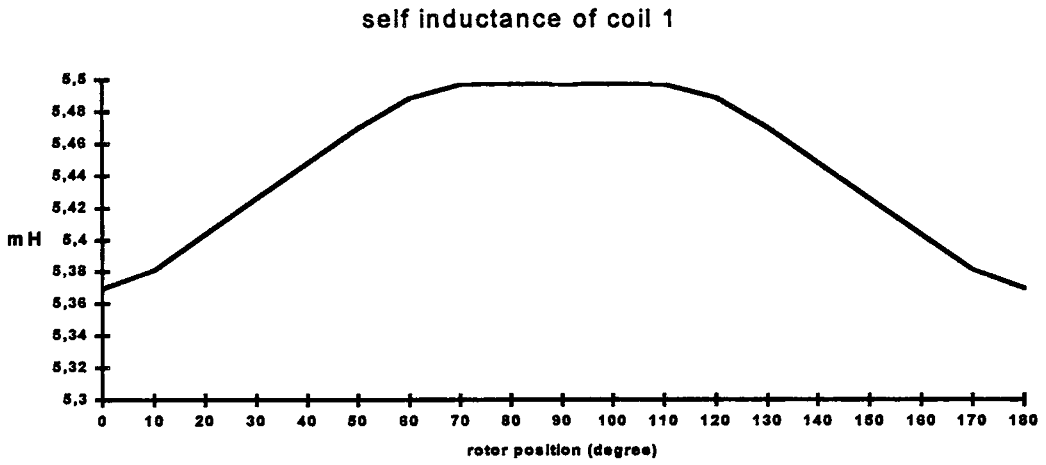

Figure 3.26 Self inductance of phase A

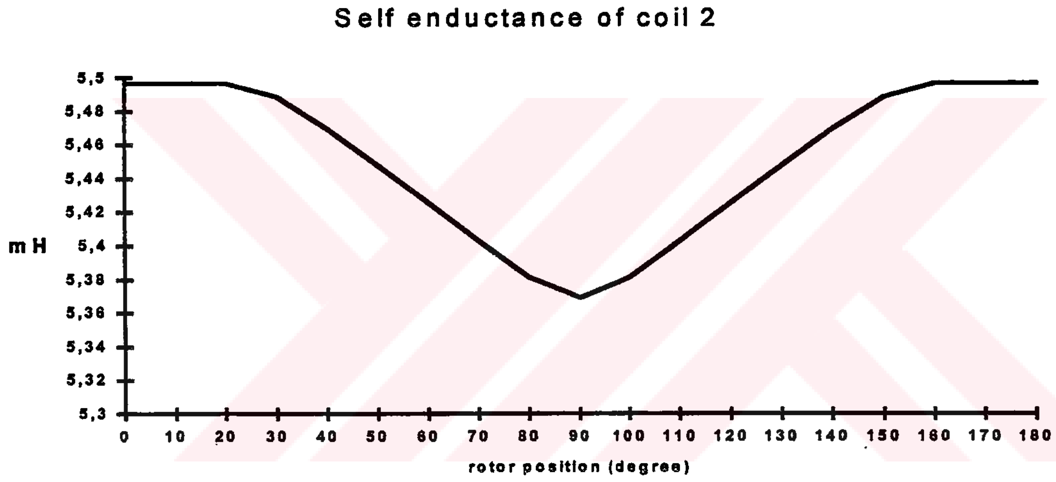

Figure 3.27 Self inductance of phase B

After the rotor rotates 90 degrees, the phase B takes place at the location that was occupied by phase A. That is the reason why the inductance of phase B lags the inductance of phase A by 90 degrees.

Self inductances are obtained as $L_{11}(\theta)=L_{33}(\theta)$ and $L_{22}(\theta)=L_{44}(\theta)$ as shown in figure 3.28 and 3.29.

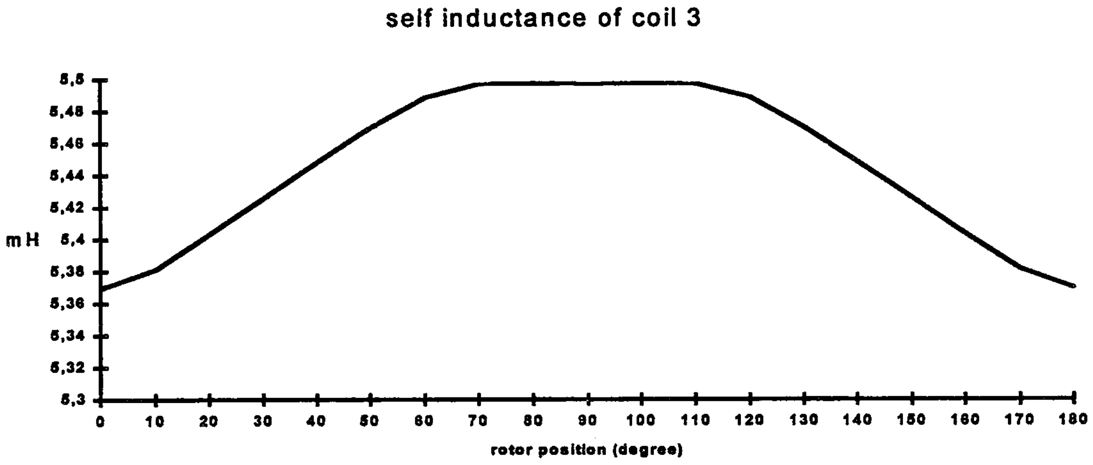

Figure 3.28 Self inductance of phase A'

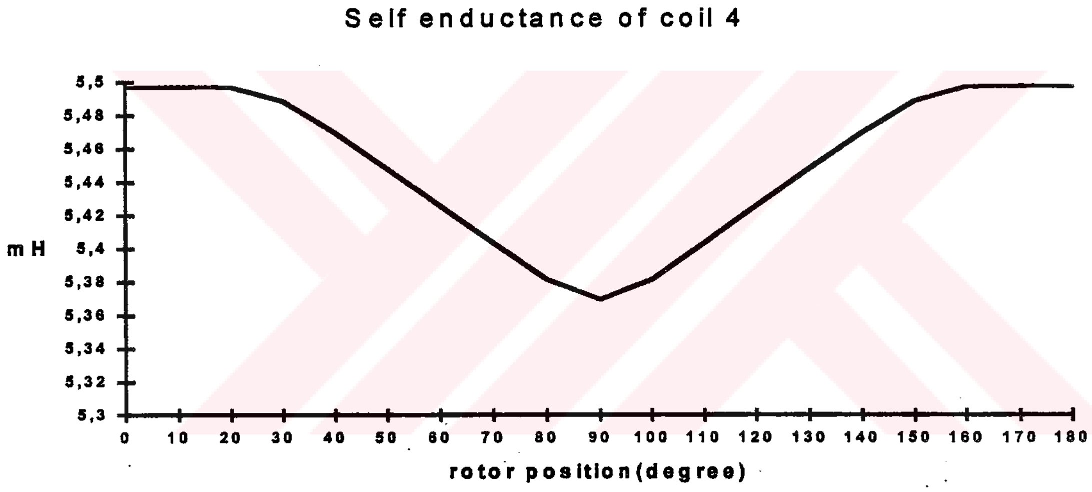

Figure 3.29 Self inductance of phase B'

Similarly, the mutual inductances $L_{12}(\theta)$, $L_{14}(\theta)$,$L_{32}(\theta)$, and $L_{34}(\theta)$ are identical. Therefore, the only $L_{12}(\theta)$ is given in figure 3.30.

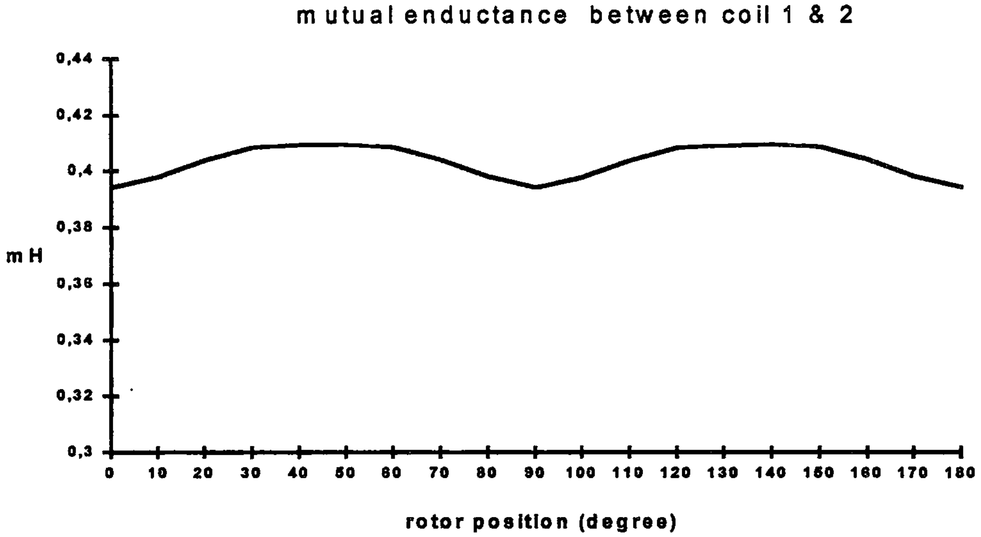

Figure 3.30 Mutual inductance between phase A and phase B

The mutual inductance between the winding A and A' is calculated as L_{13} and the mutual inductance between the winding B and B' is calculated as L_{24} as given in figure 3.31 and 3.32.

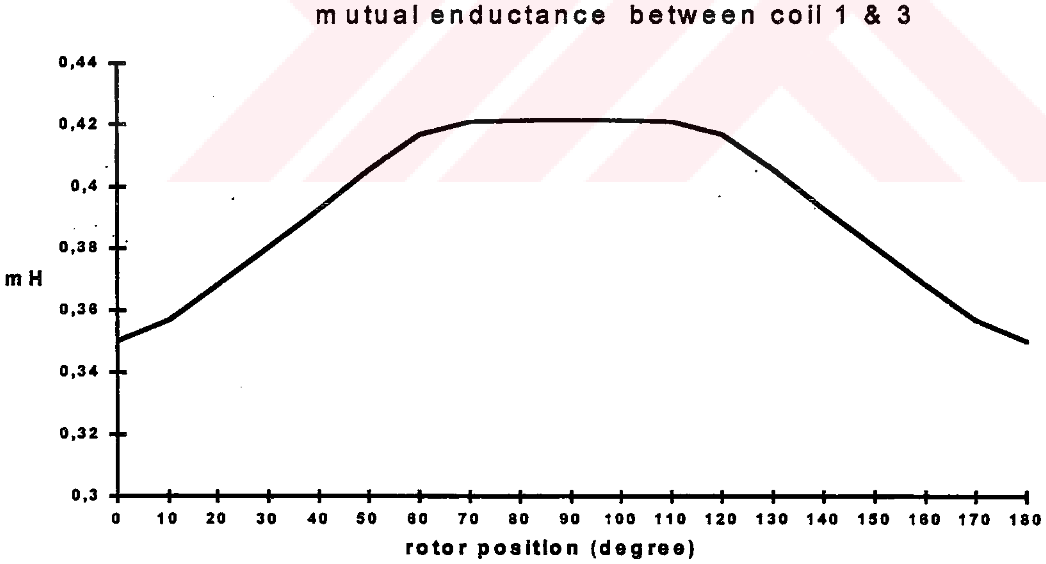

Figure 3.31 Mutual inductance between A and A'

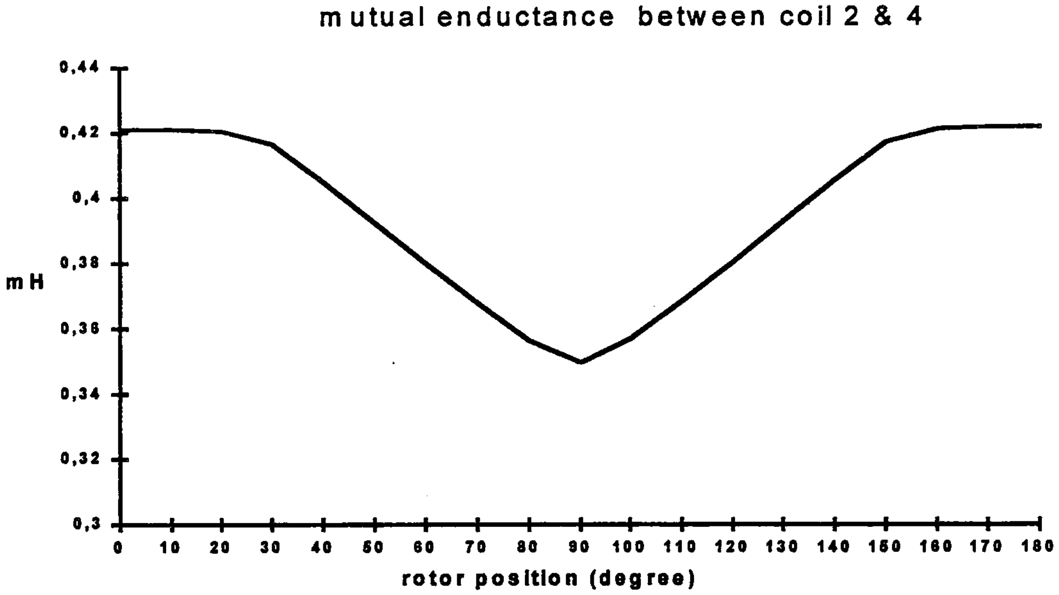

Figure 3.32 Mutual inductance between B and B'

The phase delay between $L_{13}(\theta)$ and $L_{24}(\theta)$ is 90 degrees as being similar to self inductances.

3.6.2.2 Calculation of Inductances with Energy and Current Perturbation

This method is based on the perturbation of the magnetic field distribution inside the machine for a given set of winding currents by means of small current increments.

The electrical behavior of any electromechanical device can be modeled as a set of n coupled winding. The voltage at the terminals of the j-th winding can be written as follow [N. A. Demerdash & F. A. Fouad & T. W. Nehl 1982], [N. A. Demerdash & J. M. Hijazi & A. A. Arkadan 1988], [T. W. Nehl & N. A. O. Demerdash 1992]:

$$V_J = R_J . i_J + \frac{\partial}{\partial t} \lambda_J \qquad (3.34)$$

This equation can be written in terms of the current applied to j-th winding

This equation can be written in terms of the current applied to j- th winding

$$V_J = R_J.i_J + \frac{\partial}{\partial i_1}\lambda_J.\frac{d i_1}{d t} + \frac{\partial}{\partial i_2}\lambda_J.\frac{d i_2}{d t} + \ldots$$
$$+ \frac{\partial}{\partial i_n}\lambda_J.\frac{d i_n}{d t} + \frac{\partial}{\partial \theta}\lambda_J.\frac{d \theta}{d t} \qquad (3.35)$$

The first term of this equation represents the ohmic voltage drop in the j-th coil. The final term is the rotational voltage due to relative motion between the windings and it is dropped because of rotor position is fixed at operating point. The other terms in the equation are transformer voltages produced by time variations in the current vector. These terms can be rewritten as partial derivation - the derivative of flux linkage with respect to current and the derivative of current with respect to time-. Equation (3.35) can be written again as follows:

$$V_J = R_J.i_J + \frac{\partial \lambda_j}{\partial i_1}.\frac{d i_1}{d t} + \frac{\partial \lambda_j}{\partial i_2}.\frac{d i_2}{d t} + \ldots + \frac{\partial \lambda_j}{\partial i_n}.\frac{d i_n}{d t} \qquad (3.36)$$

This type of coefficient is known as differential inductance, and is defined as follows for the mutuals between the j- th and k-th in windings:

$$L_{jk} = \frac{\partial \lambda_{jk}}{\partial i_k} = \frac{\partial \lambda_{kj}}{\partial i_k} = L_{kj} \qquad (3.37)$$

Similarly, for the j- th self terms:

$$L_{jj} = \frac{\partial \lambda_{jj}}{\partial i_j} \qquad (3.38)$$

The instantaneous terminal power of the j-th winding may be obtained by multiplying equation (3.36) with the coil current, [T. W: Nehl & F. A: Fouad & N. A. Demerdash 1982], [M. A. Alhamadi & N. A. Demerdash 1994],

$$P_J = V_J . I_J = R_J . i_J^2 + i_J . L_{J1} . \frac{di_1}{dt} + i_J . L_{J2} . \frac{di_2}{dt} + ... + i_J . L_{Jn} . \frac{di_n}{dt} \tag{3.39}$$

The first term in this equation, represents the instantaneous power dissipated in the j-th coil. The remaining terms represent the instantaneous magnetic energy storage of the j- th winding . That is:

$$W_J = \sum_{k=1}^{n} \int_{i_k(0)}^{i_k(t)} \left(L_{Jk} . i_J \right) . di_k \tag{3.40}$$

Therefore, the total energy stored in a system of n coupled windings can be written as follow:

$$W = \sum_{J=1}^{n} W_J = \sum_{J=1}^{n} \left(\sum_{k=1}^{n} \int_{i_k(0)}^{i_k(t)} \left(L_{Jk} . i_J \right) . di_k \right) \tag{3.41}$$

The n currents are disturbed increment at so small range, the inductance can be assumed to remain constant. Therefore, it can be mentioned from the corresponding incremental change, ΔW, in the total energy W.

$$\Delta W = \sum_{J=1}^{n} \left(\sum_{k=1}^{n} L_{Jk} . \int_{i_k}^{i_k + \Delta i_k} i_J . di_k \right) \tag{3.42}$$

In reference [N. A: Demerdash & F. A. Fouad & T. W. Nehl 1982] the theory of the perturbed excitation currents is given and in reference [T.W. Nehl & F. A. Fouad &N. A. Demerdash 1982], [N. A. Demerdash & J. M. Hijazi & A. A Arkadan 1988] it was shown that the self and mutual inductance terms of the various n windings can be expressed as the partial derivatives of the stored energy with respect to various winding current perturbations as follows:

$$L_{JJ} = \frac{\partial^2 W}{\partial(\Delta i_J)^2} \qquad (3.43)$$

and

$$L_{Jk} = L_{kJ} = \frac{\partial^2 W}{\partial(\Delta i_J).\partial(\Delta i_k)} \qquad (3.44)$$

These derivatives can be expanded around a 'quiescent' magnetic field solution obtained for a given set of winding currents in terms of various current perturbation $\pm\Delta i_j$ and $\pm\Delta i_k$ in the j-th and k-th windings and the change in the stored energy.

$$L_{JJ} \cong \frac{\left[W(i_J - \Delta i_J) - 2.W(i_J) + W(i_J + \Delta i_J)\right]}{(\Delta i_J)^2} \qquad (3.45)$$

and

$$L_{Jk} \cong \left\{W(i_J + \Delta i_J, i_k + \Delta i_{Jk}) - W(i_J - \Delta i_J, i_k + \Delta i_{Jk})\right.$$

$$\left. - W(i_J + \Delta i_J, i_k - \Delta i_{Jk}) + W(i_J + \Delta i_J, i_k + \Delta i_{Jk})\right\} / (4.\Delta i_J.\Delta i_k)$$

$$(3.46)$$

When the equation (3.45) and (3.46) are used to compute the inductances a straight line between the origin and operating point is still employed to replace the non linear magnetization characteristic of the magnetic circuit. As it can be observed from figure 3.33, a perturbation is applied on the operating current i_j at the amount of Δi_j.

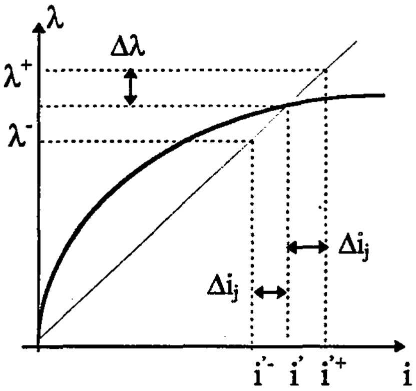

Figure 3.33 perturbation of excitation current

This computation is carried out at different rotor positions, which cover the 180 electrical degree cycle. So, the inductances are obtained as a functions of the rotor position.

The results obtained from two methods are collected in same figure. The self inductances of phase A and B are given in figure 3.34 and 3.35 respectively. It can be easily seen that there is a slightly difference between the values obtained from two methods.

Since the waveshape of inductances given in Figures 3.26- 3.32 are periodical, the Fourier analysis technique can be employed to find a mathematical expression for them. The following basic relation has been used to calculate the Fourier coefficients A_{hjk} and φ_{hjk}.

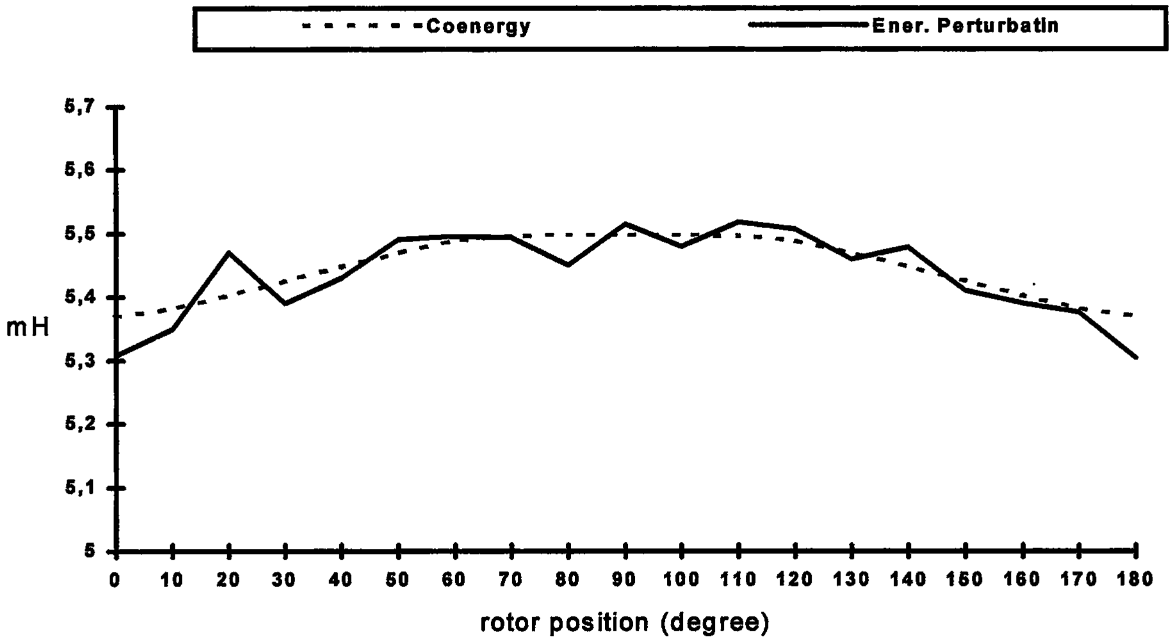

Figure 3.34 Self enductance of phase A with two different method

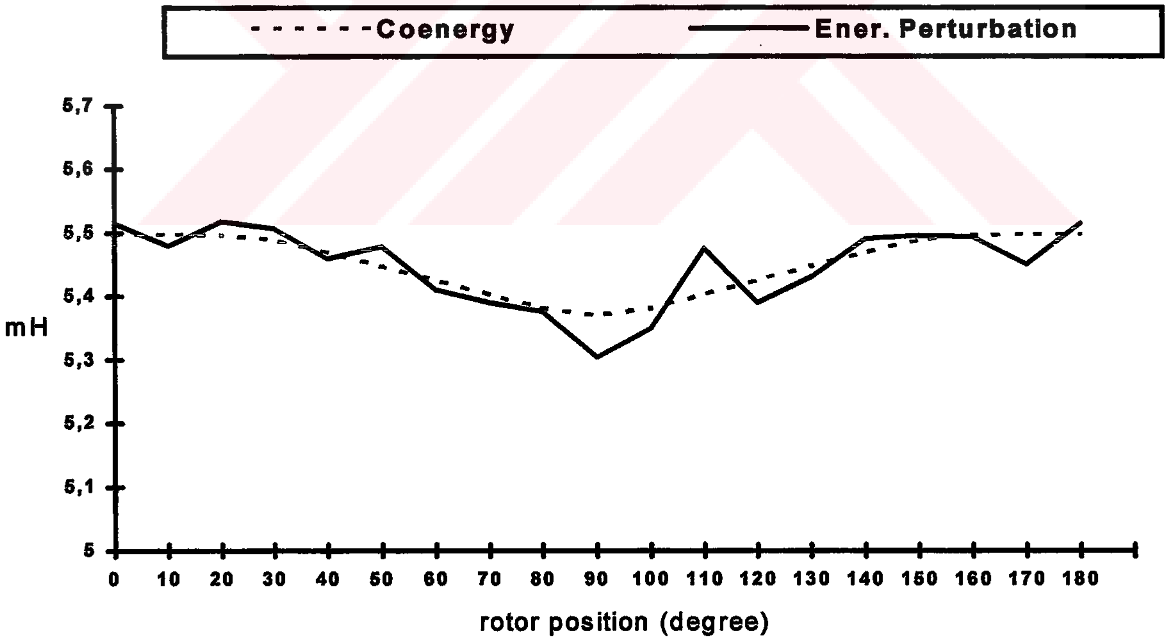

Figure 3.35 Self enductance of phase B with two different method

$$L_{jk}(\theta) = A_{0_{jk}} + \sum_{h=1}^{H} A_{h_{jk}}.Cos(h\theta + \varphi_{h_{jk}}) \qquad (3.47)$$

where

$j=1,2,3,...N$ & $k=1,2,3,...N$

h is the harmonic order 1,2,3,...,H,

A_{hjk} is the harmonic coefficient of order h,

A_{ojk} is the average inductance value,

φ_{hjk} is the harmonic phase shift in space.

The following numerical values have been obtained by using a numerical formulation and programming of the Fourier analysis in Fortran language;

$L_{11}(\theta)$= 5.754172E-3 + 6.121691E-5 Cos(2θ -180) H,

$L_{22}(\theta)$= 5.747510E-3 + 5.487284E-5 Cos(2θ) H,

$L_{12}(\theta)$=4.255903E-4 + 1.624186E-6 Cos(4θ -180) H,

$L_{13}(\theta)$= 4.177232E-4 + 3.375929E-5 Cos(2θ -180) H,

$L_{24}(\theta)$= 4.136995E-4 + 3.094121E-5 Cos(2θ) H.

3.6.3 Armature Winding Resistance

For AWG23, the wire resistance is given 21 Ω for 1000 ft(=304.8 mt)in the table on the reference [D.G. Fink & H.W. Besty 1993]. So the winding length must be calculated.

$$l_a = 2.N.(l + l_c' + l_p) \qquad (3.48)$$

where l_a is the length of the coil, l is the axial armature core length, l_p is the average width of the main pole on the armature core, and l_c' is the width of the cross sectional area of coil group as being shown in figure 3.36.

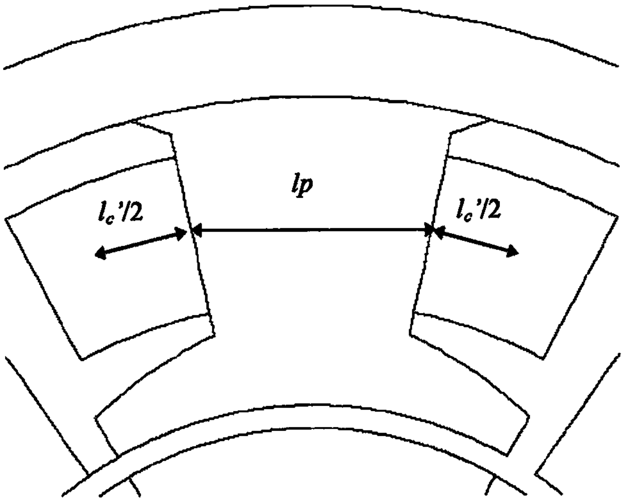

Figure 3.36 The cross section of the motor geometry

The armature winding resistance is obtained as 0,892 Ω for 96 turn per phase.

CHAPTER FOUR

SIMULATION OF THE PERMANENT MAGNET VARIABLE RELUCTANCE MOTOR DRIVE

A non-linear model for the permanent magnet variable reluctance machine has been developed in order to predict the transient and steady-state behavior of the machine. This non-linear model has been combined with the model of the drive circuit. The drive circuit contains two closed loops. The outer loop is the speed feedback having a proportional-integral (PI) type of controller and the inner loop is the current feedback having a hysteresis current control. The closed loop control of machine is also included into the model.

The entire drive system consists of the motor, speed and current transducers, speed and current controllers, chopper, and the dc power supply. The block diagram of the complete drive system is shown in figure 4.1.

The motor core losses in the study has not been calculated due to the fact that it is impossible to define core losses in the model based on the generalized machine theory.

The whole system is separated into three parts for the modeling purpose:

- motor
- drive circuit
- closed-loop controllers

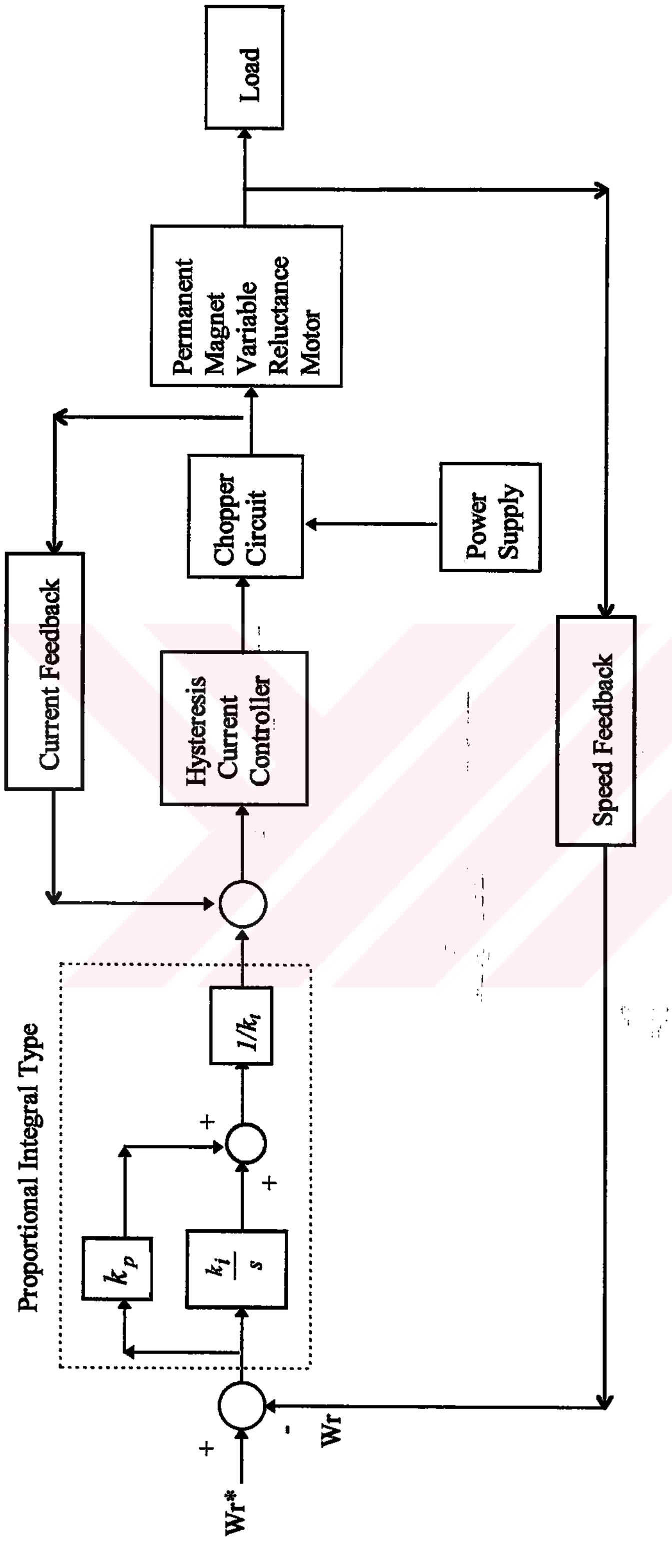
Load
Permanent Magnet Variable Reluctance Motor
Chopper Circuit
Power Supply
Current Feedback
Hysteresis Current Controller
Speed Feedback
Proportional Integral Type
k_p
$\frac{k_i}{s}$
$1/k_t$
+
+
+
-
Wr*
Wr

Figure 4.1 The complete drive circuit

4.1 Modeling of the Motor

In general the instantaneous relationship between the voltages and currents of permanent magnet variable reluctance motor can be written in matrix form:

$$\underline{V} = \underline{R}.\underline{I} + \frac{d}{dt}(\underline{\Lambda}) \qquad (4.1)$$

and

$$\underline{\Lambda} = \underline{L}.\underline{I} \qquad (4.2)$$

where $\underline{V}$ is the vector of motor armature terminal voltages, $\underline{R}$ is the armature resistance matrix, $\underline{I}$ is the armature current vector, $\underline{L}$ is the motor inductance matrix computed using the 2D finite element magnetic field solution , and $\underline{\Lambda}$ is the vector of the corresponding flux linkages.

The machine is considered as consisting of five coupled windings depicted in figure 4.2. Four out of five windings represent the two armature phase windings, a, b, a', and b'. The fifth, a fictitious winding, f, is an equivalent field winding that represents the effect of the permanent magnet on the rotor. The permanent magnet system is equivalent to a constant current field winding, whose ampere turns are proportional to coercivity of the permanent magnet material and the magnet geometries; therefore the field current i_f is constant [M. Rizzo 1992], [T. W. Nehl & N. A. O. Demerdash 1992], [V. Gangla & J. De La Ree 1991], [M. Wing & J. F. Gieras 1992], [M. A. Alhamadi & N.Demerdash 1994], [N. A. O. Demerdash & M. A. Alhamadi 1996], [N. A. Demerdash & T. A. Nyamusa 1985].

In expanded matrix form, equation (4.1) can be written in terms of terminal voltages, winding currents and fictitious field current representing the effects of the permanent magnet mounted on the rotor as follows;

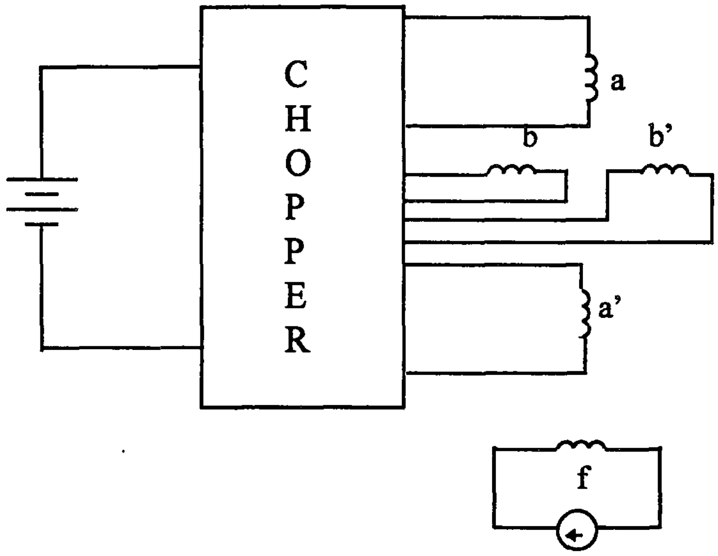

Figure 4.2 Five winding PM machine model

$$\begin{bmatrix} V_a \\ V_b \\ V_{a'} \\ V_{b'} \\ V_f \end{bmatrix} = \begin{bmatrix} r_a & 0 & 0 & 0 & 0 \\ 0 & r_b & 0 & 0 & 0 \\ 0 & 0 & r_{a'} & 0 & 0 \\ 0 & 0 & 0 & r_{b'} & 0 \\ 0 & 0 & 0 & 0 & r_f \end{bmatrix} . \begin{bmatrix} i_a \\ i_b \\ i_{a'} \\ i_{b'} \\ i_f \end{bmatrix} +$$

$$\frac{d}{dt}\left\{ \begin{bmatrix} L_{11} & L_{12} & L_{13} & L_{14} & L_{1f} \\ L_{21} & L_{22} & L_{23} & L_{24} & L_{2f} \\ L_{31} & L_{32} & L_{33} & L_{34} & L_{3f} \\ L_{41} & L_{42} & L_{43} & L_{44} & L_{4f} \\ L_{f1} & L_{f2} & L_{f3} & L_{f4} & L_{ff} \end{bmatrix} . \begin{bmatrix} i_a \\ i_b \\ i_{a'} \\ i_{b'} \\ i_f \end{bmatrix} \right\} \qquad (4.3)$$

where r_a, r_b, $r_{a'}$, and $r_{b'}$ are the winding resistances, r_f is the field winding resistance, L_{11}, L_{22}, L_{33}, and L_{44} are the self inductances, L_{ff} is the field winding self inductance, and L_{12}, L_{13}, ..., L_{34} are the mutual inductances. L_{f1}, L_{f2}, L_{f3}, L_{f4}, L_{1f}, L_{2f}, L_{3f}, L_{4f} are the fictitious field inductances.

In unsaturated or lightly saturated machines, the last term of equation (4.3) can be written with two parts [M. A. Alhamadi & N. A. Demerdash 1994];

$$\frac{d}{dt}(\underline{\Lambda}) = w.\left(\frac{d}{d\theta}.\underline{L}\right).\underline{I} + \underline{L}.\frac{d}{dt}\underline{I} \tag{4.4}$$

where w = dθ/dt is the rotor speed in electrical rad/sec. If the equation (4.3) is rearranged by using equation (4.4), then

$$\begin{bmatrix} V_a \\ V_b \\ V_{a'} \\ V_{b'} \\ V_f \end{bmatrix} = \begin{bmatrix} r_a & 0 & 0 & 0 & 0 \\ 0 & r_b & 0 & 0 & 0 \\ 0 & 0 & r_{a'} & 0 & 0 \\ 0 & 0 & 0 & r_{b'} & 0 \\ 0 & 0 & 0 & 0 & r_f \end{bmatrix} . \begin{bmatrix} i_a \\ i_b \\ i_{a'} \\ i_{b'} \\ i_f \end{bmatrix} +$$

$$w.\left\{ \frac{d}{d\theta} \begin{bmatrix} L_{11} & L_{12} & L_{13} & L_{14} & L_{1f} \\ L_{21} & L_{22} & L_{23} & L_{24} & L_{2f} \\ L_{31} & L_{32} & L_{33} & L_{34} & L_{3f} \\ L_{41} & L_{42} & L_{43} & L_{44} & L_{4f} \\ L_{f1} & L_{f2} & L_{f3} & L_{f4} & L_{ff} \end{bmatrix} \right\} . \begin{bmatrix} i_a \\ i_b \\ i_{a'} \\ i_{b'} \\ i_f \end{bmatrix} +$$

$$\begin{bmatrix} L_{11} & L_{12} & L_{13} & L_{14} & L_{1f} \\ L_{21} & L_{22} & L_{23} & L_{24} & L_{2f} \\ L_{31} & L_{32} & L_{33} & L_{34} & L_{3f} \\ L_{41} & L_{42} & L_{43} & L_{44} & L_{4f} \\ L_{f1} & L_{f2} & L_{f3} & L_{f4} & L_{ff} \end{bmatrix} . \left\{ \frac{d}{dt} \begin{bmatrix} i_a \\ i_b \\ i_{a'} \\ i_{b'} \\ i_f \end{bmatrix} \right\} \tag{4.5}$$

The equivalent fictitious field current is constant in value for a permanent magnet field excitation. Also, the armature currents have little effects on the magnet flux distributions under normal load operating conditions. The fifth row in the equation (4.5) can be eliminated from it without significantly affecting the accuracy of the modeling approach. But the effects of i_f current on the remainder state variables must be kept. Hence, the equation (4.5) can be rewritten as follows;

$$\begin{bmatrix} V_a \\ V_b \\ V_{a'} \\ V_{b'} \end{bmatrix} = \begin{bmatrix} r_a & 0 & 0 & 0 \\ 0 & r_b & 0 & 0 \\ 0 & 0 & r_{a'} & 0 \\ 0 & 0 & 0 & r_{b'} \end{bmatrix} . \begin{bmatrix} i_a \\ i_b \\ i_{a'} \\ i_{b'} \end{bmatrix} +$$

$$w. \left\{ \frac{d}{d\theta} \begin{bmatrix} L_{11} & L_{12} & L_{13} & L_{14} \\ L_{21} & L_{22} & L_{23} & L_{24} \\ L_{31} & L_{32} & L_{33} & L_{34} \\ L_{41} & L_{42} & L_{43} & L_{44} \end{bmatrix} \right\} . \begin{bmatrix} i_a \\ i_b \\ i_{a'} \\ i_{b'} \end{bmatrix} +$$

$$\begin{bmatrix} L_{11} & L_{12} & L_{13} & L_{14} \\ L_{21} & L_{22} & L_{23} & L_{24} \\ L_{31} & L_{32} & L_{33} & L_{34} \\ L_{41} & L_{42} & L_{43} & L_{44} \end{bmatrix} . \frac{d}{dt} \left\{ \begin{bmatrix} i_a \\ i_b \\ i_{a'} \\ i_{b'} \end{bmatrix} \right\} + \frac{d}{dt} \left\{ \begin{bmatrix} L_{1f}.i_f \\ L_{2f}.i_f \\ L_{3f}.i_f \\ L_{4f}.i_f \end{bmatrix} \right\} \tag{4.6}$$

[M. A. Alhamadi & N. A. Demerdash 1994], [T. W. Nehl & F. A. Fouad & N. A. Demerdash & E. A. Maslowski 1982], [T. W. Nehl & N. A. O. Demerdash 1992].

The first term on the right hand side of equation (4.6) represents the ohmic voltage drop in the armature windings of the machine, the second term represents the rotational voltage components due to self and mutual effects of the armature windings, the third term represents the transformer voltage components due to the self and mutual effects of the armature windings, and the last term represents the rotational voltage components due to the permanent magnets mounted on the rotor, that is the no load armature induced emfs in the armature windings of the machine. Last term can be rewritten as partial derivative;

$$\frac{d}{dt}\begin{bmatrix} i_f . L_{1f} \\ i_f . L_{2f} \\ i_f . L_{3f} \\ i_f . L_{4f} \end{bmatrix} = \left[i_f\right].\frac{d}{dt}\begin{bmatrix} L_{1f} \\ L_{2f} \\ L_{3f} \\ L_{4f} \end{bmatrix} + \begin{bmatrix} L_{1f} \\ L_{2f} \\ L_{3f} \\ L_{4f} \end{bmatrix}.\frac{d}{dt}\left[i_f\right] \tag{4.7}$$

Since the coercivity force of the permanent magnet material is constant, the fictitious field current i_f is constant. Therefore the last term of equation (4.7) is zero. The time derivative of inductance can be written as a position derivative;

$$\frac{d}{dt}\begin{bmatrix} i_f . L_{1f} \\ i_f . L_{2f} \\ i_f . L_{3f} \\ i_f . L_{4f} \end{bmatrix} = \left[i_f\right].\left\{\frac{d}{d\theta}\begin{bmatrix} L_{1f} \\ L_{2f} \\ L_{3f} \\ L_{4f} \end{bmatrix}\right\}.\frac{d\theta}{dt} = w.\left[i_f\right].\frac{d}{d\theta}\begin{bmatrix} L_{1f} \\ L_{2f} \\ L_{3f} \\ L_{4f} \end{bmatrix} \tag{4.8}$$

The right hand side of equation (4.8) is the no load induced emf. This back emf can be expresses as follows;

$$\begin{bmatrix} e_a \\ e_b \\ e_{a'} \\ e_{b'} \end{bmatrix} = w\left[i_f\right]\frac{d}{d\theta}\begin{bmatrix} L_{1f} \\ L_{2f} \\ L_{3f} \\ L_{4f} \end{bmatrix} \tag{4.9}$$

The model in equation (4.6) can be rearranged as given below after substituting equation (4.9) into (4.8) and (4.6). The state variables are i_a, i_b, $i_{a'}$, and $i_{b'}$.

$$\frac{d}{dt}\begin{bmatrix} i_a \\ i_b \\ i_{a'} \\ i_{b'} \end{bmatrix} = \begin{bmatrix} L_{11} & L_{12} & L_{13} & L_{14} \\ L_{21} & L_{22} & L_{23} & L_{24} \\ L_{31} & L_{32} & L_{33} & L_{34} \\ L_{41} & L_{42} & L_{43} & L_{44} \end{bmatrix}^{-1} . \left(\begin{bmatrix} V_a \\ V_b \\ V_{a'} \\ V_{b'} \end{bmatrix} - \begin{bmatrix} e_a \\ e_b \\ e_{a'} \\ e_{b'} \end{bmatrix} - \right.$$

$$\left\{ w.\frac{d}{d\theta}\begin{bmatrix} L_{11} & L_{12} & L_{13} & L_{14} \\ L_{21} & L_{22} & L_{23} & L_{24} \\ L_{31} & L_{32} & L_{33} & L_{34} \\ L_{41} & L_{42} & L_{43} & L_{44} \end{bmatrix} + \begin{bmatrix} r_a & 0 & 0 & 0 \\ 0 & r_b & 0 & 0 \\ 0 & 0 & r_{a'} & 0 \\ 0 & 0 & 0 & r_{b'} \end{bmatrix} \right\} . \begin{bmatrix} i_a \\ i_b \\ i_{a'} \\ i_{b'} \end{bmatrix} \Bigg)$$

(4.10)

The torque balance equation for the mechanical motion may be written as follows by neglecting the coefficient of friction and windage:

$$T_E - T_L = J.\frac{dw}{dt} \qquad (4.11)$$

where J is the moment of inertia constant , T_E is the electro magnetic torque developed by the motor, T_L is the load torque, and w is the rotor angular speed. Therefore,

$$\frac{d}{dt}w = \frac{1}{J}.(T_E - T_L) \qquad (4.12)$$

and

$$\frac{d}{dt}\theta = w \qquad (4.13)$$

4.1.1 The Electromagnetic Torque

When all stator windings of the motor are energized, the coenergy in the motor is given;

$$W_c = \frac{1}{2}\left(\lambda_a.i_a + \lambda_{a'}.i_{a'} + \lambda_b.i_b + \lambda_{b'}.i_{b'} + \lambda_f.i_f\right) \qquad (4.14)$$

where all of λ are the flux linkage which belong to these coils. These flux linkage can be written in explicit form as follows;

$$\lambda_a = i_a.L_{11} + i_b.L_{12} + i_{a'}.L_{13} + i_{b'}.L_{14} + i_f.L_{1f}$$

$$\lambda_b = i_a.L_{21} + i_b.L_{22} + i_{a'}.L_{23} + i_{b'}.L_{24} + i_f.L_{2f}$$

$$\lambda_{a'} = i_a.L_{31} + i_b.L_{32} + i_{a'}.L_{33} + i_{b'}.L_{34} + i_f.L_{3f} \quad (4.15)$$

$$\lambda_{b'} = i_a.L_{41} + i_b.L_{42} + i_{a'}.L_{43} + i_{b'}.L_{44} + i_f.L_{4f}$$

$$\lambda_f = i_a.L_{f1} + i_b.L_{f2} + i_{a'}.L_{f3} + i_{b'}.L_{f4} + i_f.L_{ff}$$

The equation (4.14) can be rewritten in matrix notation;

$$W_c = \frac{1}{2}.[I]^T.L.[I] \qquad (4.16)$$

where $[I]$ is the winding currents vector and L is the inductance matrix of the motor. Electromagnetic torque for a motor is described as a position derivative of coenergy [S. H-Y. Li & F. Liang & Y. Zhao & T. A. Lipo 1995], [T-S. Low & C. Bi & K-T. Chang 1996];

$$T_E = \frac{dW_c}{d\theta} = \frac{1}{2}.[I]^T.\frac{d}{d\theta}L.[I] \qquad (4.17)$$

The electro magnetic torque can be rewritten in explicit form;

$$T_E = \frac{1}{2}\begin{bmatrix} i_a & i_b & i_{a'} & i_{b'} & i_f \end{bmatrix} \cdot \left\{ \frac{d}{d\theta} \begin{bmatrix} L_{11} & L_{12} & L_{13} & L_{14} & L_{1f} \\ L_{21} & L_{22} & L_{23} & L_{24} & L_{2f} \\ L_{31} & L_{32} & L_{33} & L_{34} & L_{3f} \\ L_{41} & L_{42} & L_{43} & L_{44} & L_{4f} \\ L_{f1} & L_{f2} & L_{f3} & L_{f4} & L_{ff} \end{bmatrix} \right\} \cdot \begin{bmatrix} i_a \\ i_b \\ i_{a'} \\ i_{b'} \\ i_f \end{bmatrix}$$

(4.18)

Equation (4.18) can be arranged ;

$$T_E = \frac{1}{2}\left\{ i_a^2 . \left(\frac{d}{d\theta} L_{11} \right) + i_b^2 . \left(\frac{d}{d\theta} L_{22} \right) + i_{a'}^2 . \left(\frac{d}{d\theta} L_{33} \right) + i_{b'}^2 . \left(\frac{d}{d\theta} L_{44} \right) \right\} +$$

$$\frac{1}{2} . i_f^2 . \left(\frac{d}{d\theta} L_{ff} \right) + \left\{ i_a . i_b . \left(\frac{d}{d\theta} L_{12} \right) + i_a . i_{a'} . \left(\frac{d}{d\theta} L_{13} \right) + i_a . i_{b'} . \left(\frac{d}{d\theta} L_{14} \right) + \right.$$

$$\left. i_b . i_{a'} . \left(\frac{d}{d\theta} L_{23} \right) + i_b . i_{b'} . \left(\frac{d}{d\theta} L_{24} \right) + i_{b'} . i_{a'} . \left(\frac{d}{d\theta} L_{34} \right) \right\} +$$

$$\left\{ i_f . i_a . \left(\frac{d}{d\theta} L_{f1} \right) + i_f . i_b . \left(\frac{d}{d\theta} L_{f2} \right) + i_f . i_{a'} . \left(\frac{d}{d\theta} L_{f3} \right) + i_f . i_{b'} . \left(\frac{d}{d\theta} L_{f4} \right) \right\}$$

(4.19)

The second term on the right-hand side of equation (4.19) expresses a torque component which is due to the variation of self inductance of the field coil. The self inductance of the field coil depends on the rotor position. This variation produce the torque which is denoted by T_f, is a reluctance torque and it is not related to armature current [T-S Low & C. Bi & K-T. Chang 1996].

$$T_f = \frac{1}{2} . i_f^2 . \frac{d}{d\theta} L_{ff} \qquad (4.20)$$

This reluctance torque is calculated from the finite element analysis by using equation (3.10). The variation of this torque with respect to the rotor position is depicted in figure 3.19.

The last term on the right-hand side of equation (4.19) is the expression related to induced emf and armature currents as it can be clearly seen from the by using equation (4.9). This part of the equation is given below;

$$T_{E4} = \left\{ i_a . \left(i_f . \frac{d}{d\theta} L_{1f} \right) + i_b . \left(i_f . \frac{d}{d\theta} L_{2f} \right) + i_{a'} . \left(i_f . \frac{d}{d\theta} L_{3f} \right) + i_{b'} . \left(i_f . \frac{d}{d\theta} L_{4f} \right) \right\} \tag{4.21}$$

In equation (4.9), the components of back emf which are e_a, e_b, $e_{a'}$, $e_{b'}$ were given as a function of time derivative of inductances and i_f.

By substituting the equation (4.9) into equation (4.21), the following equation can be obtained.

$$T_{E4} = i_a \frac{e_a}{w} + i_b \frac{e_b}{w} + i_{a'} \frac{e_{a'}}{w} + i_{b'} \frac{e_{b'}}{w} \tag{4.22}$$

e_a, $e_{a'}$, e_b, and $e_{b'}$ have been obtained from the finite element analysis. Their change in time during the solution of the rotor is given in figure 3.24 and figure 3.25.

4.2 Drive Circuit

According to the static torque waveforms obtained in section 3.5.3, it is appropriate to transmit the current through the motor windings only in one direction. That's why a unipolar drive type has been chosen. Otherwise, the drive circuit would be bi-polar since current would pass through the windings in both direction. A unidirectional drive circuit supplies current to each phase during 90 degrees of rotor position. Therefore, important input parameter for drive circuit is the rotor position detected.

The chopper drive circuit that is used in this study, is shown in figure 4.3. This drive is fed by a constant dc source, and it is feeding power to one phase of the motor. The semiconductor switches ,T_1 and T_2 (i.e., BJT transistor, IGBT, MOSFET, or GTO) are in on state if the winding is connected to the power source. Since the winding resistance is low, the steady state current will be very high. Therefore, the current should be limited by the current controller dictating the status of T_2. If the current is less than the hysteresis limit, T_2 is turned-on, otherwise it is turned-off. In that case, the armature current will circulate through T_1, D_1, and winding. After completing the conduction period of the phase, both T_1 and T_2 are turned-off and the winding current will flow through D_2, power source V_{dc} and D_1 until the current reaches to zero. The winding current should be monitored to specify the status of the semiconductor switch T_2. In order to perform this application, a small resistance in series with the winding, i.e. R_c shown in the figure 4.3, or a dc current transformer can be used [P. P . Acarnley & R. J. Hill & C. W. Hooper 1985], [P. P. Acarnley 1992].

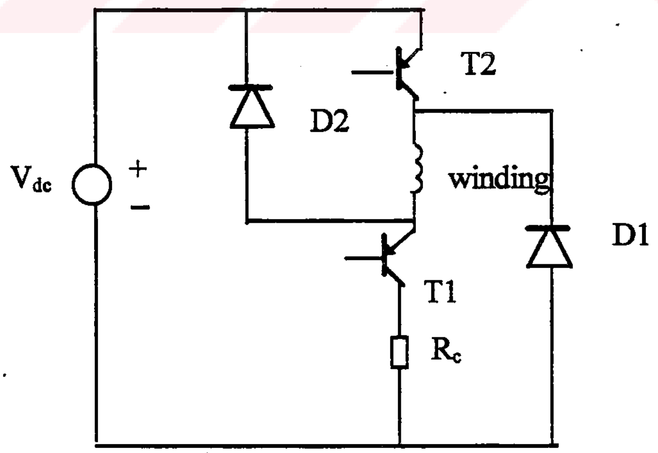

Figure 4.3 The chopper drive circuit

This period is repeated for the excitation cycle of each phase. The timing diagram of the chopper circuit is given at figure 4.4.

Each phase of the motor is excited during 90 mechanical degrees of rotation as shown in figure 3.15 since the motor has two phases. One phase is opened while the other phase is drawing current from the drive circuit. Therefore, the terminal voltage of the winding that is disconnected from the source should be estimated from the analysis of the motor in order to predict the performance of the machine by using the equation set given in (4.10) - (4.19) or the effect of this open-circuited winding can be eliminated by rearranging the equations of (4.10)- (4.19) after substituting zero for the currents corresponding to open-circuited windings. [E. Akpinar & P. Pillay 1990]

The equation (4.6) is rearranged in two states as being described below according to the disconnection of the windings from the source. During the connection of phase A to the power source by means of the chopper drive, the system is described by the state 1. In this case, phase B is completely disconnected. During the connection of phase B to the power source via the chopper drive, the system is described by the state 2. In this case, phase A is completely disconnected.

The following voltage - current relation can be written from the equation (4.6).

$$V_a = r_a.i_a + w.\frac{d}{d\theta}(L_{11}).i_a + w.\frac{d}{d\theta}(L_{12}).i_b + w.\frac{d}{d\theta}(L_{13}).i_{a'} + w.\frac{d}{d\theta}(L_{14}).i_{b'}$$

$$+ L_{11}.\frac{d}{dt}i_a + L_{12}.\frac{d}{dt}i_b + L_{13}.\frac{d}{dt}i_{a'} + L_{14}.\frac{d}{dt}i_{b'} + e_a \qquad (4.23)$$

$$V_b = r_b.i_b + w.\frac{d}{d\theta}(L_{21}).i_a + w.\frac{d}{d\theta}(L_{22}).i_b + w.\frac{d}{d\theta}(L_{23}).i_{a'} + w.\frac{d}{d\theta}(L_{24}).i_{b'}$$

$$+ L_{21}\frac{d}{dt}i_a + L_{22}.\frac{d}{dt}i_b + L_{23}.\frac{d}{dt}i_{a'} + L_{24}.\frac{d}{dt}i_{b'} + e_b \qquad (4.24)$$

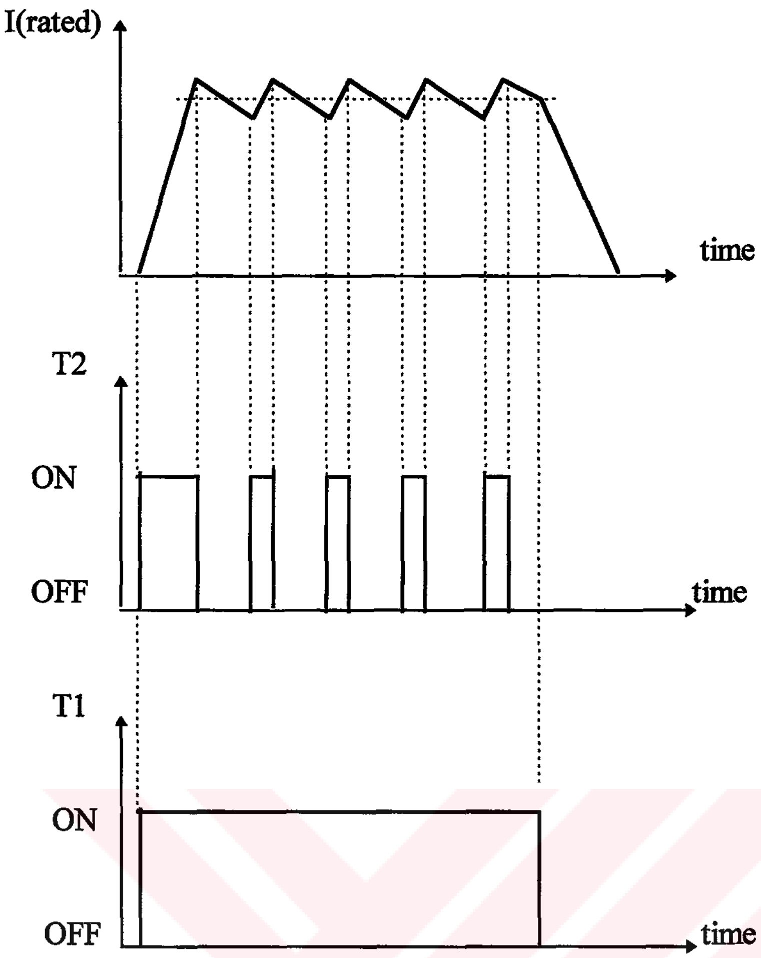

Figure 4.4 Chopper drive current waveform and transistor switching time

$$V_{a'} = r_{a'}.i_{a'} + w.\frac{d}{d\theta}\left(L_{31}\right).i_a + w.\frac{d}{d\theta}\left(L_{32}\right).i_b + w.\frac{d}{d\theta}\left(L_{33}\right).i_{a'} + w.\frac{d}{d\theta}\left(L_{34}\right).i_{b'}$$

$$+ L_{31}.\frac{d}{dt}i_a + L_{32}.\frac{d}{dt}i_b + L_{33}.\frac{d}{dt}i_{a'} + L_{34}.\frac{d}{dt}i_{b'} + e_{a'}$$

(4.25)

$$V_{b'} = r_{b'}.i_{b'} + w.\frac{d}{d\theta}\left(L_{41}\right).i_a + w.\frac{d}{d\theta}\left(L_{42}\right).i_b + w.\frac{d}{d\theta}\left(L_{43}\right).i_{a'} + w.\frac{d}{d\theta}\left(L_{44}\right).i_{b'}$$

$$+ L_{41}\frac{d}{dt}i_a + L_{42}.\frac{d}{dt}i_b + L_{43}.\frac{d}{dt}i_{a'} + L_{44}.\frac{d}{dt}i_{b'} + e_{b'}$$

(4.26)

STATE_1:

i_b and $i_{b'}$ are equal to zero, when only phase A is excited. Two equations out of four equations are taken into account. These are equation (4.23) and (4.25). After substituting zero for i_b and $i_{b'}$ in (4.23) and (4.25), the following can be obtained;

$$V_a = r_a.i_a + w.\frac{d}{d\theta}(L_{11}).i_a + w.\frac{d}{d\theta}(L_{13}).i_{a'} + L_{11}.\frac{d}{dt}i_a + L_{13}.\frac{d}{dt}i_{a'} + e_a$$

(4.27)

$$V_{a'} = r_{a'}.i_{a'} + w.\frac{d}{d\theta}(L_{31}).i_a + w.\frac{d}{d\theta}(L_{33}).i_{a'} + L_{31}.\frac{d}{dt}i_a + L_{33}.\frac{d}{dt}i_{a'} + e_{a'}$$

The equation (4.27) can be written in matrix notation;

$$\begin{bmatrix} V_a \\ V_{a'} \end{bmatrix} = \begin{bmatrix} r_a & 0 \\ 0 & r_{a'} \end{bmatrix} . \begin{bmatrix} i_a \\ i_{a'} \end{bmatrix} + w.\left(\frac{d}{d\theta} \begin{bmatrix} L_{11} & L_{13} \\ L_{31} & L_{33} \end{bmatrix} \right) . \begin{bmatrix} i_a \\ i_{a'} \end{bmatrix} + \begin{bmatrix} L_{11} & L_{13} \\ L_{31} & L_{33} \end{bmatrix} . \frac{d}{dt} \begin{bmatrix} i_a \\ i_{a'} \end{bmatrix} + \begin{bmatrix} e_a \\ e_{a'} \end{bmatrix}$$

(4.28)

The equation (4.28) can be rearranged in state space form in order to solve it with the numerical integration method.

$$\frac{d}{dt} . \begin{bmatrix} i_a \\ i_{a'} \end{bmatrix} = \begin{bmatrix} L_{11} & L_{13} \\ L_{31} & L_{33} \end{bmatrix}^{-1} . \left\{ \begin{bmatrix} V_a - e_e \\ V_{a'} - e_{a'} \end{bmatrix} - \left(\begin{bmatrix} r_a & 0 \\ 0 & r_{a'} \end{bmatrix} + w.\frac{d}{d\theta} \begin{bmatrix} L_{11} & L_{13} \\ L_{31} & L_{33} \end{bmatrix} \right) \begin{bmatrix} i_a \\ i_{a'} \end{bmatrix} \right\}$$

(4.29)

When T_1 and T_2 are turned on, the V_a and $V_{a'}$ are equal to V_{dc}. When T_1 and D_1 are conducting, then V_a and $V_{a'}$ are equal to zero. When T_1, D_1 and D_2 are conducting, then V_a and $V_{a'}$ are equal to $-V_{dc}$. In addition, electro magnetic torque expression can be given for motor by arranging equation (4.19) ;

$$T_{EA}=\frac{1}{2}\cdot\left(i_a^2\cdot\frac{d}{d\theta}L_{11}+i_{a'}^2\cdot\frac{d}{d\theta}L_{33}\right)+\frac{1}{2}i_f^2\cdot\frac{d}{d\theta}L_{ff}+i_a.i_{a'}.\frac{d}{d\theta}L_{13}+\frac{i_a.e_a+i_{a'}.e_{a'}}{w}$$

(4.30)

STATE_2:

Similar equations can be derived when only phase B is excited. When T_1 and T_2 are turned on, then V_b and $V_{b'}$ are equal to V_{dc} as shown in figure 4.3. When T_1 and D_1 are conducting, then V_b and $V_{b'}$ are equal to zero. When T_1, D_1 and D_2 are conducting, then V_b and $V_{b'}$ are equal to $-V_{dc}$. The zero are substituted into the current i_a and $i_{a'}$ at the equation (4.24) and (4.26). Thus following equations are obtained;

$$V_b=r_b.i_b+w.\frac{d}{d\theta}\left(L_{22}\right).i_b+w.\frac{d}{d\theta}\left(L_{24}\right).i_{b'}+L_{22}.\frac{d}{dt}i_b+L_{24}.\frac{d}{dt}i_{b'}+e_b$$

(4.31)

$$V_{b'}=r_{b'}.i_{b'}+w.\frac{d}{d\theta}\left(L_{24}\right).i_b+w.\frac{d}{d\theta}\left(L_{44}\right).i_{b'}+L_{42}.\frac{d}{dt}i_b+L_{44}.\frac{d}{dt}i_{b'}+e_{b'}$$

The equation (4.31) can be rewritten as matrix notation;

$$\begin{bmatrix}V_b\\V_{b'}\end{bmatrix}=\begin{bmatrix}r_b&0\\0&r_{b'}\end{bmatrix}\cdot\begin{bmatrix}i_b\\i_{b'}\end{bmatrix}+w.\left(\frac{d}{d\theta}\begin{bmatrix}L_{22}&L_{24}\\L_{42}&L_{44}\end{bmatrix}\right)\cdot\begin{bmatrix}i_b\\i_{b'}\end{bmatrix}+\begin{bmatrix}L_{22}&L_{24}\\L_{42}&L_{44}\end{bmatrix}\cdot\frac{d}{dt}\begin{bmatrix}i_b\\i_{b'}\end{bmatrix}+\begin{bmatrix}e_b\\e_{b'}\end{bmatrix}$$

(4.32)

The equation (4.32) can be arranged in state space form:

$$\frac{d}{dt}\begin{bmatrix}i_b\\i_{b'}\end{bmatrix}=\begin{bmatrix}L_{22}&L_{24}\\L_{42}&L_{44}\end{bmatrix}^{-1}\cdot\left\{\begin{bmatrix}V_b-e_b\\V_{b'}-e_{b'}\end{bmatrix}-\left(\begin{bmatrix}r_b&0\\0&r_{b'}\end{bmatrix}+w.\frac{d}{d\theta}\begin{bmatrix}L_{22}&L_{24}\\L_{42}&L_{44}\end{bmatrix}\right)\cdot\begin{bmatrix}i_b\\i_{b'}\end{bmatrix}\right\}$$

(4.33)

After substituting zero for i_a and $i_{a'}$ in equation (4.19), the electro magnetic torque expression can be obtained as follow;

$$T_{EB} = \frac{1}{2}.\left(i_b^2.\frac{d}{d\theta}L_{22} + i_{b'}^2.\frac{d}{d\theta}L_{44}\right) + \frac{1}{2}i_f^2.\frac{d}{d\theta}L_{ff} + i_b.i_{b'}.\frac{d}{d\theta}L_{24} + \frac{i_b.e_b + i_{b'}.e_{b'}}{w} \tag{4.34}$$

STATE_3:

When T_1 and T_2 are turned off, after completing the conduction sequence of 90 degrees, the V_a and $V_{a'}$ are equal to $-V_{dc}$. In the mean time, since T_3 and T_4 are turned on, the V_b and $V_{b'}$ are equal to V_{dc} and the i_b and $i_{b'}$ start to increase from zero as the i_a and $i_{a'}$ are decreasing to zero. For a while, all of windings can carry the currents. Thus, four terminal voltage equations belonging to two phases should be solved simultaneously. The equations (4.10) and (4.19) are solved simultaneously for this mode of operation.

4.3 Closed Loop Controllers

The closed loop control of permanent magnet variable reluctance motor basically consists of two feedback loops as shown in figure 4.5. The outer is speed feedback loop, and the inner is current feedback loop. The speed feedback is proportional integral (PI) type. The current controller is a hysteris type of controller. The closed loop speed controller is included into the simulation. The speed controller is taken into consideration in the model by adding one more state variable that is the error between reference and actual value of the rotor speed. The governing equation of PI speed controller may be obtained as given below;

$$I_{ref} = \frac{1}{K_t}.\left(K_p.\left(w_{ref} - w_{act}\right) + K_i.\int\left(w_{ref} - w_{act}\right).dt\right) \tag{4.35}$$

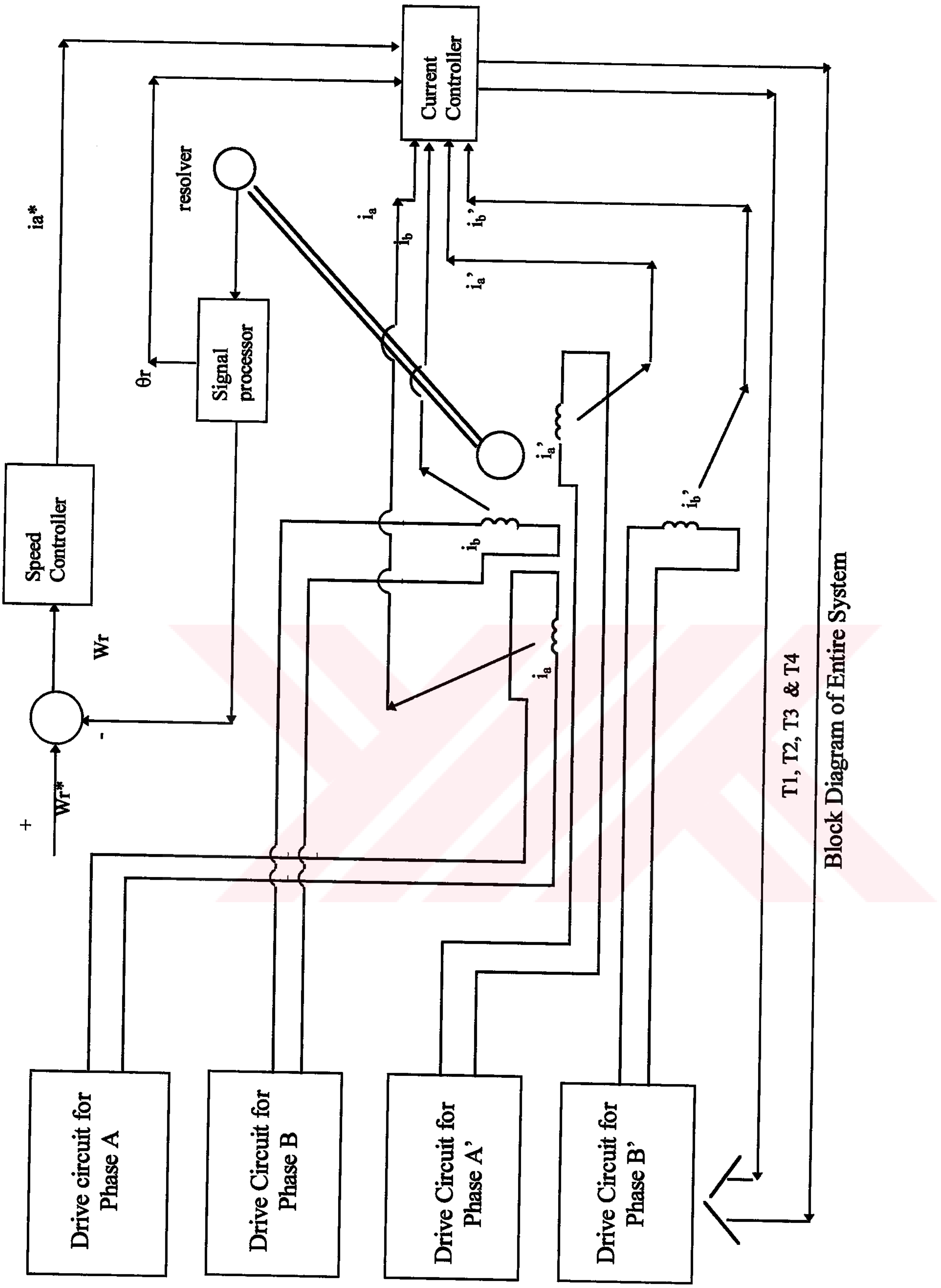
Current Controller
resolver
Signal processor
θr
ia*
Speed Controller
Wr
Wr*
+
-
i_a
i_b
i_a'
i_b'
i_a
i_b
i_a'
i_b'
T1, T2, T3 & T4
Block Diagram of Entire System
Drive circuit for Phase A
Drive Circuit for Phase B
Drive Circuit for Phase A'
Drive Circuit for Phase B'

Figure 4.5 Closed loop control of drive circuit

where I_{ref} is the reference current, K_t is the torque constant, W_{ref} is the reference speed, and W_{act} is the actual rotor speed.

The last term of right hand side of equation (4.35) is taken as the additional state variable in this system. Equation (4.35) can be computed in two steps as follows;

$$\frac{d}{dt}X = K_i.\left(w_{ref} - w_{act}\right) \tag{4.36}$$

After the X is calculated in the simulation program , reference current will be obtained,

$$I_{ref} = \frac{K_p.\left(w_{ref} - w_{cal}\right) + X}{K_t} \tag{4.37}$$

K_i , K_p and K_t are predicted for a stable operation of the entire system by using the trial and error method. These values are given below;

$K_i = 8.5$
$K_p = 1.95$
$K_t = 75$

By controlling the stator winding currents, the magnetic flux distribution in the airgap and output torque can be controlled. The actual stator current will follow the reference current generated at the output of speed controller by means of current controller.

Hysteresis Current Controller:

There are various methods of non-linear current control. The hysteresis current controller method that is used in this study, is one of them. The hysteresis controller compares the actual current with the reference current and generates the error signals. With this controller, the actual armature current is always kept in the range of hysteresis band [O. Craiu & N. Dan & E. A. Badea 1995].

An envelope of hysteresis band, Δi, consisting of the reference value of the current, i_a^* is given in figure 4.6. The actual value of current stays in the range between the maximum and minimum value of the hysteresis band by means of the controller.

The maximum level of the actual current is $i_a^* + \Delta i/2$ while the minimum level is $i_a^* - \Delta i/2$.

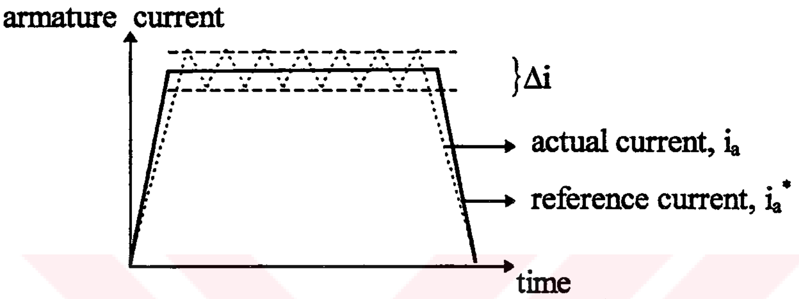

Figure 4.6 Hysteresis current control

The hysteresis current controller is employed for each winding. The status of the transistor T_2 in figure 4.4 is dictated by the current controller depending on the relation given below;

If $i_a > (i_a^* + \Delta i/2)$ then turn off transistor T2

If $i_a < (i_a^* - \Delta i/2)$ then turn on transistor T2

The reference current, i_a^* is one directional (assumed to be positive).

A disadvantage of the hysteresis controller is that the switching frequency is unknown and frequency depends on motor parameter. For example, small hysteresis band imply a high switching frequency which is a partial limitation on the power device switching capability. Increased switching frequency also implies increased chopper losses.

4.4 Detection of rotor position

The absolute position accuracy is one of the most critical requirements for PM motor drive. For most PM motor drive application, motion control of the rotor and the load connected to motor are the final purpose. Thus, a high precision position sensor is required. The position sensors used nowadays are:

- Hall switch elements
- Light-emitting diodes and phototransistors
- Electromagnetic resolvers

The most common device used in industry is a Hall Effect switches. These devices are mounted in the end of stator phase windings, thus they sense magnetic pole pieces of the rotor. If the apparent rotor pole position varies as a function of direction and of device temperature, it should be noted that matching of devices becomes more difficult because thermal hysteresis and sensitivity properties should all be identical. Despite these difficulties, it is a common solution due to the convenient and the relatively low cost of the devices.

An alternative solution is to use of opto-electronic source and receiver pairs. These consist of matched light emitting diode (LED), light source and photo diode or transistor switching devices. They operate in the photoconductive mode. That is, either reflective or shadowing transmittance of light.

In the application of electromagnetic resolvers, the output of resolver are amplitude modulated waveforms of the original excitation waveform. The modulation frequency range varies from 400 Hz to 20 kHz in general. The resolver amplitude modulation is a function of the angular position of the rotor with respect to stator. The rotor angle must be calculated from demodulation of this amplitude and may be transformed to a digital form. The disadvantages of resolver are both technical and economic [R. D. Lorenz 1991].

The transistor T_1 used in the chopper circuit given in figure 4.3 is controlled by the rotor position, θ.

4.5 The simulation program

In this section, computer program and its flowchart are presented. The purpose of simulation program is to examine the behavior of the permanent magnet variable reluctance motor. Models of the machine, current and speed controllers, and chopper circuit are taken into consideration to simulate the entire drive.

The FORTRAN programming language is used in the simulation program. In this program, the non-linear differential equation set is solved by 4th order Runga Kutta numerical integration method. The flowchart of computer program is given in figure 4.7.

The motor parameters, speed controller gains, reference angular speed, incremental time step value, hysteresis band width for current controller, initial rotor position, initial value of state variables, and the total simulation time are the input data for the computer program. Motor parameters include the induced backemf, stator winding inductance, the angles that dictate the boundary of conduction sequence, stator winding resistance, and moment of inertia constant. All of these are read in 'initialize' part of flowchart.

Firstly, it must be determined whichever phase is to be excited by reading the rotor position. Secondly both of the phase currents are read. Hysteresis current control are applied for the current of the phase to be excited and thus the terminal voltage is determined. In case the unexcited phase current is bigger than 0.05A, this indicates that the terminal voltage has been only recently cut and that the current does not decrease to zero Amps immediately. In such a case the end of the unexcited windings are given negative terminal voltages and the current equations of the both phases are workout together (STATE3). If unexcited phase current is smaller than

0.05A, then the current of this phase is quite close to zero amps, and no equation is considered. That means, the equations of only one phase are solved (STATE1 or STATE2) .

At the 'HSYCC' subroutine, the winding current is controlled. It is decided to apply terminal voltage or not according to the current value at available rotor position. If the current value is greater than $(i_a^* + \Delta i/2)$, the terminal voltage is removed from phase winding. Similarly, if the current value is less than $(i_a^* - \Delta i/2)$, the terminal voltage is applied to phase winding.

The solutions of the equations are done by applying 4th Runga Kutta integration algorithm. The subroutine (RKSYST) which is used for this purpose simultaneously solves the seven first order differential equations, four of which are current; the fifth is angle; the sixth is angular speed and the seventh is closed loop equation.

The DERIVS subroutine calculates the derivative value of state variables. But firstly, it has decided either solving of only one phase equations or simultaneously solving of two phase equations.

After, suitable state is chosen to calculate derivative value of equations. There are 3 states in this program. The 'STATE1' subroutine calculates only equation of phase A, the 'STATE2' subroutine calculates only equation of phase B, and The 'STATE3' subroutine calculates both of them.

In this modeling, induced back emf and reluctance torque versus rotor position graphics which are calculated by using finite element method, are used. In order to carry the values of these parameters into simulation program at given rotor position, the Cubic Spline that is a curve fitting algorithm is also used. A matrix inverse package program is used to invert the inductance matrix given in equation (4.10).

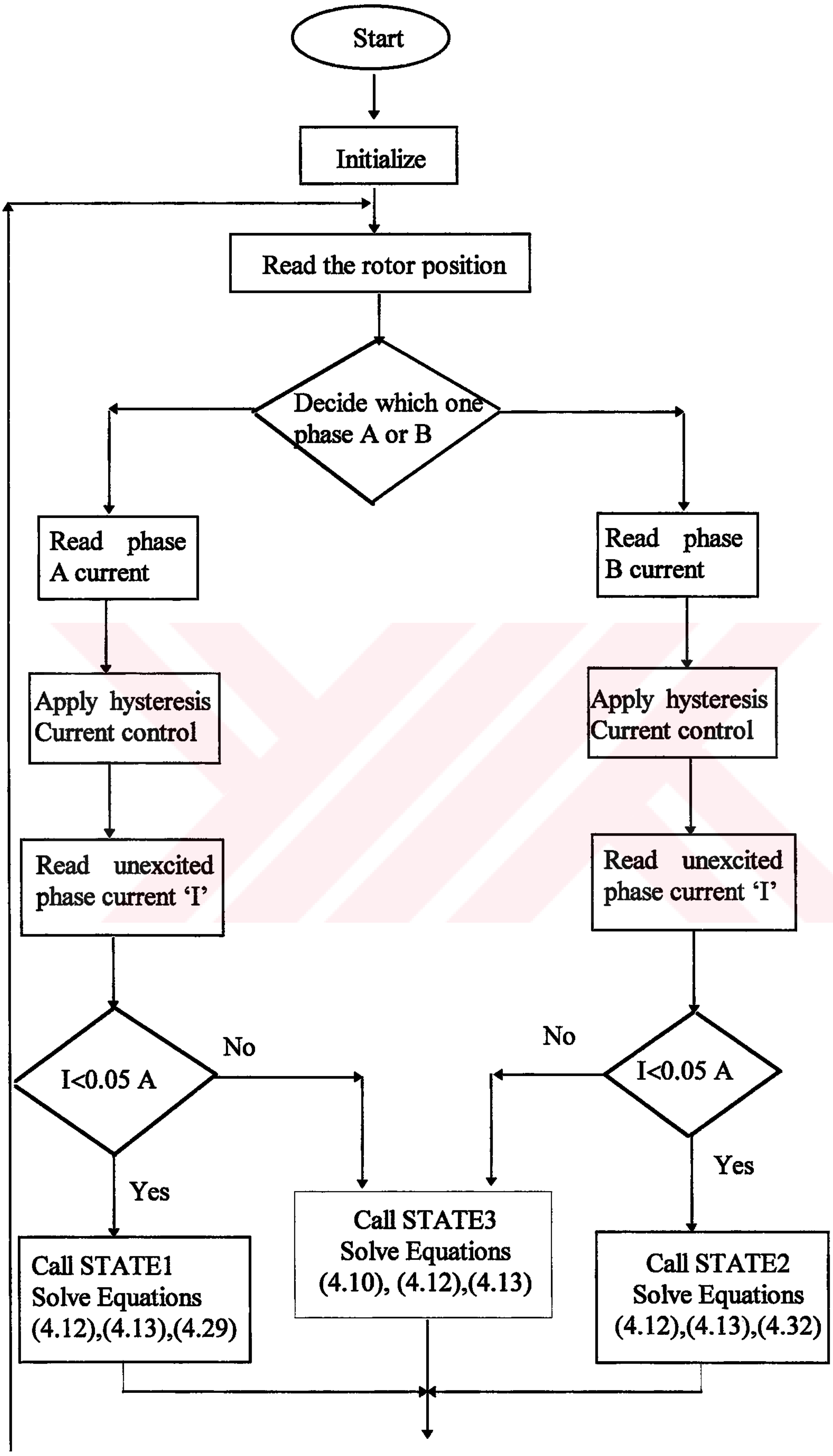
Start
Initialize
Read the rotor position
Decide which one phase A or B
Read phase A current
Read phase B current
Apply hysteresis Current control
Apply hysteresis Current control
Read unexcited phase current 'I'
Read unexcited phase current 'I'
I<0.05 A
No
Yes
I<0.05 A
No
Yes
Call STATE1 Solve Equations (4.12),(4.13),(4.29)
Call STATE3 Solve Equations (4.10), (4.12),(4.13)
Call STATE2 Solve Equations (4.12),(4.13),(4.32)

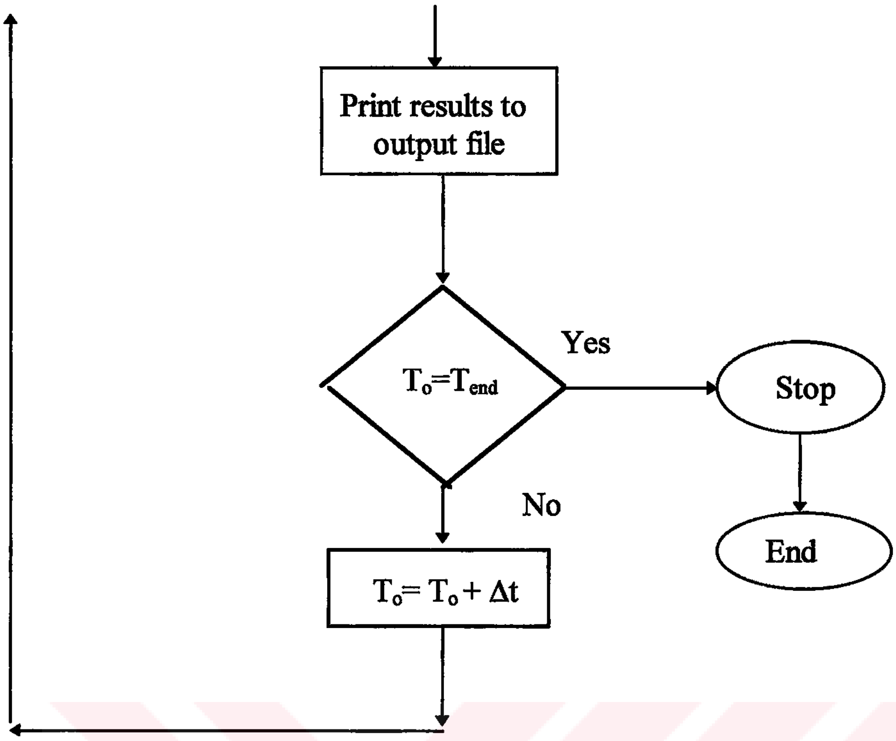

Figure 4.7 The flowchart of simulation program

The results of the equations are put down in an output file and time is increased by Δt. In the event that the simulation period is not over, the same procedures are repeated at a new t value. If the period is over, the program is ended. and the graphics of state variables are drawn by another pc tools after the simulation is completed.

The list of the simulation program is given at appendix A.

4.6 The Results of the Simulation

The simulation program is used to predict the performance of open-loop system (without the speed feedback). The torque-speed characteristics are obtained from the open loop system. Then the speed feedback is included into the model and the efficiency of the motor is investigated under the closed loop control of the system. This section is divided into two parts.

The first part will cover the result of open loop system and the second part will be dedicated to the results of closed loop system.

4.6.1 The Results of Open Loop System

The simulation of the permanent magnet variable reluctance motor is performed for the open loop which does not contain the speed feedback. The control of the rotor speed requires the control of the reference current that is the input to the current controller.

Because the torque speed characteristic is controlled by the magnitude of the actual armature current. Before employing the speed controller in this drive, the change of the torque-speed characteristic of the machine is investigated using the open loop operation. Five current levels around the rating value, which are 1A, 1.5A, 2A, 2.5A, and 3A, are selected for this purpose. The hysteresis band of the current controller is chosen as 0.1 A. In other words, the armature current is allowed to change between 0.95 and 1.05 for the reference current of 1 Amps and 2.45 and 2.55 for the reference current of 2.5 Amp.

For each current value, the simulation program has been run for the different load torques (T_L) applied on the shaft. For the stator current of 2.5 Amps and load torque T_L =0.15 Nm , the results of open loop simulation are given in figures 4.8 .

Figure 4.8-a presents the change of the rotor speed from the standstill to the steady state value.

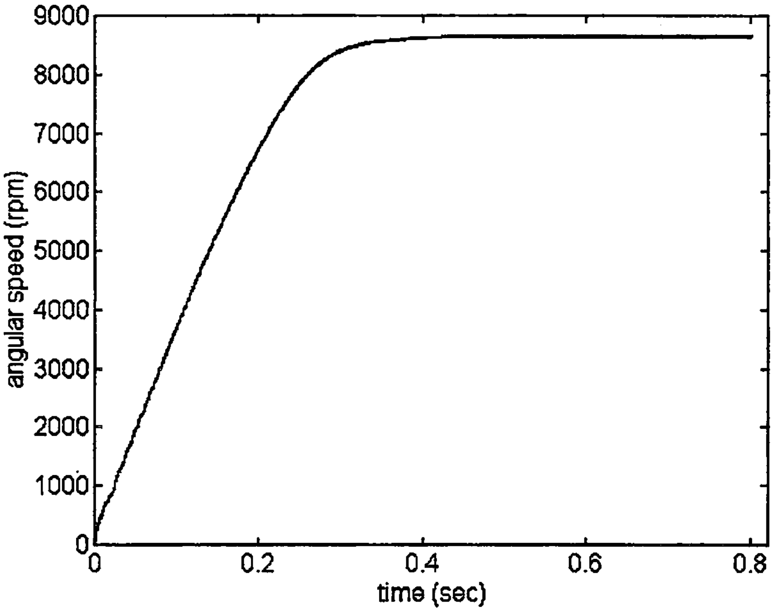

Figure 4.8-a) The rotor speed (I=2.5 A & TL=0.15 Nm)

When the load torque is adjusted to 0.15 Nm, the time of reaching to the steady state from standstill takes approximately 0.4 sec. Figure 4.8-b shows the change of the rotor speed around the steady state. The fluctuation of rotor speed is outcome of torque pulsations.

Figure 4.8-c depicts the variation of the electromagnetic torque versus time during the period of 0.05 sec.

The motor produceses 0.45 Nm starting electromagnetic torque to provide the first motion while it has a 0.15 Nm load torque.

The electromagnetic torque graphics fluctuates approximately between 0.15 Nm and 0.3 Nm in first 0.2 seconds of its complete simulation period and between 0.05 and 0.25 Nm. in the remainder period. Therefore, when the motor passes transient zone and reaches steady state, it produce enough electromagnetic torque for demanded by the load.

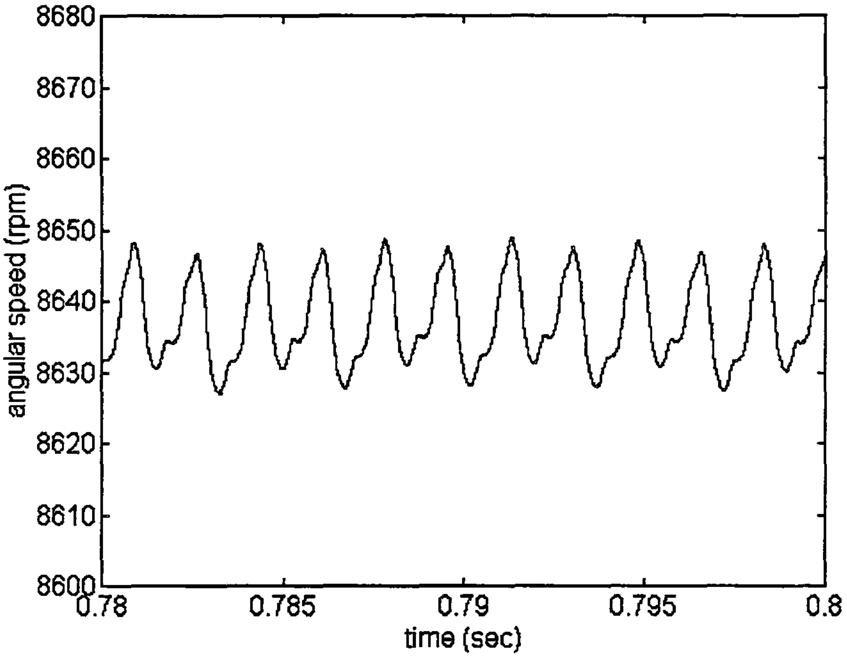

Figure 4.8-b) The extended rotor speed (I=2.5 A & TL=0.15 Nm)

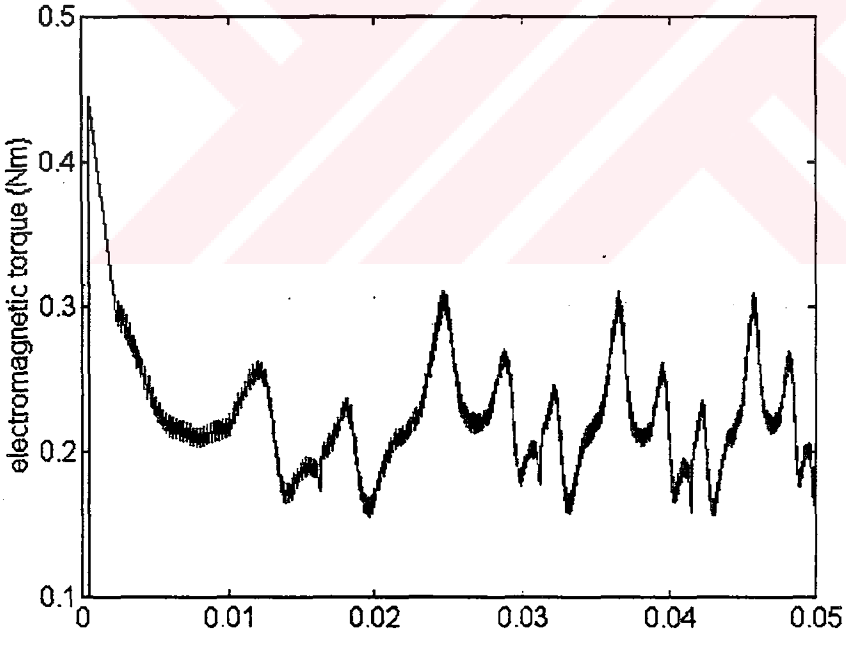

Figure 4.8-c) The electromagnetic torque at standstill (I=2.5 A & TL=0.15 Nm)

When we examine the expanded form of the 0.05 second period of the electromagnetic torque graphics shown in figure 4.8-c, it is easily observed that there are some fluctuations and electromagnetic torque periods lessen because the motor accelerates gradually and thus it is seen that a shape gets tighten gradually.

Small fluctuations in graphics are caused from the ripples due to applied current control. There are also some sharp descent in a period of graphics. The one of sharp ascents which is between 0.18 Nm and 0.14 Nm (at 0.015 sec and 0.032 sec) is caused from current commutation between phases. When one terminal voltage of the phase is cut off, the current of this phase equals to zero during very short time period. At this short period, the other phase current increases to 2.5 Amps. The decreasing of the electromagnetic torque appears at this time.

Abrupt rises reaching 0.3 Nm are related to the back emf waveform of each phase. Since the multiplication of back emf and the winding current is the biggest component of electromagnetic torque, it is easily noticed that the increasing of the back emf has the effect on electromagnetic torque.

At the steady state, the average value of electromagnetic torque is 0.15 Nm as shown in figure 4.8-d, that is equal to load torque. Figure 4.8-e and 4.8-f show the current commutation between the phases. Because of the current controller, the phase current is kept constant at 2.5 Amps. During the starting of the motor, the current of the stator winding exceed the current limits of the current controller. Some time later, the stator current will be within the limits. The shape of electromagnetic torque waveform at steady state is related to current waveform.

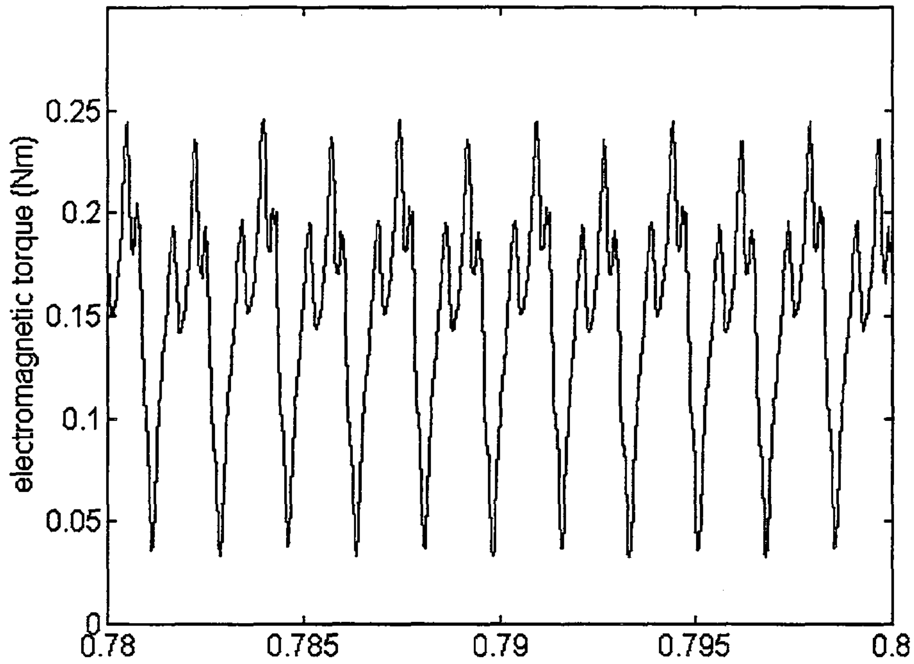

Figure 4.8-d) The electromagnetic torque at steady state(I=2.5 A & TL=0.15 Nm)

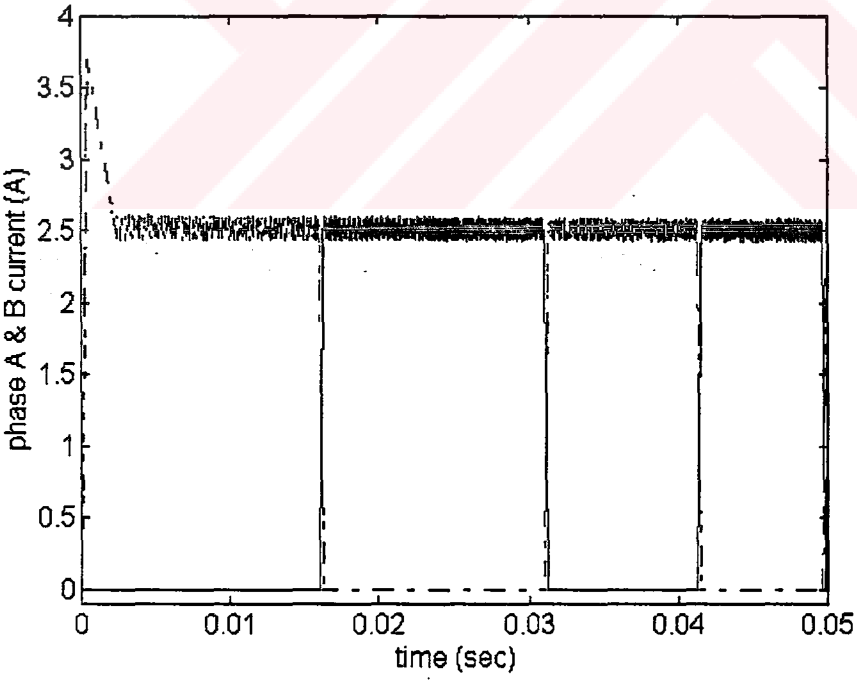

Figure 4.8-e) The phase currents at standstill (I=2.5 A & TL=0.15 Nm)

The phase current A whose terminal voltage applied to winding is cut off, decreases to zero in very short time. Similarly, the current of the phase B reaches to rated value in very short time, after applying terminal voltage as it is observed from figure 4.8-f. Since the hysteresis band of current controller is 0.1 Amps, the current approximately fluctuates between 2.45 Amps and 2.55 Amps.

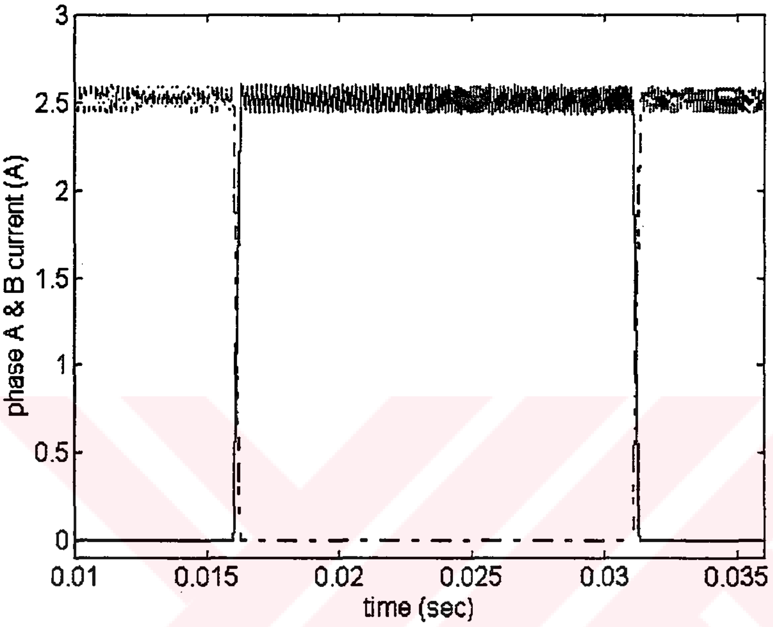

Figure 4.8-f) The phase currents at standstill(I=2.5 A & TL=0.15 Nm)

The stator phase currents at steady state are presented in figure 4.8-g. Each phase is energized during the time of almost 2 msec as it can be seen from figure 4.8-g.

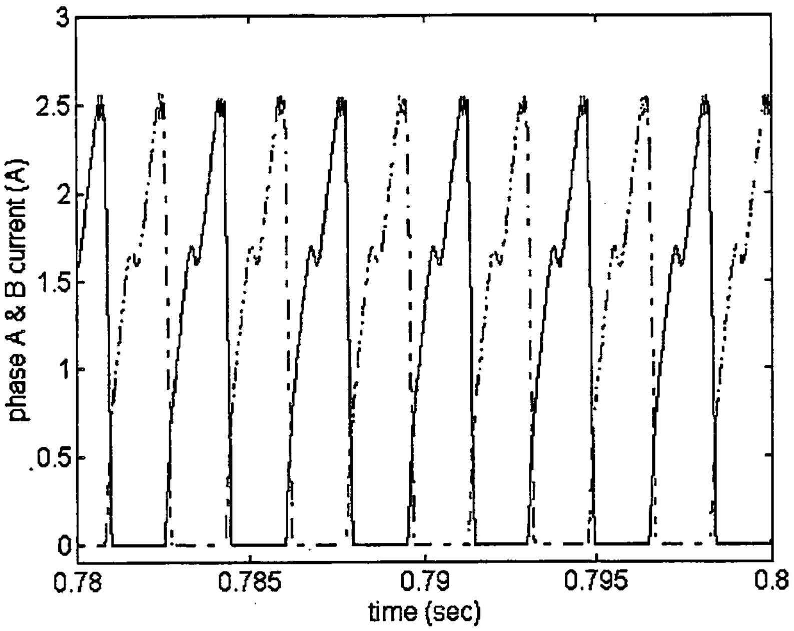

Figure 4.8-g) The phase currents at steady state (I=2.5 A & TL=0.15 Nm)

The steady state operating speed corresponding to the load torque at the specific stator current has been obtained. The collection of these data presents the torque-speed characteristics of the machine shown in figure 4.9. Five stator current levels have been used to generate these data, but it could be extended to the current levels out of the range between 1 and 3 Amps. The aim here is to investigate the change of torque-speed curve and search the possibility whether a proportional integral (PI) controller can be employed for the speed feedback or not. Figure 4.9 represents that the torque developed by the motor decreases as the speed increases at a particular stator current. Also, the electromagnetic torque is almost proportional to the stator current. Therefore, the torque-speed control of the motor can be carried out by the current-speed controller using PI.

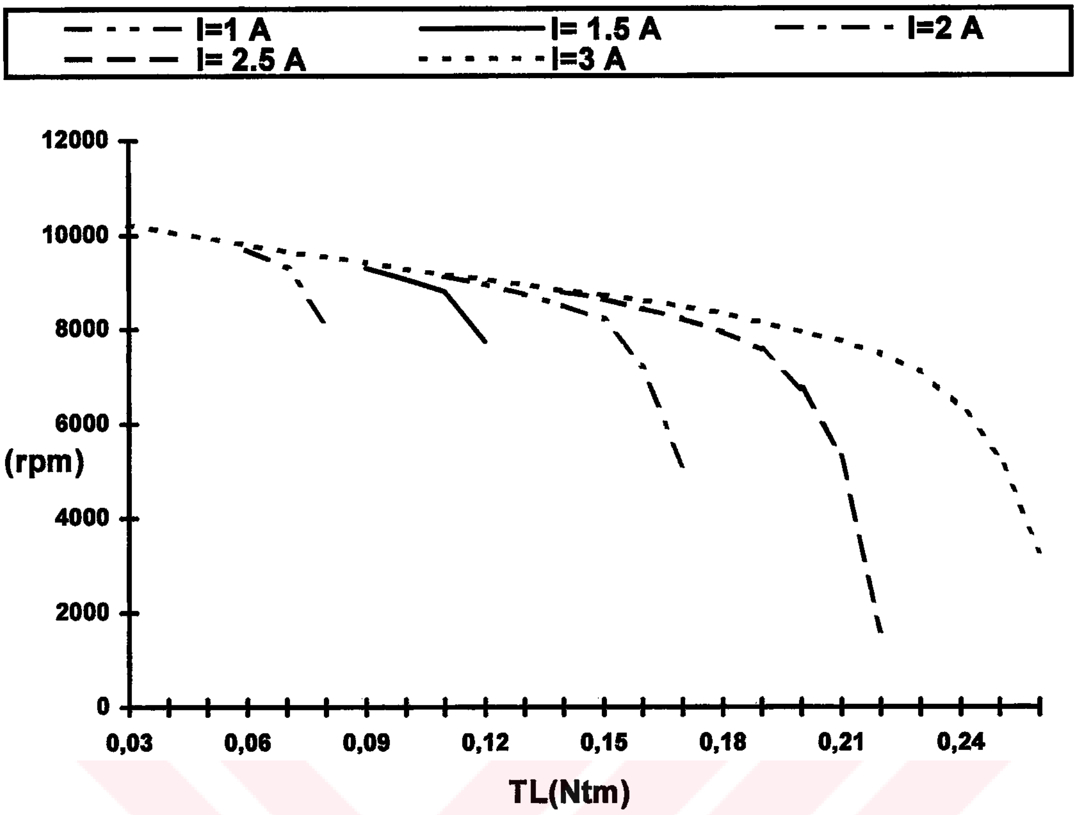

Figure 4.9 Electromagnetic torque versus angular rotor speed

4.6.2 The Results of Closed Loop System

The analysis of closed loop system is carried out by adding one more state variable to the model of the open loop system. This state variable is the error between the reference and actual speeds.

After employing speed controller in the drive circuit, the waveforms of the current, angular rotor speed, and electromagnetic torque are obtained for different value of reference speed (from 300 rad/sec to 860 rad/sec). For these speed values, input and output power are calculated in order to predict the efficiency of the motor. In the closed loop system, the output of the speed controller as shown in figure 4.1 is the reference current for the current controller. Therefore, the reference current is automatically set by the speed controller.

In this study, it is assumed that the motor drives a mechanical load whose torque requirements vary with the speed at which it is driven. This type of load can be described as fan type. The torque speed equation below is used to represent the mechanical load.

$$T_L = k.w \qquad (4.38)$$

where k is constant and w is the rotor speed in rad/sec. In this study, k is chosen as 2.5E-4 Nm.sec/rad .

In the analysis of closed loop system, stator winding currents are limited by 4 Amps to protect winding from over heat and magnets against demagnetization.

Figure 4.10-a shows the rotor speed in terms of revolution per minute (rpm) with respect to time in seconds. Since the reference speed was given as 5729.57 rpm (= 600 rad/sec) the rotor speed settles down that value at the steady state in a very short time.

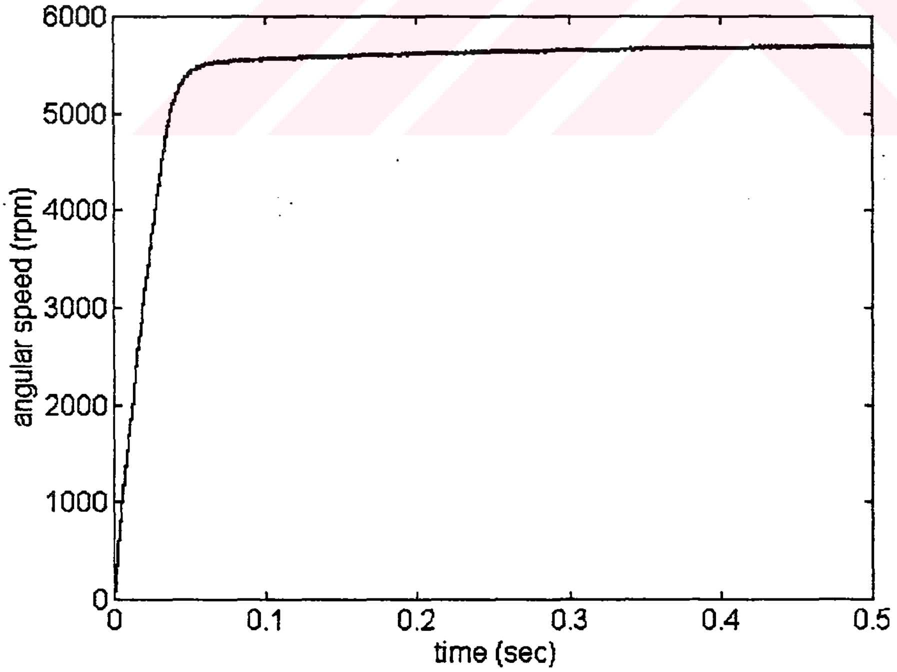

Figure 4.10-a) The angular speed graphic of closed loop

Since the system has been changed from open loop to closed loop, it reaches steady state in a very short time via high starting current. Therefore, it will be sufficient to take the total simulation time as 0.5 seconds.

Figure 4.10-b shows the electromagnetic torque developed by the motor during the 0.5 sec. The electromagnetic torque shows fluctuations during the starting transient. After the motor reaches the steady state, the average electromagnetic torque settles down 0.15 Nm which is equal to load torque.

The variation of the phase current with respect to time is shown in figure 4.10-c.

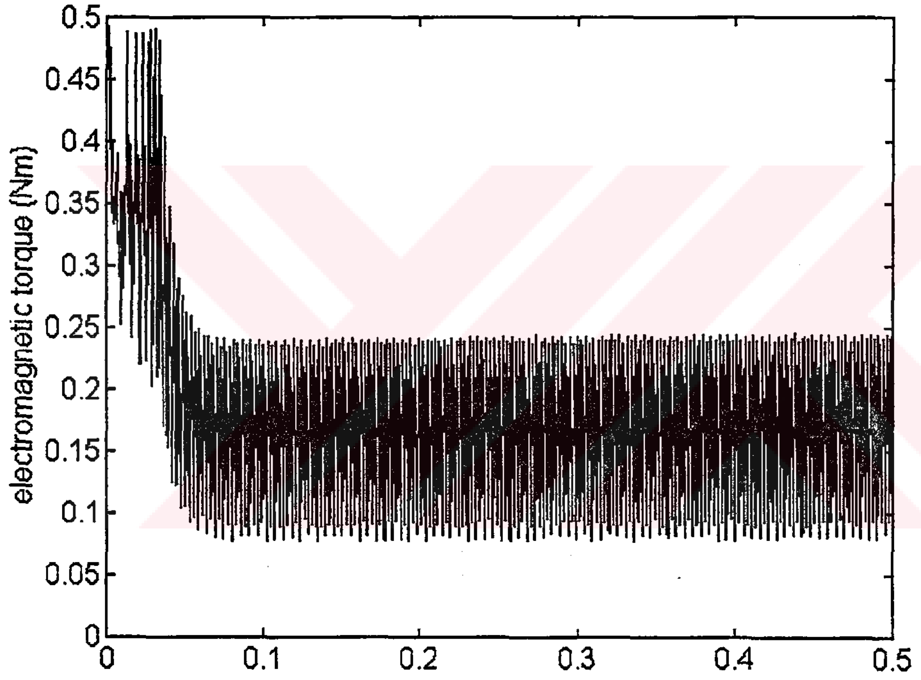

Figure 4.10-b) The electromagnetic torque of closed loop

At the starting, the phase current is at 4 Amps which is approximately 2 times of rated current. It reaches the steady state gradually and remains around 2 Amps.

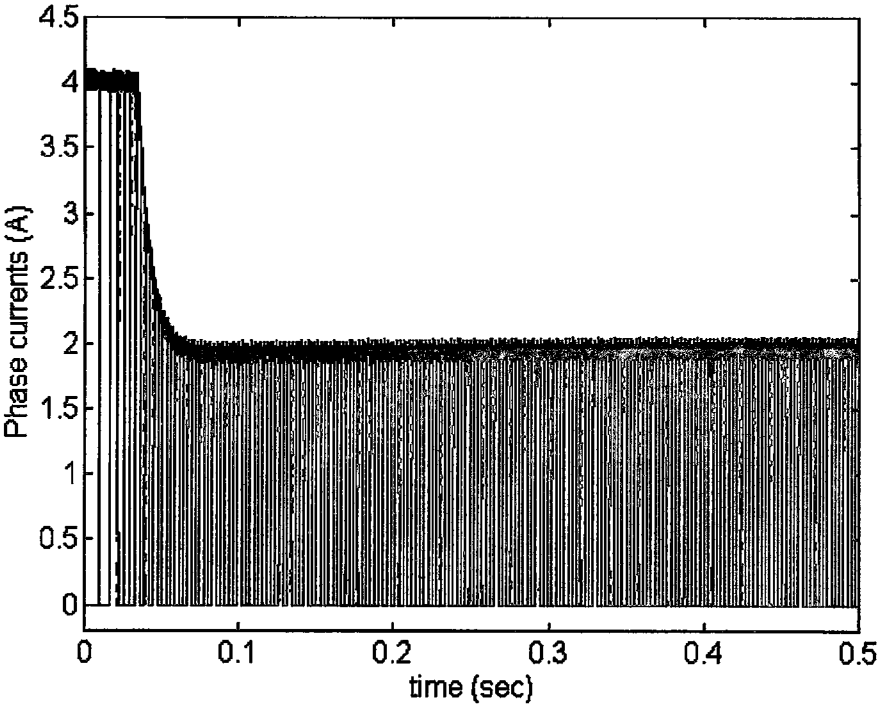

Figure 4.10-c) The phase currents of closed loop

The instantaneous input power shown in figure 4.10-d, described by equation (4.38), is the sum of the multiplications of the terminal voltage of each phase by its current. On the other hand, since the terminal voltage applied to the phases is 50V, the waveform of the input power is similar to the envelope of the phase currents.

The output power of the motor shown in figure 4.10-e, as is formulated in equation (4.38), is the multiplication of the electromagnetic torque and angular speed.

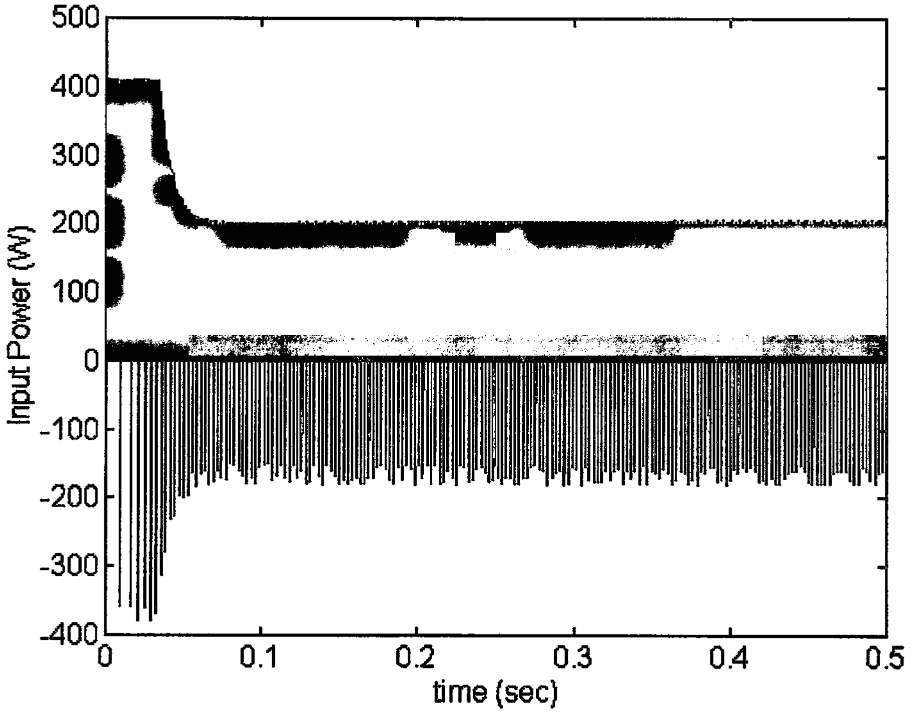

Figure 4.10-d) The input power of closed loop

The starting transient takes approximately 0.05 sec. Hence the envelope of waveforms are dense in drawings, the time axis of the angular speed is zoomed to see the pulsation of rotor speed during the period of between 0.49 and 0.5 sec. These detailed graphics are given in figure 4.11. The first graphic given in figure 4.11-a belongs to the rotor speed. The value of the steady state angular speed seems to be fluctuating in a smaller range. This results from the pulsation of electromagnetic torque at the steady state. The steady state value of speed is 5690 rpm, that is it is very close to referance speed which is 5729 rpm.

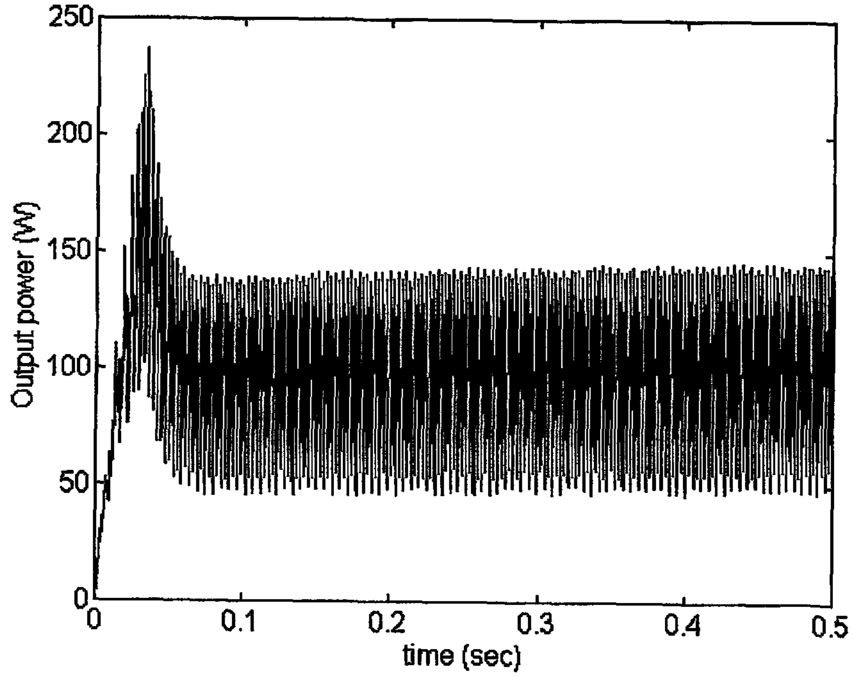

Figure 4.10-e) The output Power of Closed Loop

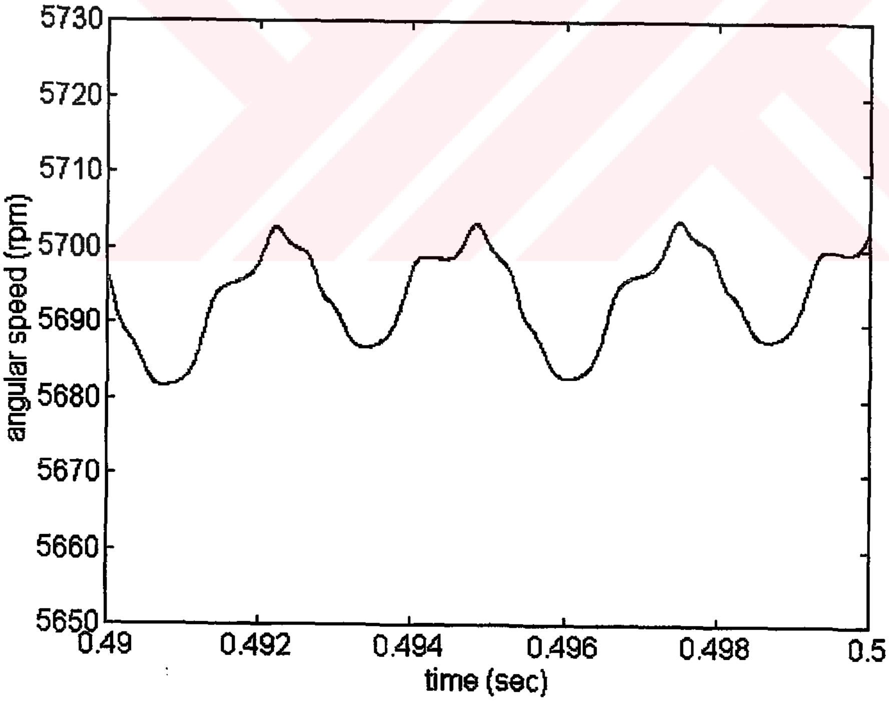

Figure 4.11-a) The extended angular speed graphic

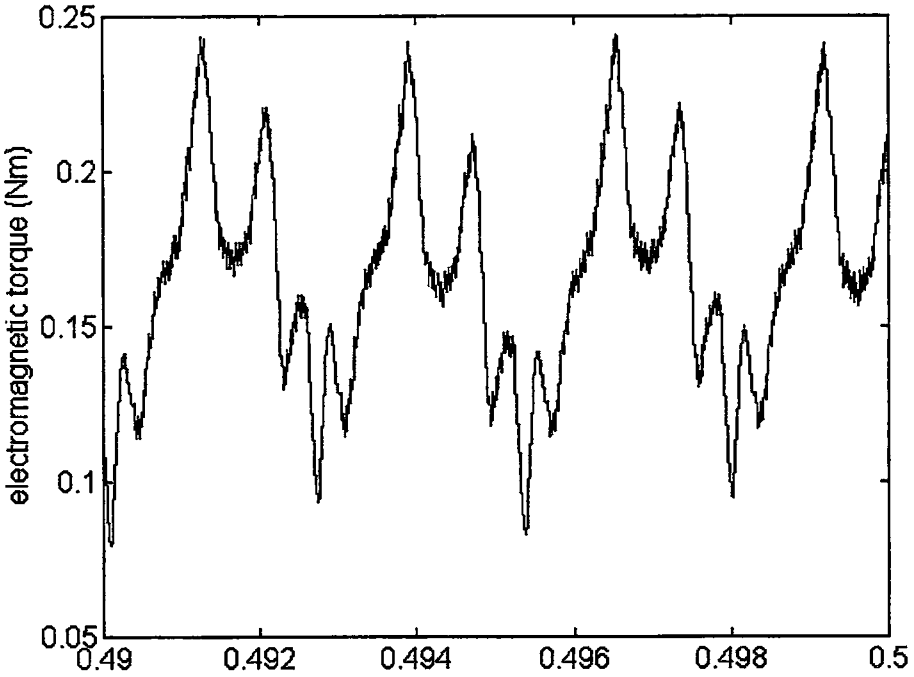

Figure 4.11-b) The extended electromagnetic torque graphic

There are considerable fluctuations in the electromagnetic torque as being observed from the figure 4.11-b at the steady state in the case of closed loop operation. As being described in the previous section, these periodical transients are caused by the phase commutation, changes in the back emf waveform, and the current ripples formed by the current controller.

The extended graphic of phase currents is shown in figure 4.11-c. The period of the phase currents is constant and the amplitude is also held constant between 1.95 Amps and 2.05 Amps by the current controller.

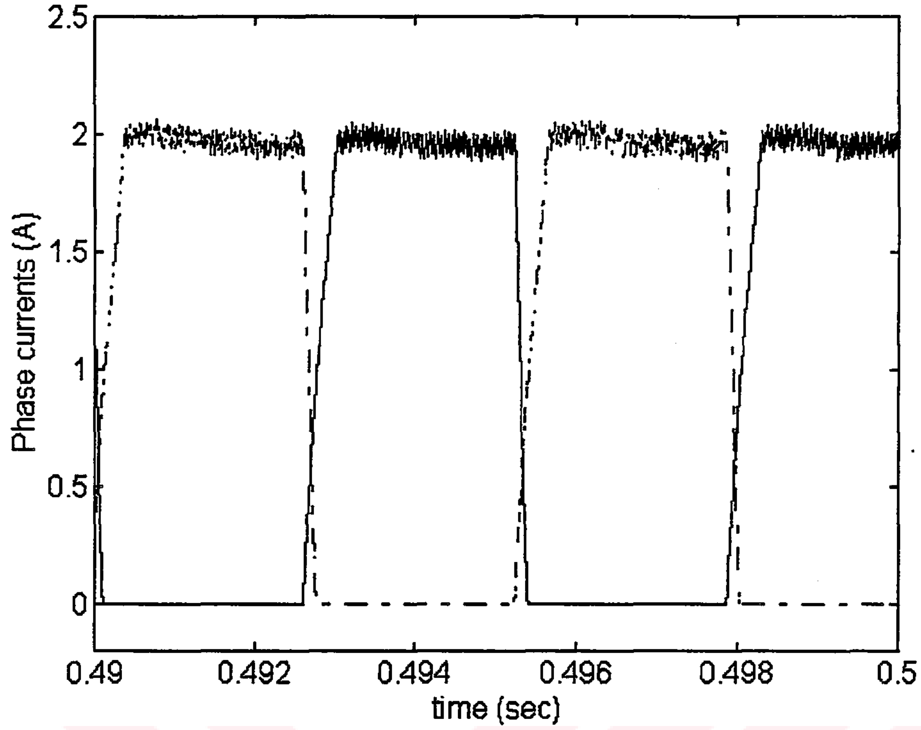

Figure 4.11-c) The extended phase currents graphic

The input and output power graphics are given in figure 4.11-d and 4.11-e respectively. When a small interval such as 50 m seconds is extended and the input power is examined, the effect which is shown like impulsive waveform are completely caused by the terminal voltage. The output power waveform is similar to the electromagnetic torque waveform, since the rotor speed is almost constant.

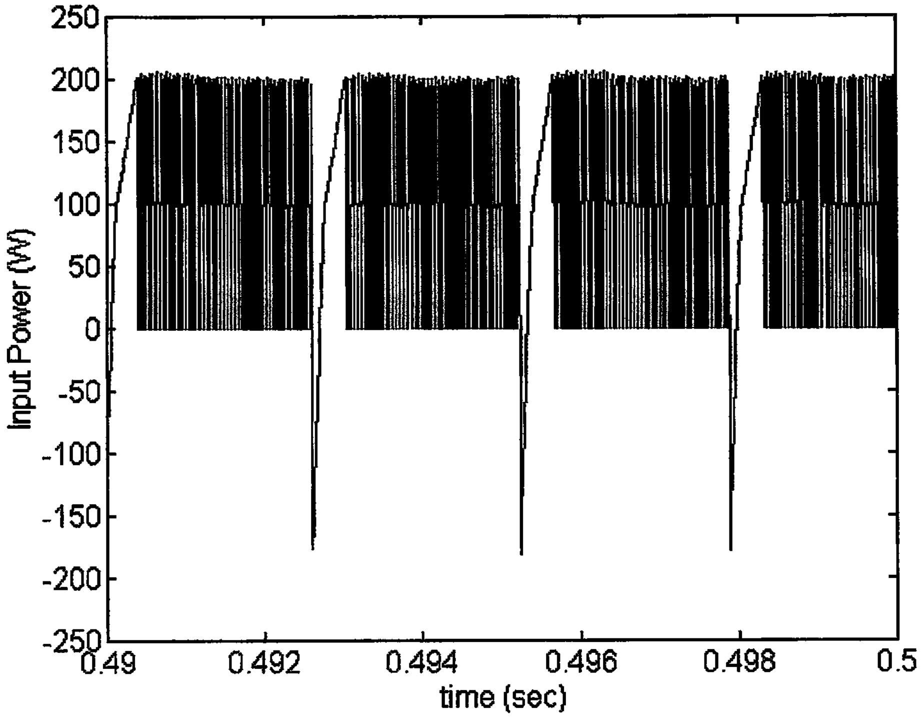

Figure 4.11-d) The extended input power graphic

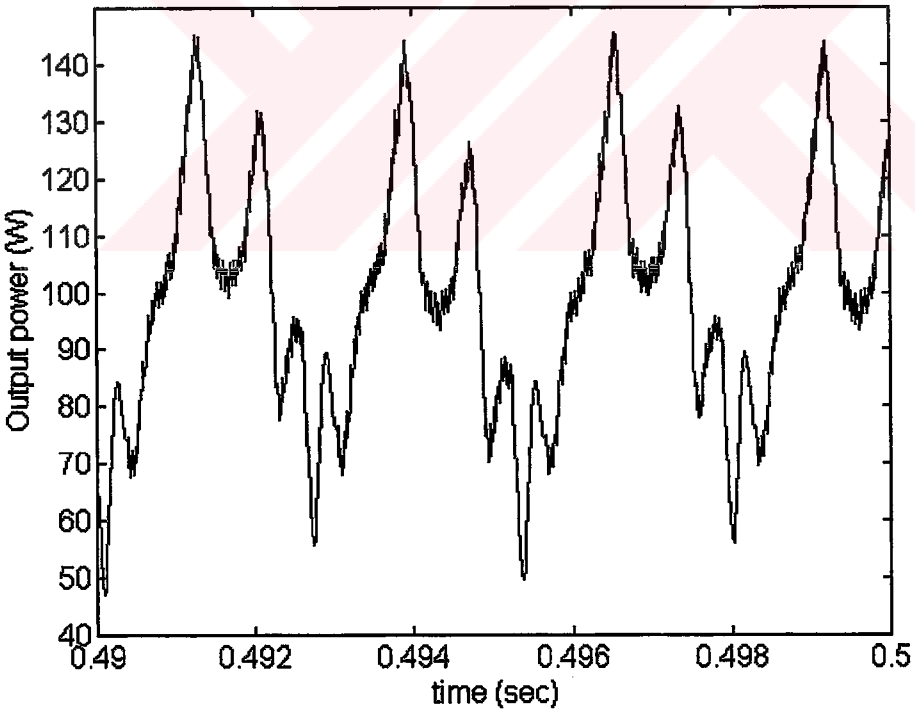

Figure 4.11-e) The extended output power graphic

Figure 4.11-f shows the terminal voltages applied to each phase. A period of the terminal voltage first covers a large area and then the impulsive effects are observed. Since an ideal switch model is being used for the semiconductor devices in chopper circuit, the terminal voltage changes immediately instead of taking a finite time.

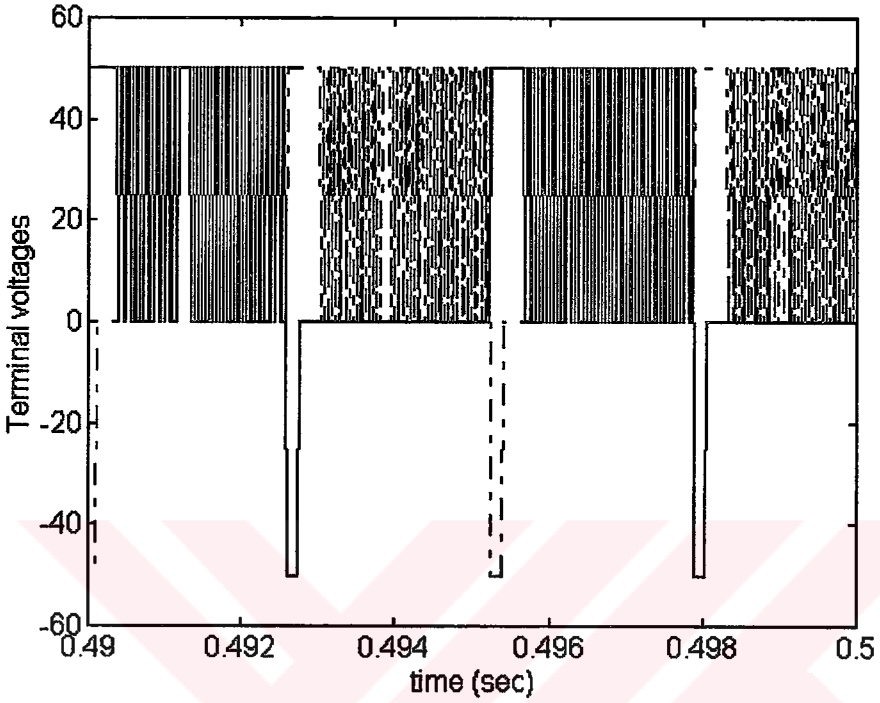

Figure 4.11-f) The extended terminal voltages graphic

4.6.3. Computation Of The Machine Efficiency

The efficiency at the steady-state operating speed has been computed by using the one period of the input and output power waveforms. The ratio between the output power and input power is the efficiency of the motor at the steady-state operating speed. These calculation is repeated for the steady-state rotor speed from 300 rad/sec to 860 rad/sec at 29 points.

$$\eta = \frac{\int_0^T P_o(t).dt}{\int_0^T P_i(t).dt}$$

$$\eta = \frac{\int_0^T T_E(t).w(t).dt}{\int_0^T V_a(t).i_a(t) + V_b(t).i_b(t) + V_{a'}(t).i_{a'}(t) + V_{b'.dt}(t).i_{b'}(t).dt} \tag{4.38}$$

where $P_o(t)$ is the output power and $P_i(t)$ is the input power of the motor. $V_a(t)$, $V_b(t)$, $V_{a'}(t)$, and $V_{b'}(t)$ are the terminal voltages. All variables of the equation (4.38) are the function of the time. The average value of the output power and input power can be calculated over the period of the waveshapes, T as given below;

$$\overline{P_o} = \frac{1}{T}\int_0^T P_o(t).dt \tag{4.39}$$

where $\overline{P_o}$ is the average value. Similarly average value of input power can be written;

$$\overline{P_i} = \frac{1}{T}\int_0^T P_i(t).dt \tag{4.40}$$

The integration can be taken as the total of least square. So equation (4.39) and (4.40) can be rewritten;

$$\overline{P_o} = \frac{1}{T}\left(T_1.w_1.\Delta t + T_2.w_2.\Delta t + ... + T_n.w_n.\Delta t + ...\right) \tag{4.41}$$

and

$$\overline{P_i} = \frac{1}{T}\left(P_1.\Delta t + P_2\Delta t + ... + P_n.\Delta t. + ...\right) \tag{4.42}$$

after these, efficiency can be written [G. Richard & P. Pillay 1994];

$$\eta = \frac{\sum_i T_i . w_i}{\sum_i P_i} \tag{4.43}$$

The figure 4.12 shows the efficiency-rotor speed characteristic of the machine.

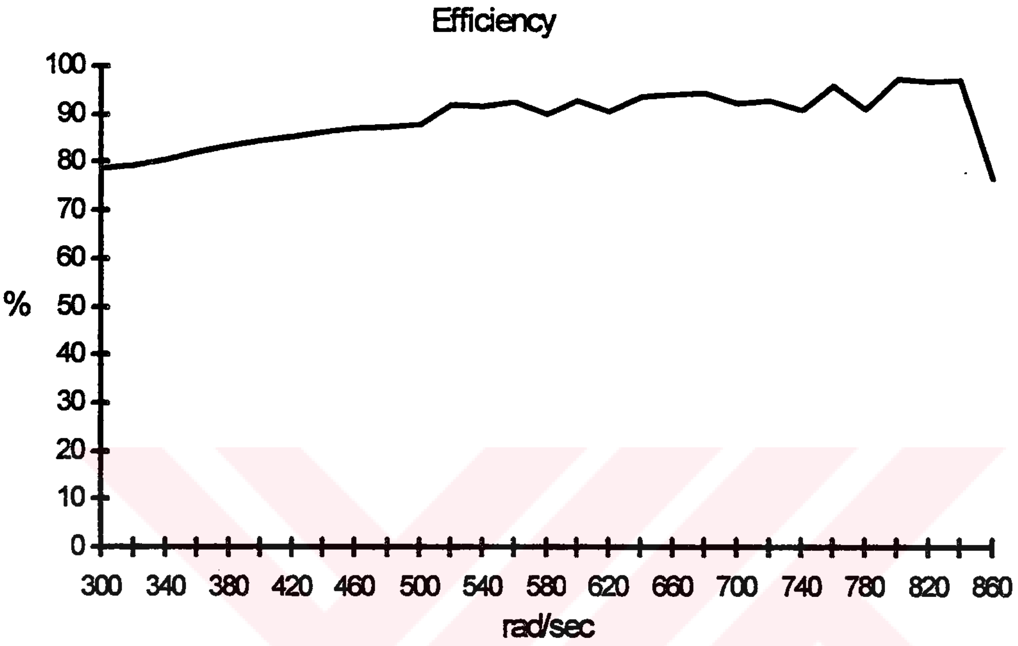

Figure 4.12 The efficiency graphic

4.6.4 The Closed Loop Analysis While The Inductances Are Constant

If self and mutual inductances of the stator winding is accepted as a constant value, the second term on the right hand side of equation (4.6) is omitted. Because these inductances are not a function of rotor position and the derivative of inductances with respect to rotor position are equal to zero. Thus equation (4.6) can be rewritten as follows;

$$\begin{bmatrix} V_a \\ V_b \\ V_{a'} \\ V_{b'} \end{bmatrix} = \begin{bmatrix} r_a & 0 & 0 & 0 \\ 0 & r_b & 0 & 0 \\ 0 & 0 & r_{a'} & 0 \\ 0 & 0 & 0 & r_{b'} \end{bmatrix} \cdot \begin{bmatrix} i_a \\ i_b \\ i_{a'} \\ i_{b'} \end{bmatrix} +$$

$$\begin{bmatrix} L_{11} & L_{12} & L_{13} & L_{14} \\ L_{21} & L_{22} & L_{23} & L_{24} \\ L_{31} & L_{32} & L_{33} & L_{34} \\ L_{41} & L_{42} & L_{43} & L_{44} \end{bmatrix} \cdot \frac{d}{dt} \left\{ \begin{bmatrix} i_a \\ i_b \\ i_{a'} \\ i_{b'} \end{bmatrix} \right\} + \frac{d}{dt} \left\{ \begin{bmatrix} L_{1f}.i_f \\ L_{2f}.i_f \\ L_{3f}.i_f \\ L_{4f}.i_f \end{bmatrix} \right\} \tag{4.44}$$

The last term on the right hand side of equation (4.44) is induced back emf.

$$\begin{bmatrix} e_a \\ e_b \\ e_{a'} \\ e_{b'} \end{bmatrix} = w[i_f] \frac{d}{d\theta} \begin{bmatrix} L_{1f} \\ L_{2f} \\ L_{3f} \\ L_{4f} \end{bmatrix} \tag{4.45}$$

The equation (4.44) can be rearranged as given below after substituting equation (4.45) into (4.44).

$$\frac{d}{dt} \begin{bmatrix} i_a \\ i_b \\ i_{a'} \\ i_{b'} \end{bmatrix} = \begin{bmatrix} L_{11} & L_{12} & L_{13} & L_{14} \\ L_{21} & L_{22} & L_{23} & L_{24} \\ L_{31} & L_{32} & L_{33} & L_{34} \\ L_{41} & L_{42} & L_{43} & L_{44} \end{bmatrix}^{-1} \cdot$$

$$\left(\begin{bmatrix} V_a \\ V_b \\ V_{a'} \\ V_{b'} \end{bmatrix} - \begin{bmatrix} e_a \\ e_b \\ e_{a'} \\ e_{b'} \end{bmatrix} - \begin{bmatrix} r_a & 0 & 0 & 0 \\ 0 & r_b & 0 & 0 \\ 0 & 0 & r_{a'} & 0 \\ 0 & 0 & 0 & r_{b'} \end{bmatrix} \cdot \begin{bmatrix} i_a \\ i_b \\ i_{a'} \\ i_{b'} \end{bmatrix} \right) \tag{4.46}$$

The other state variables of the motor are the time derivative of the angular speed and rotor position. These equations were given in equation (4.12) and (4.13). The electromagnetic torque can be written in matrix form a follows;

$$T_E = \frac{1}{2}\begin{bmatrix} i_a & i_b & i_{a'} & i_{b'} & i_f \end{bmatrix}.\left\{\frac{d}{d\theta}\begin{bmatrix} L_{11} & L_{12} & L_{13} & L_{14} & L_{1f} \\ L_{21} & L_{22} & L_{23} & L_{24} & L_{2f} \\ L_{31} & L_{32} & L_{33} & L_{34} & L_{3f} \\ L_{41} & L_{42} & L_{43} & L_{44} & L_{4f} \\ L_{f1} & L_{f2} & L_{f3} & L_{f4} & L_{ff} \end{bmatrix}\right\}.\begin{bmatrix} i_a \\ i_b \\ i_{a'} \\ i_{b'} \\ i_f \end{bmatrix}$$

(4.47)

Equation (4.47) can be rearranged in explicit form:

$$T_E = \frac{1}{2}\left\{i_a^2.\left(\frac{d}{d\theta}L_{11}\right)+i_b^2.\left(\frac{d}{d\theta}L_{22}\right)+i_{a'}^2.\left(\frac{d}{d\theta}L_{33}\right)+i_{b'}^2.\left(\frac{d}{d\theta}L_{44}\right)\right\}+$$

$$\frac{1}{2}.i_f^2.\left(\frac{d}{d\theta}L_{ff}\right)+\left\{i_a.i_b.\left(\frac{d}{d\theta}L_{12}\right)+i_a.i_{a'}.\left(\frac{d}{d\theta}L_{13}\right)+i_a.i_{b'}.\left(\frac{d}{d\theta}L_{14}\right)+\right.$$

$$\left.i_b.i_{a'}.\left(\frac{d}{d\theta}L_{23}\right)+i_b.i_{b'}.\left(\frac{d}{d\theta}L_{24}\right)+i_{b'}.i_{a'}.\left(\frac{d}{d\theta}L_{34}\right)\right\}+$$

$$\left\{i_f.i_a.\left(\frac{d}{d\theta}L_{f1}\right)+i_f.i_b.\left(\frac{d}{d\theta}L_{f2}\right)+i_f.i_{a'}.\left(\frac{d}{d\theta}L_{f3}\right)+i_f.i_{b'}.\left(\frac{d}{d\theta}L_{f4}\right)\right\}$$

(4.48)

The first row, second term of second row, and third row on the right hand side of equation (4.48) are dropped. Hence,

$$T_E = \frac{1}{2}.i_f^2.\frac{d}{d\theta}L_{ff}+\left\{i_a.\left(i_f.\frac{d}{d\theta}L_{1f}\right)+i_b.\left(i_f.\frac{d}{d\theta}L_{2f}\right)+i_{a'}.\left(i_f.\frac{d}{d\theta}L_{3f}\right)+i_{b'}.\left(i_f.\frac{d}{d\theta}L_{4f}\right)\right\}$$

(4.49)

The self inductance of the field coil depends on rotor position and this term is defined as reluctance torque. This reluctance torque is calculated from the finite element analysis. The second term on the right hand side of equation (4.49) is the expression related to induced emf and armature currents. Equation (4.49) can be rearranged ;

$$T_E = \frac{1}{2}.i_f^2.\frac{d}{d\theta}L_{ff} + i_a\frac{e_a}{w} + i_b\frac{e_b}{w} + i_{a'}\frac{e_{a'}}{w} + i_{b'}\frac{e_{b'}}{w} \tag{4.50}$$

e_a, $e_{a'}$, e_b, and $e_{b'}$ have been obtained from the finite element analysis. Their change in time is given in figure 3.23 and figure 3.24.

The simulation program written in Fortran is run for 600 rad/sec reference speed and it solves equations (4.12), (4.13), and (4.46). Equation (4.50) is substituted into equation (4.12). The inductance matrix in equation (4.46) is not a function of θ, therefore, it is invented just once hence the program execution time is reduced. The results of the simulation are presented in figure 4.13. With this part of study, it is aimed to investigate the error on the results if the inductance matrix is used in the form independent to the rotor angle, θ.

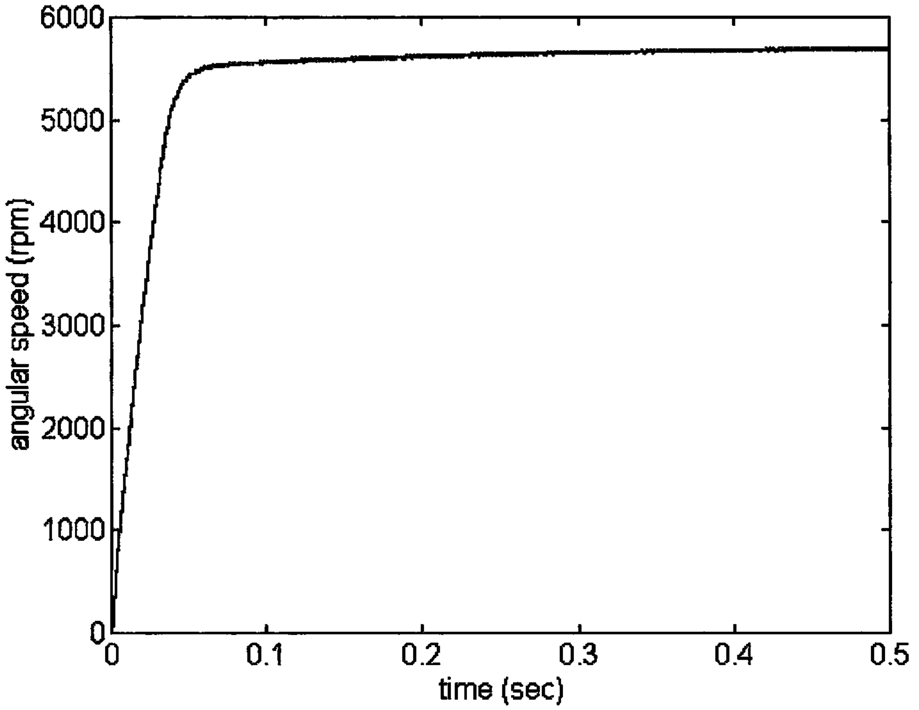

Figure 4.13-a) The angular speed for L=constant

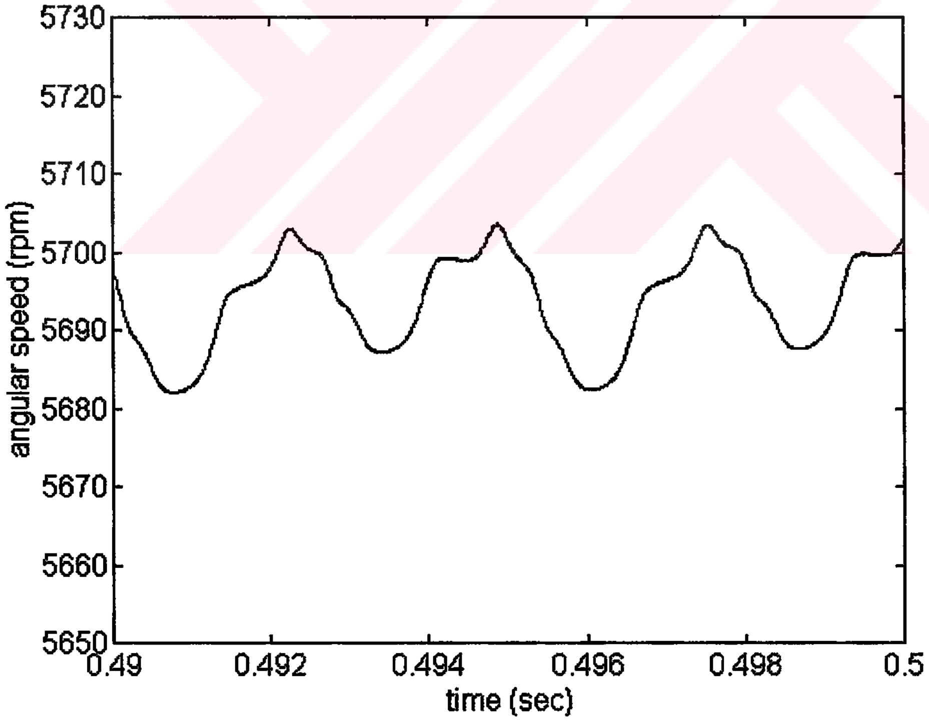

Figure 4.13-b) The extended angular speed for L=constant

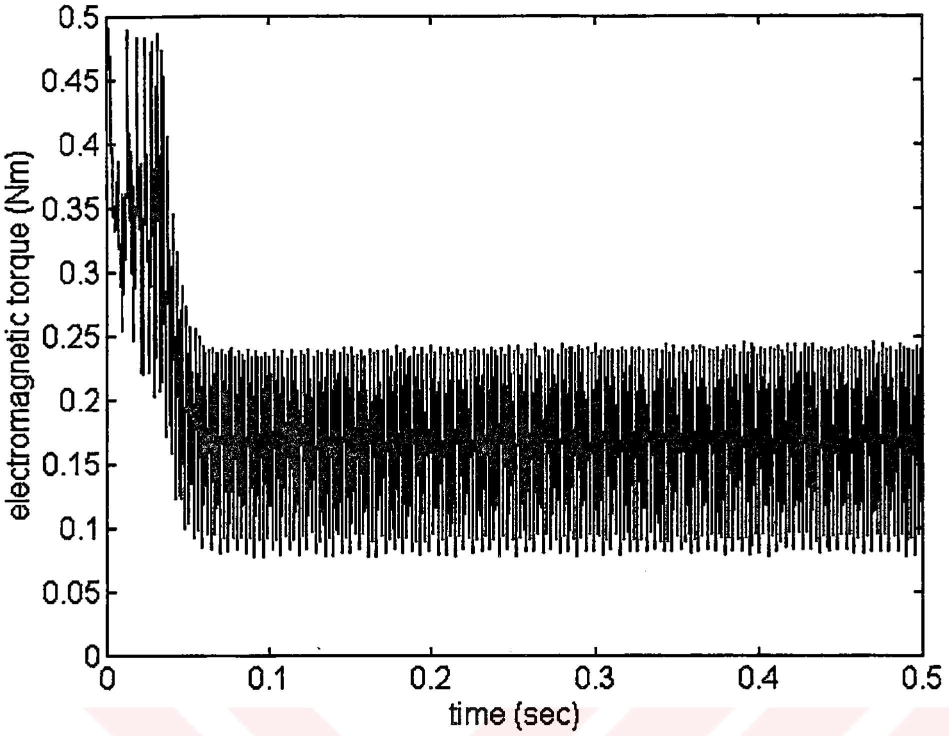

Figure 4.13-c) The electromagnetic torque for L=constant

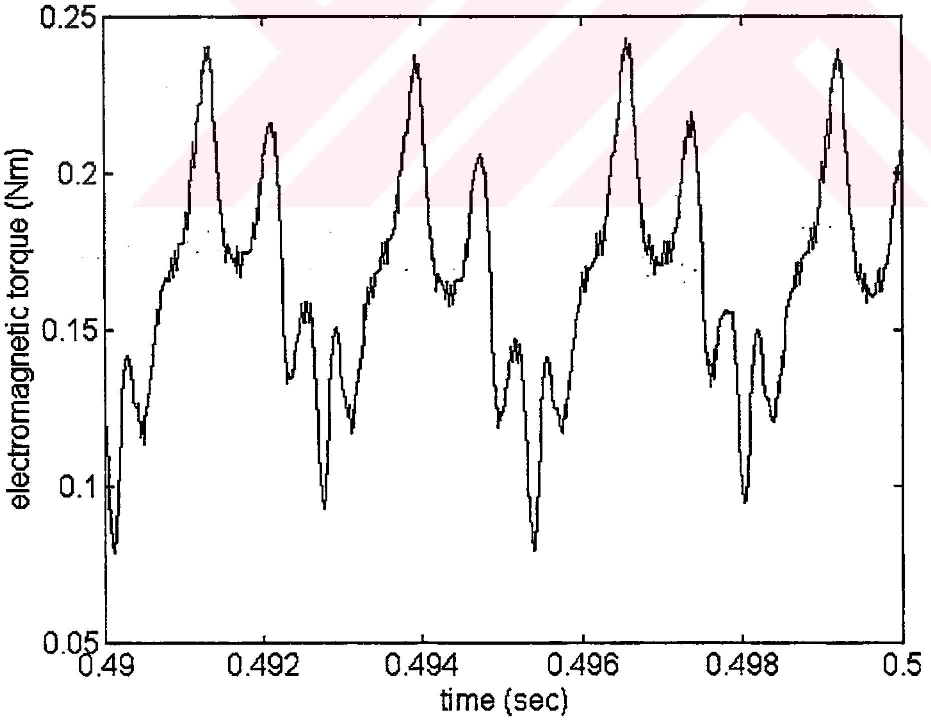

Figure 4.13-d) The extended electromagnetic torque for L=constant

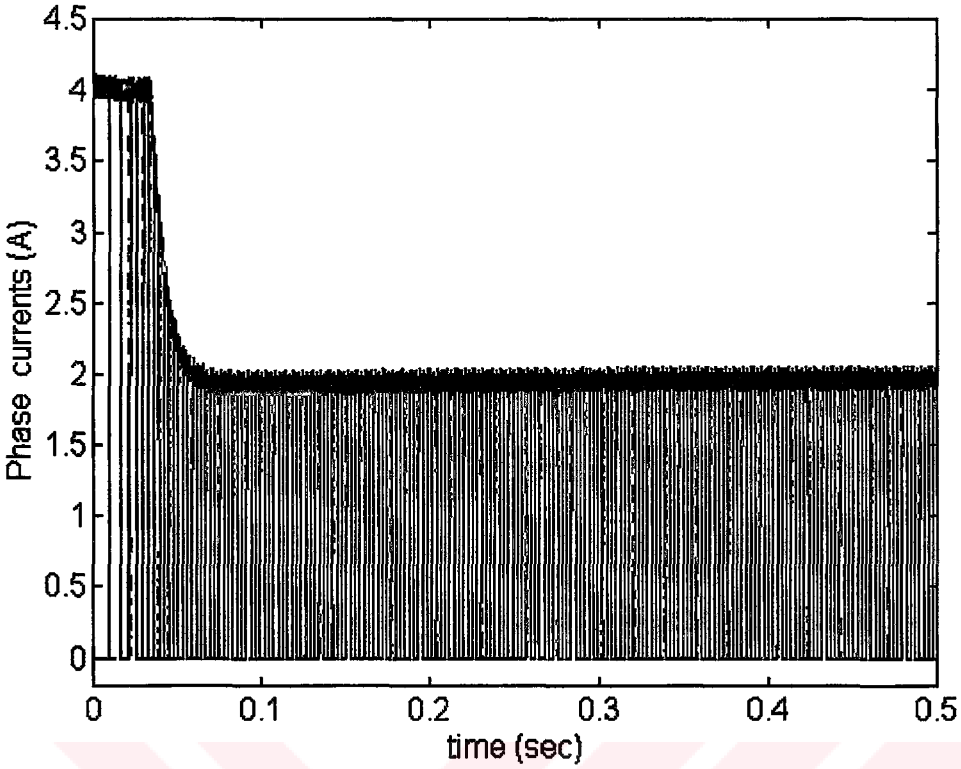

Figure 4.13-e) The phase currents for L=constant

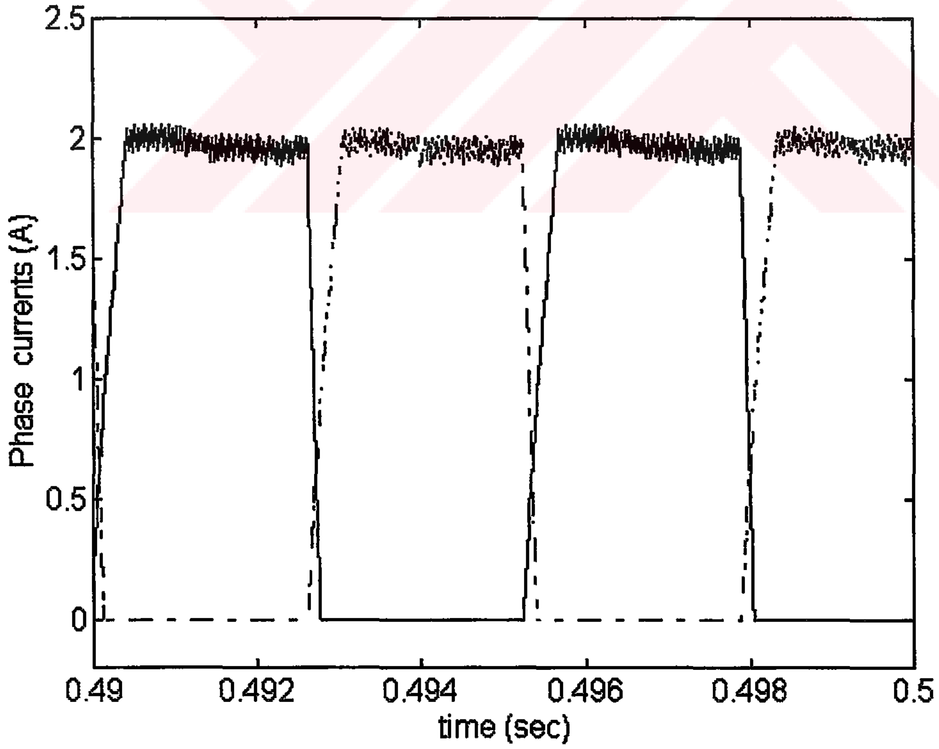

Figure 4.13-f) The extended phase currents for L=constant

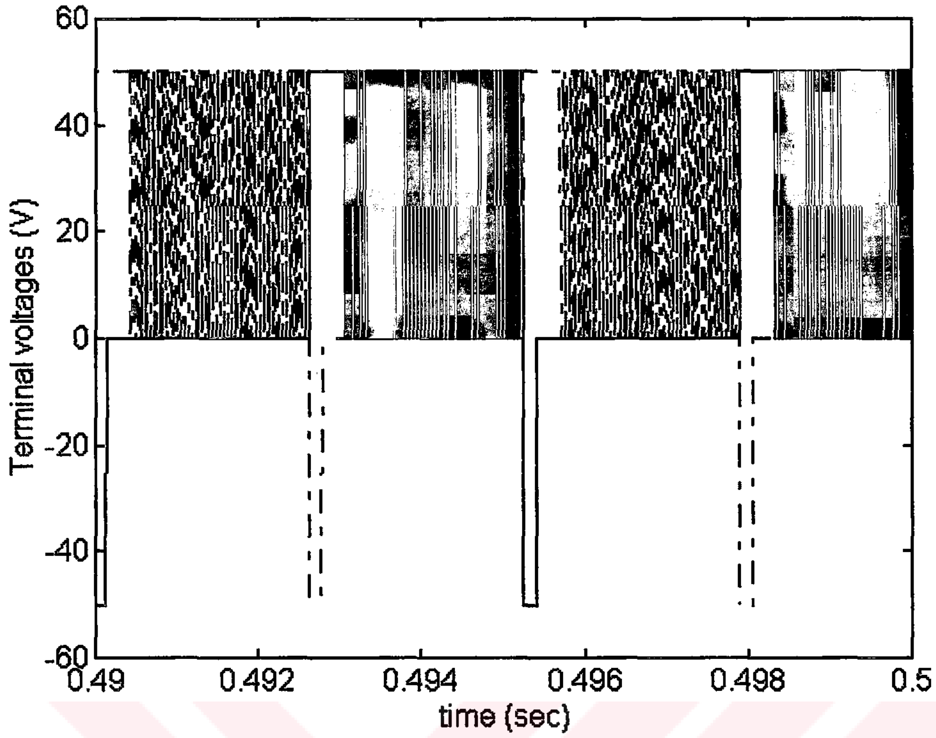

Figure 4.13-g) The extended terminal voltages for L=constant

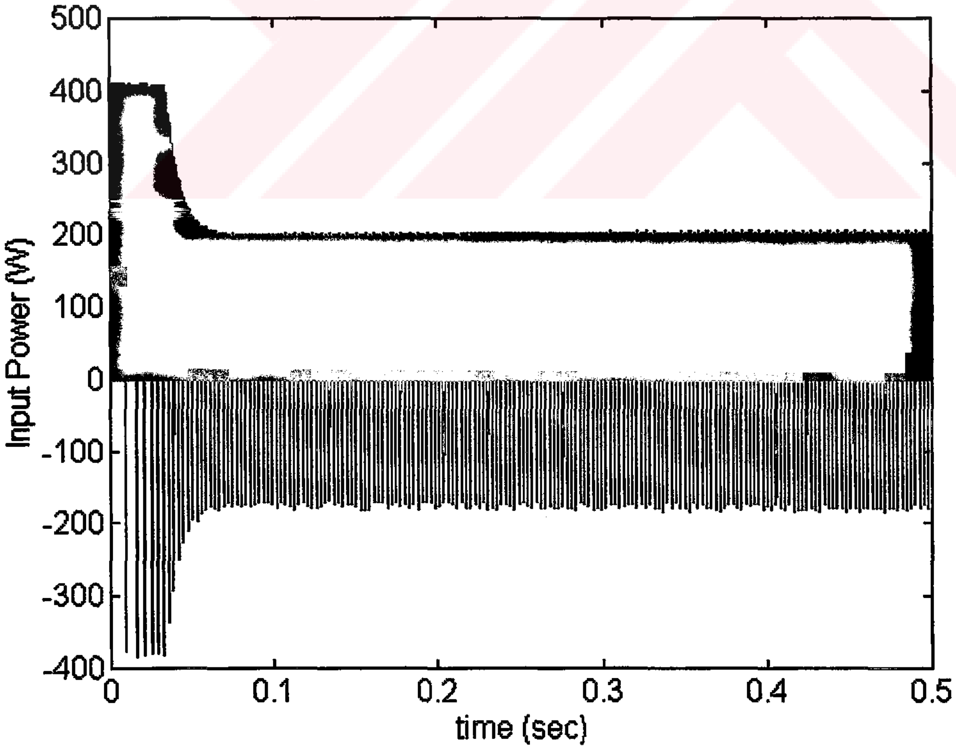

Figure 4.13-h) The input power for L=constant

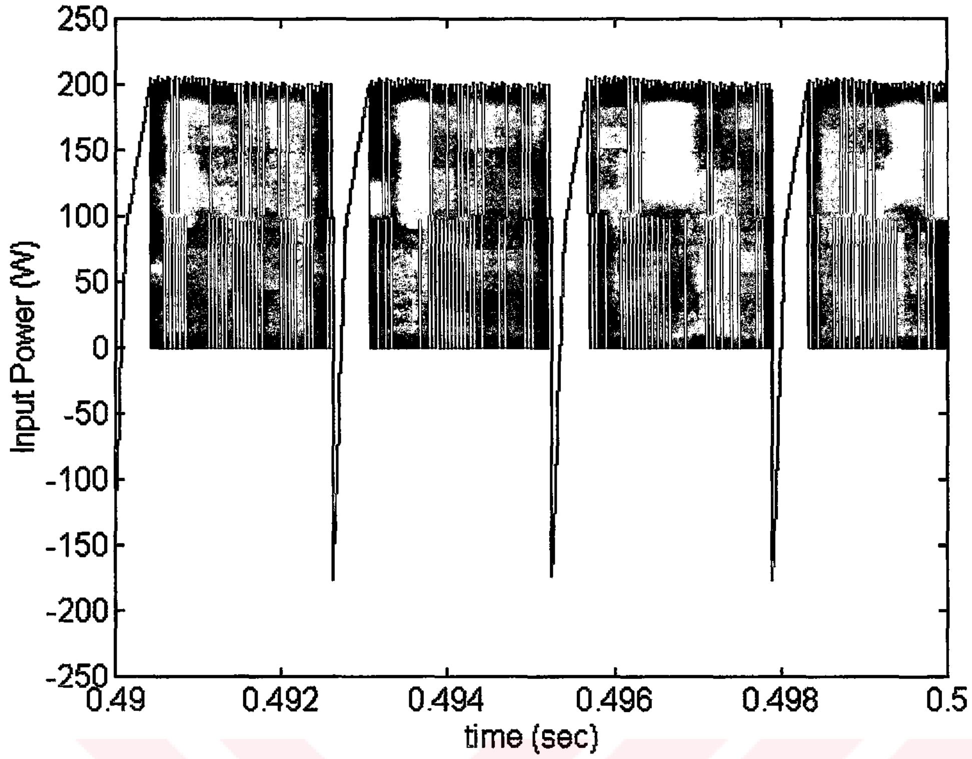

Figure 4.13-i) The extended input power for L=constant

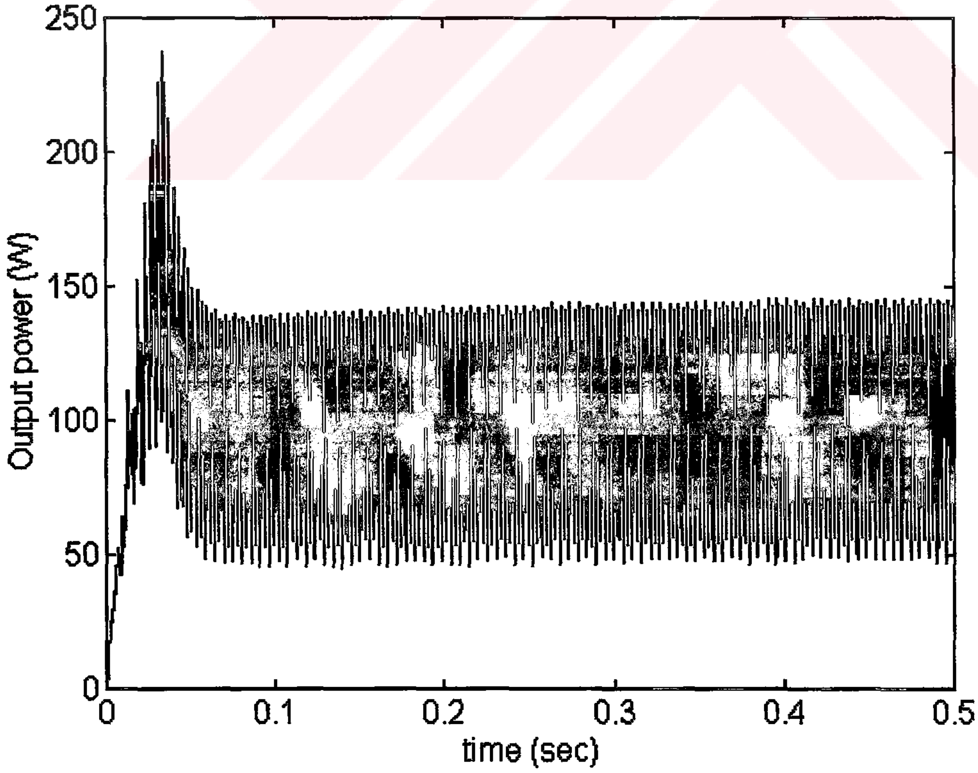

Figure 4.13-j) The output power for L=constant

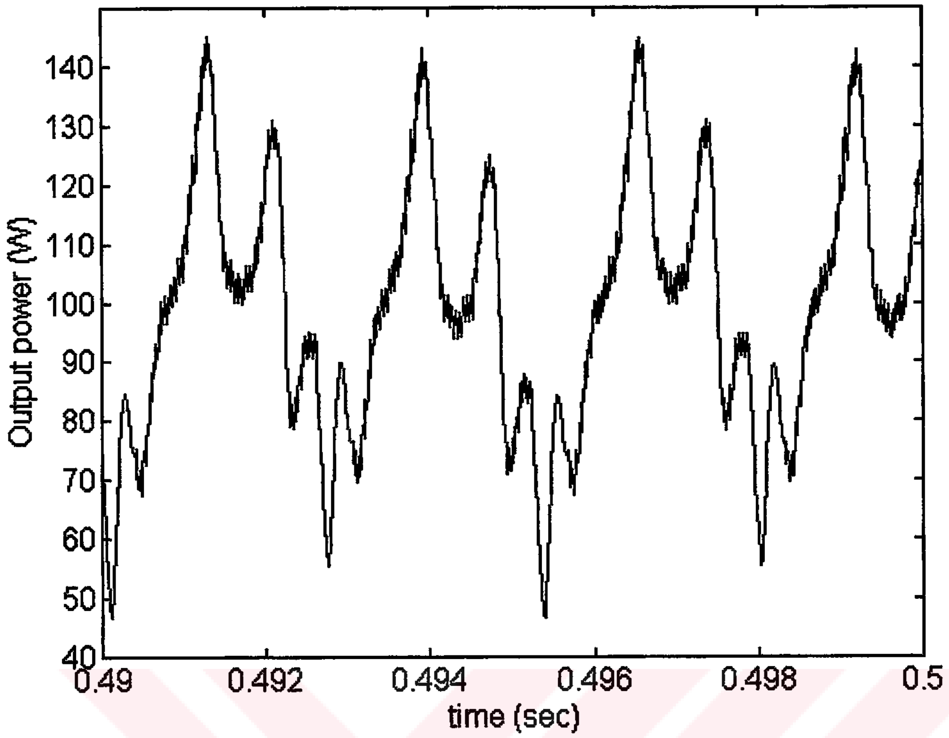

Figure 4.13-k) The extended output power for L=constant

If these graphics are compared with figure 4.10 and 4.11 obtained in the case that the inductance is a function of the rotor position. It is clearly observed that the results are very close. The reason of this that the relative permeability of permanent magnets used in this machine almost unity. Hence, the rotor can be considered as a cylindrical shape. This reasonable assumption yields the stator inductances to be constant and independent of rotor position.

4.6.5 Load Disturbances

In order to analyze the dynamic response of current and speed controllers the transients are applied to the system after the simulation has reached the steady state. The load torque and angular speed has been increased and decreased 20% in step change and the responses of the controllers to this change have been observed.

4.6.5.1 Applying Positive Step Change on Load Torque

The load torque is increased approximately from 0.17 Nm to 0.204 Nm while the machine is running. The response of the controllers and performance of the motor are investigated. The variation of the torque, rotor speed, armature current are given in figure 4.14 after the load torque is increased to 0.204 Nm at 0.3 seconds.

Figure 4.14-a shows the rotor speed with respect to the time. As the rotor is running at steady-state, the load torque is increased 20 % at 0.3 sec. Since the reference speed is kept at the same value from the input of the speed controller, the deviation of actual rotor speed from the reference value is controlled by the PI controller. PI controller reduces the error between reference and actual rotor speed. As it can be seen from figure 4.14-b, the maximum change on the rotor speed due to the disturbances on load is 2.1 %. This corresponds to 120 rpm of steady-state speed.

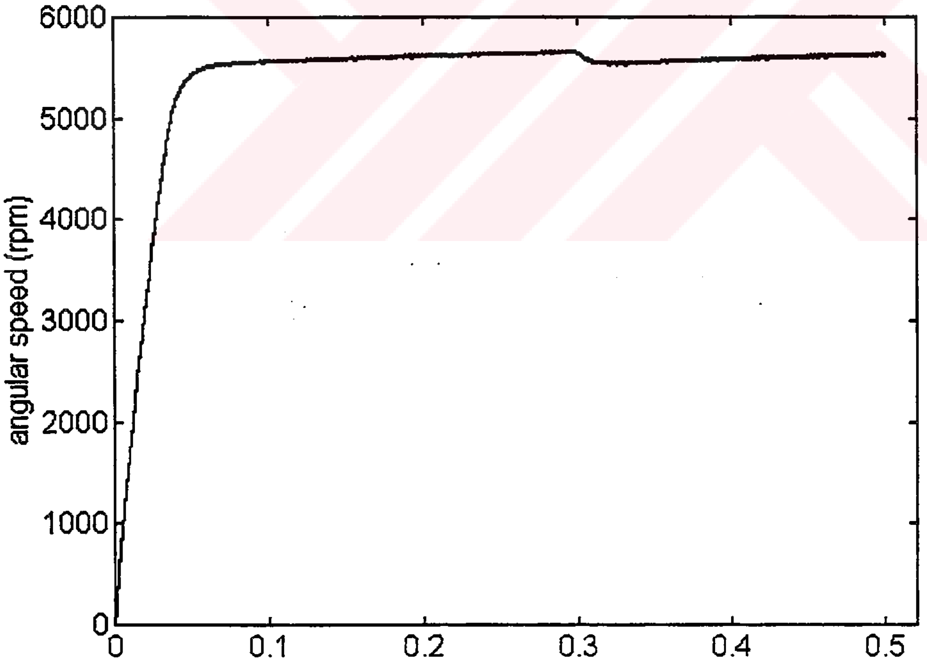

Figure 4.14-a) The rotor speed

The angular speed which suddenly decreases with the rise in the load torque will gradually increase. The electromagnetic torque and current will increase while the angular speed is decreasing. This is because, more current needs to be drawn from the source and more electromagnetic torque needs to be developed by the motor in order to balance the load.

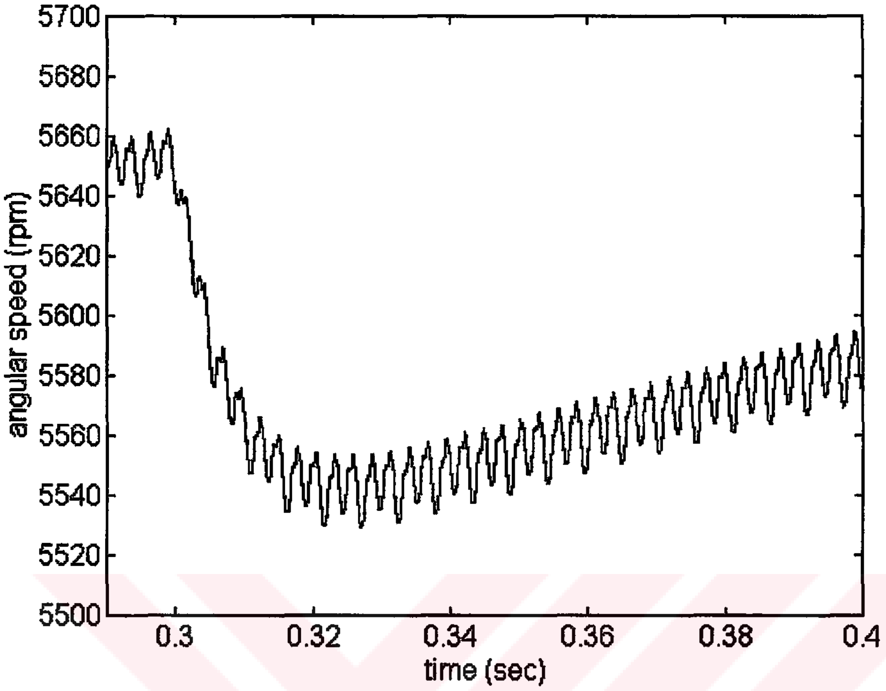

Figure 4.14-b) The extended rotor speed

The electromagnetic torque developed by the motor, as shown in figures 4.14-c and 4.14-d, has been increased, because of 20 % of disturbance applied on load torque.

As it is clearly observed from figure 4.14-e, the value of the phase current increases together with the electromagnetic torque. Since the biggest component of electromagnetic torque is developed by the stator current, the 20 % change on the load is balanced by approximately 20 % of change on the stator current. It should be noted that the magnitude of back emf does not change enormously since the rotor speed is kept almost constant at the pre-disturbed value because of speed controller. The stator current changes around 0.3Amp (from 2 Amps to 2.3 Amps) as it is shown from figure 4.14-f.

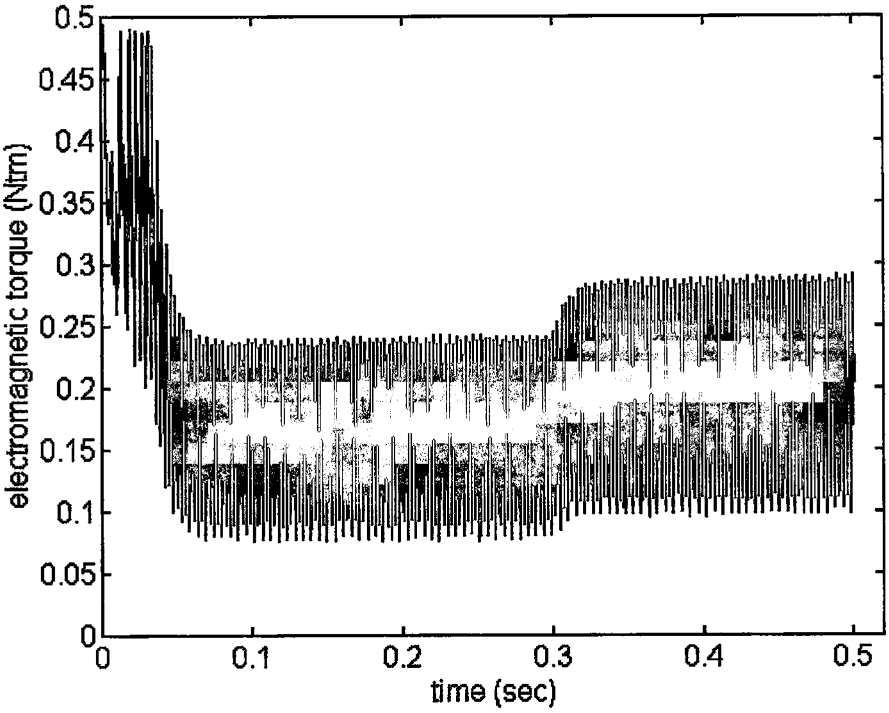

Figure 4.14-c) The electromagnetic torque

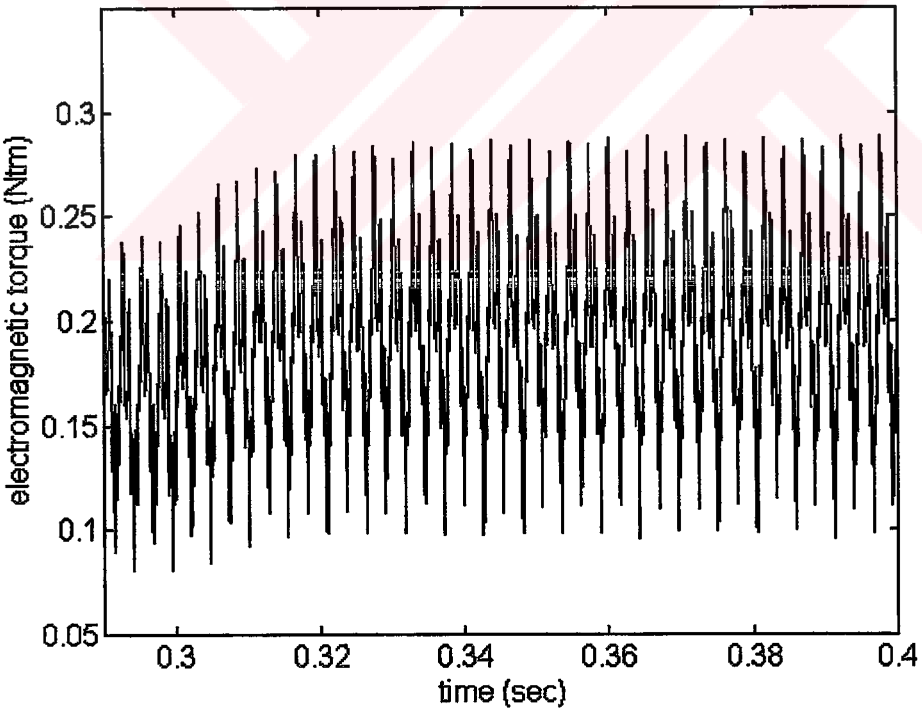

Figure 4.14-d) The extended electromagnetic torque

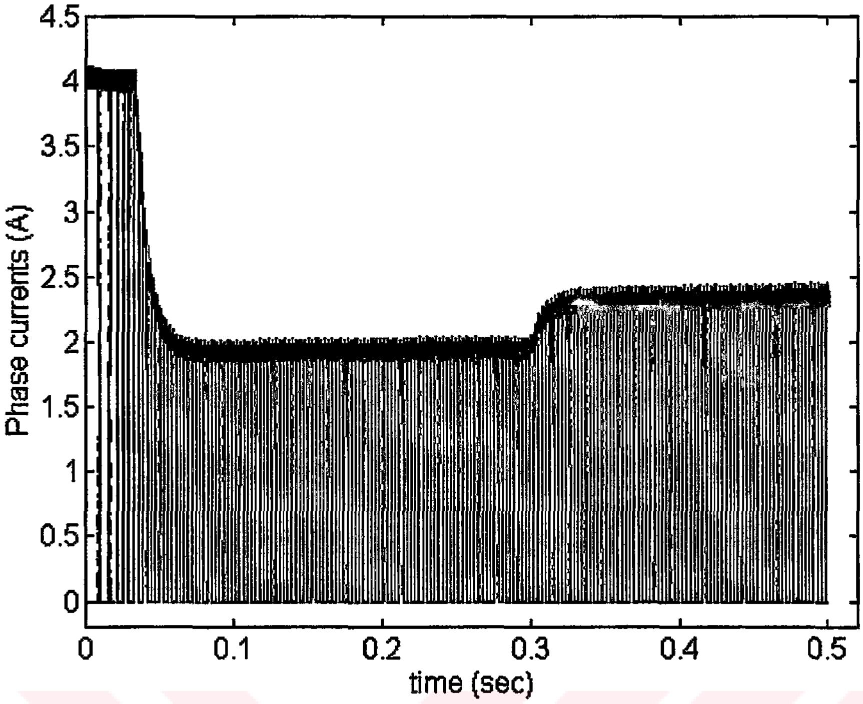

Figure 4.14-e) The phase currents

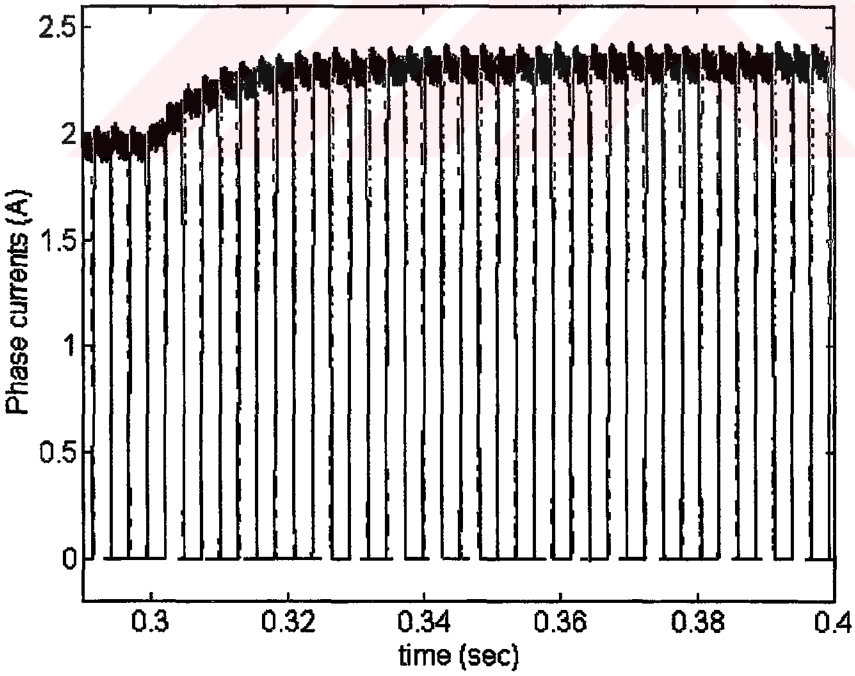

Figure 4.14-f) The extended phase currents

4.6.5.2 Applying Negative Step Change on Load Torque

The compatibility of the current and speed controllers for this drive has been also investigated by decreasing the load torque from 0.17 Nm to 0.141 Nm at 0.3 sec after the motor is run up. This change of load torque is also retained as 20 %. The results of simulation program are given in figure 4.15.

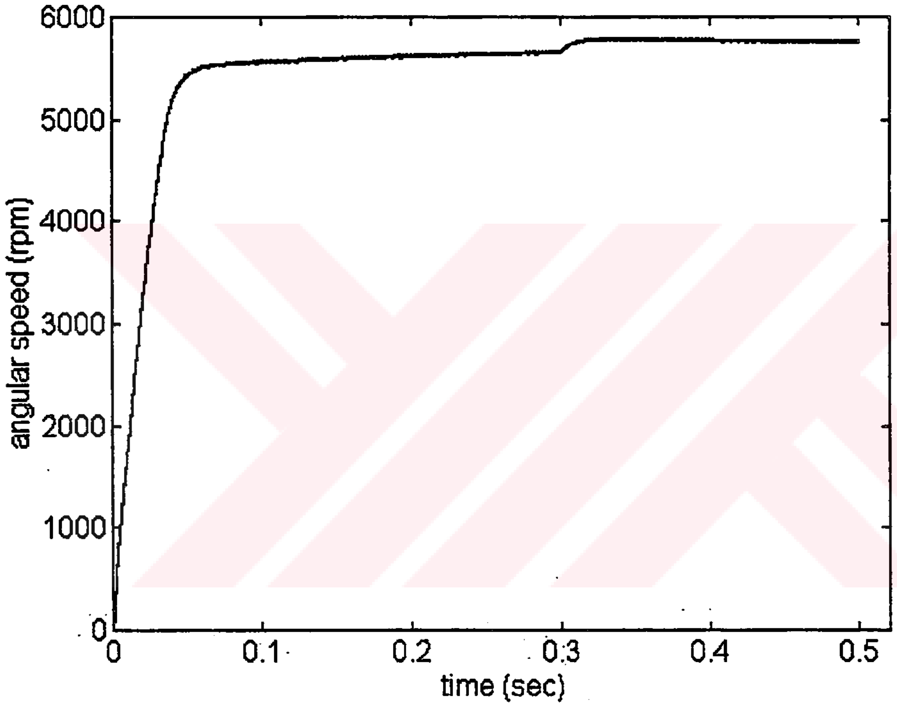

Figure 4.15-a) The rotor speed

The change of the rotor speed in time is presented in figures 4.15-a and figure 4.15-b. The load disturbance is being reflected to the rotor speed as it is clearly observed from figure 4.15-b, but this change is around 150 rpm corresponding to approximately 2.65 % as the load is decreased 20 %. The reason of why the actual rotor speed is almost constant is that the PI controller is used in speed feedback and is eliminating the error between actual and reference value of rotor speed.

Figures 4.15-c and figure 4.15-d show the electromagnetic torque developed by the motor. As it is clearly mentioned before, the average electromagnetic torque is almost proportional to the stator current. Therefore, the percentage of armature current change is more or less same as the value of that on the load torque.

Figure 4.15-e and 4.15-f show that the decrease of stator current is approximately 20 % following the same rate of change on the electromagnetic torque.

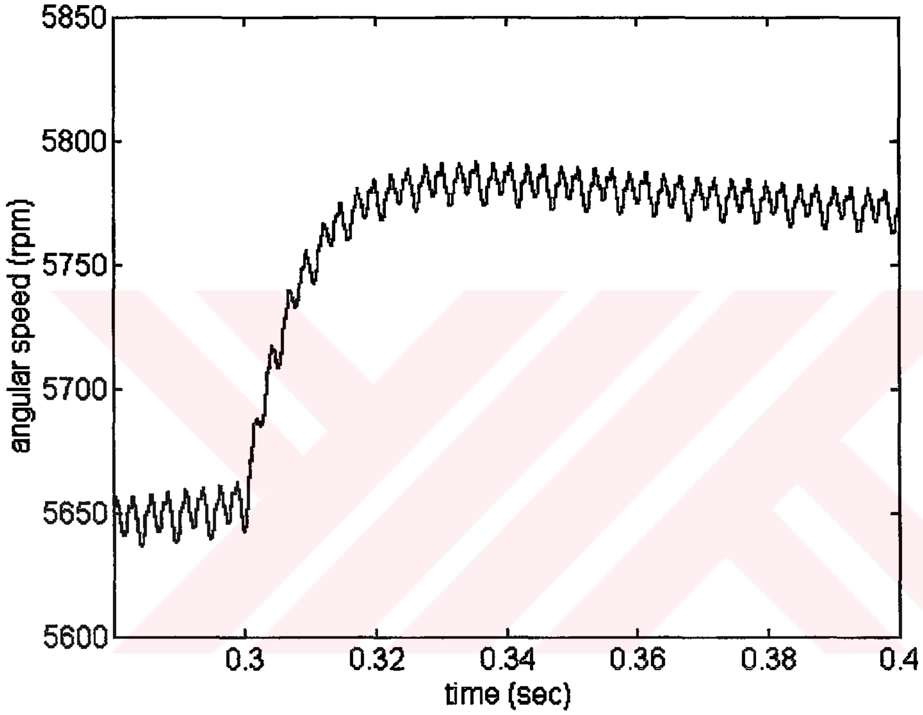

Figure 4.15-b) The extended rotor speed

With the decrease in the load torque, the motor is expected to draw less current from the source; to generate less electromagnetic torque.

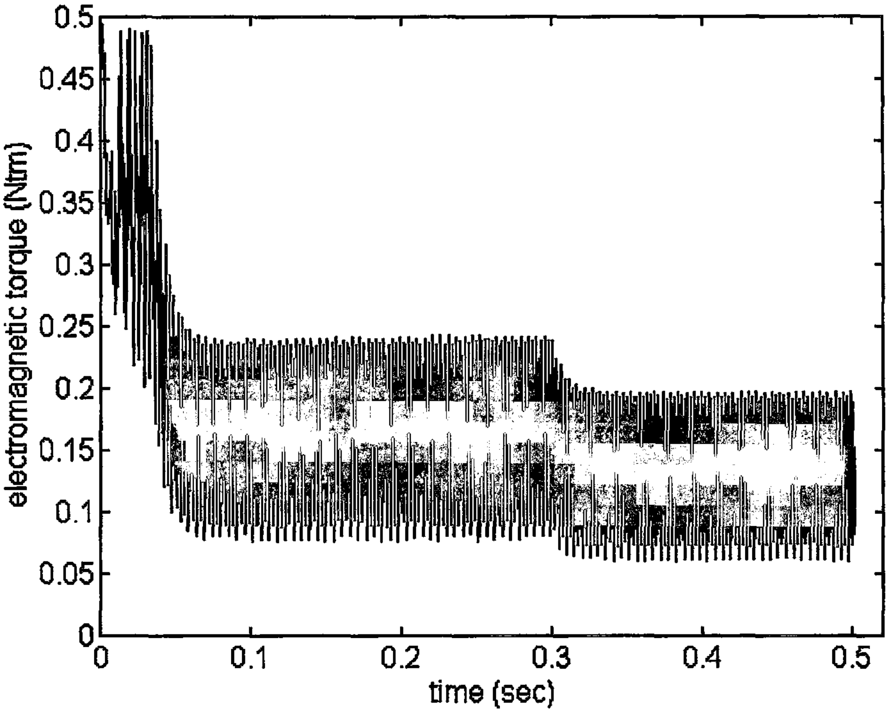

Figure 4.15-c)The electromagnetic torque

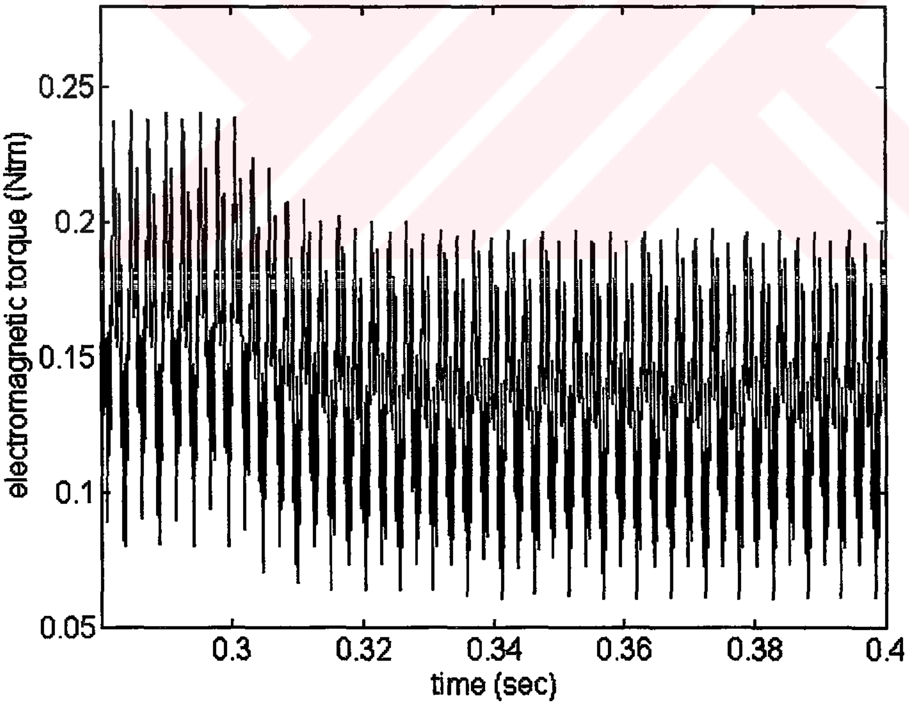

Figure 4.15-d) The extended electromagnetic torque

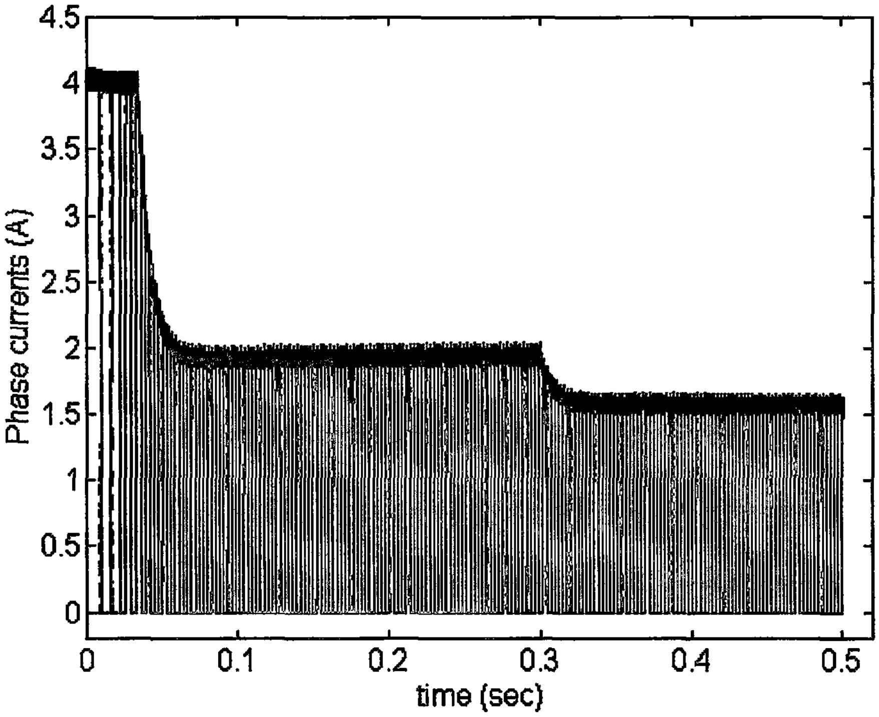

Figure 4.15-e) The stator current

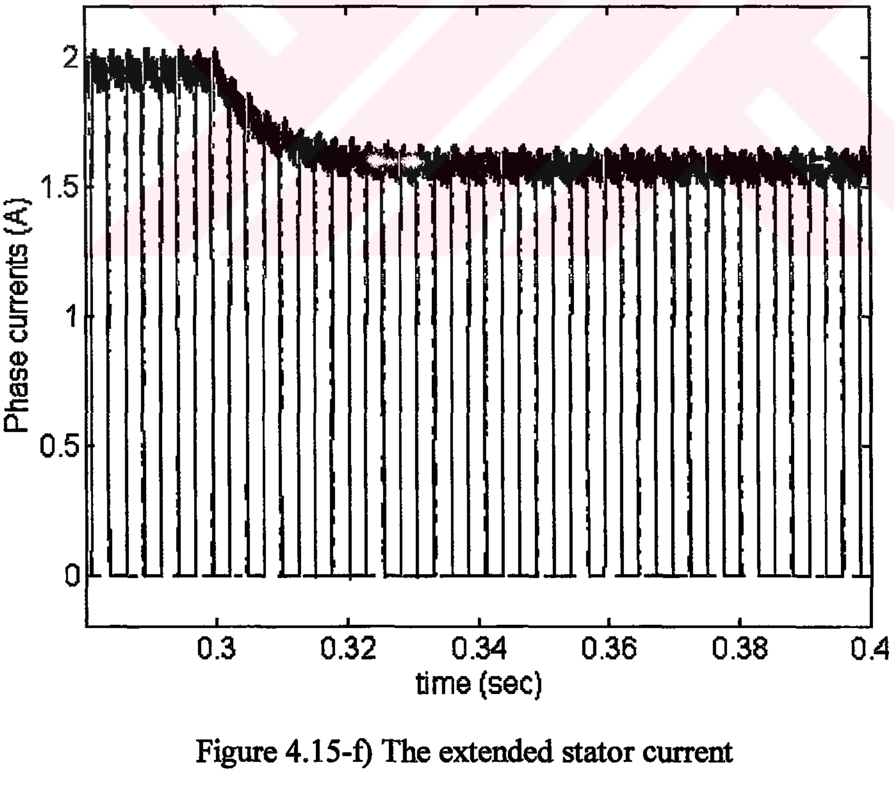

Figure 4.15-f) The extended stator current

4.6.5.3 Step Change on Reference Speed

In this part of study, the reference rotor speed is increased +%20 at 0.3 sec after the motor is run up. The variation of the state variables are examined. The results are presented in figure 4.16.

Figures 4.16-a and 4.16-b show the rotor speed with respect to time. As the reference speed is increased as a step function at 0.3 sec., the actual rotor speed settles down that value by taking an exponential rise, from pre-disturbed setting value to final setting, because of mechanical time constant of the machine.

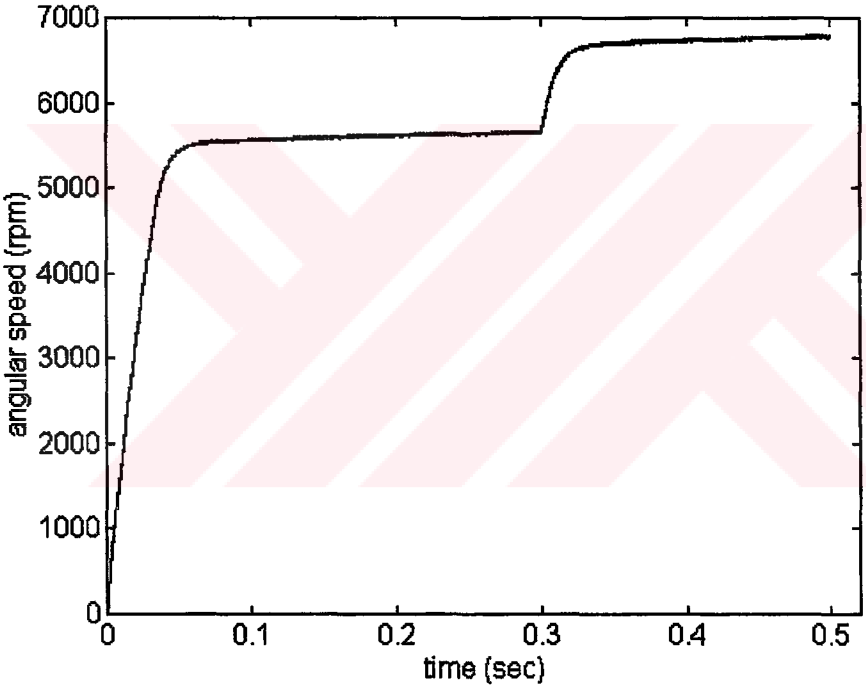

Figure 4.16-a) The rotor speed

.

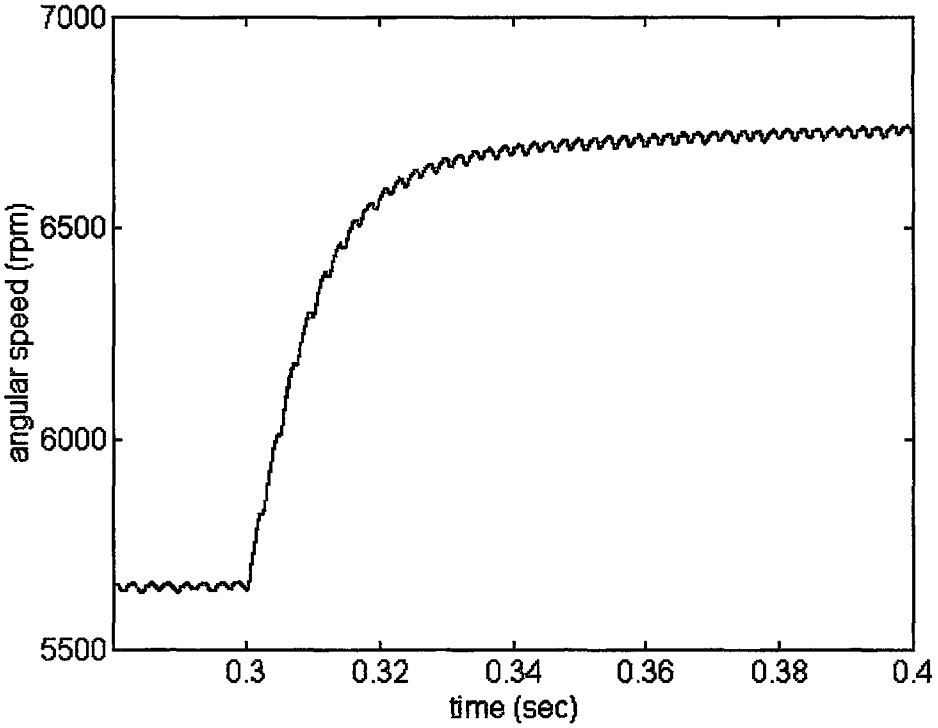

Figure 4.16-b) The extended rotor speed

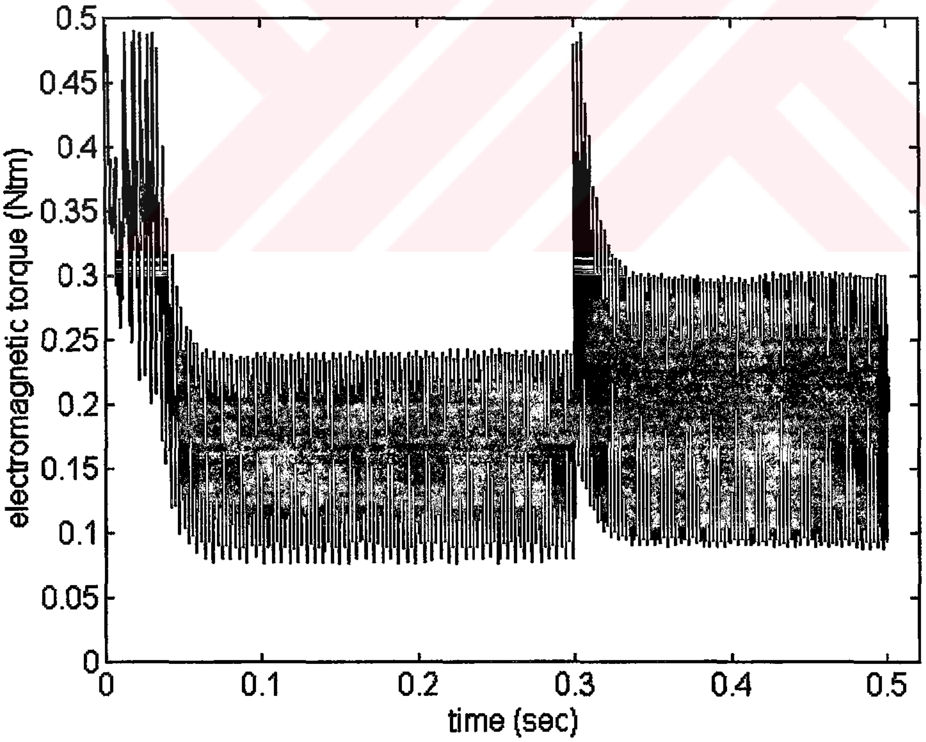

Figure 4.16-c)The electromagnetic torque

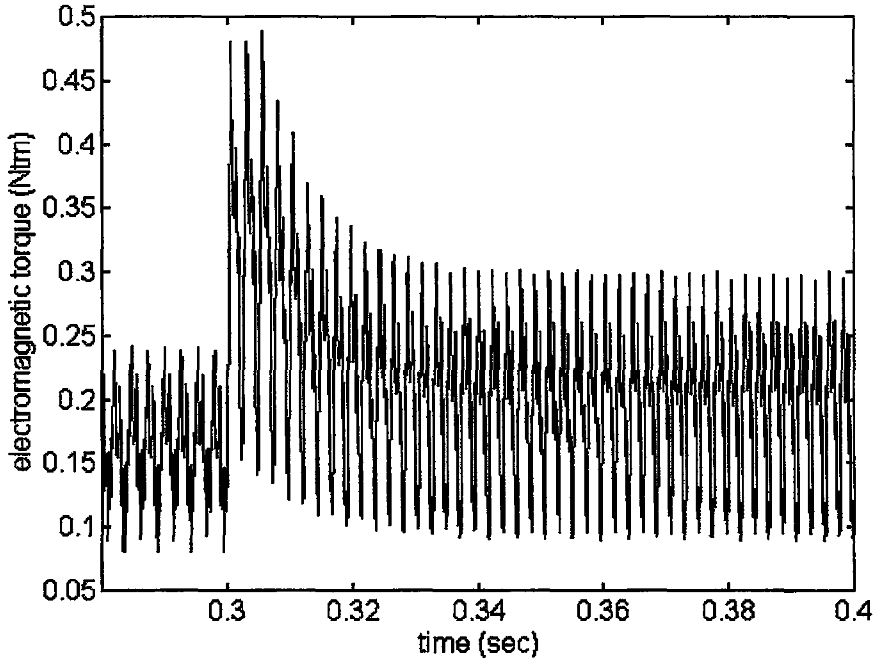

Figure 4.16-d) The extended electromagnetic torque

By increasing the rotor speed, the load torque which is described as a function of speed will increase. Finally, the torque developed by the motor will increase in order to balance the demand of the load as it is shown in figures 4.16-c and 4.16-d. The envelopes of the stator current and electromagnetic torque are similar to each other.

After increasing the rotor reference speed with a step change, the error between actual and reference speeds arises. As a result of that, the reference current which is followed by the actual current will increase for a while. This can be observed from figures 4.16-e and 4.16-f.

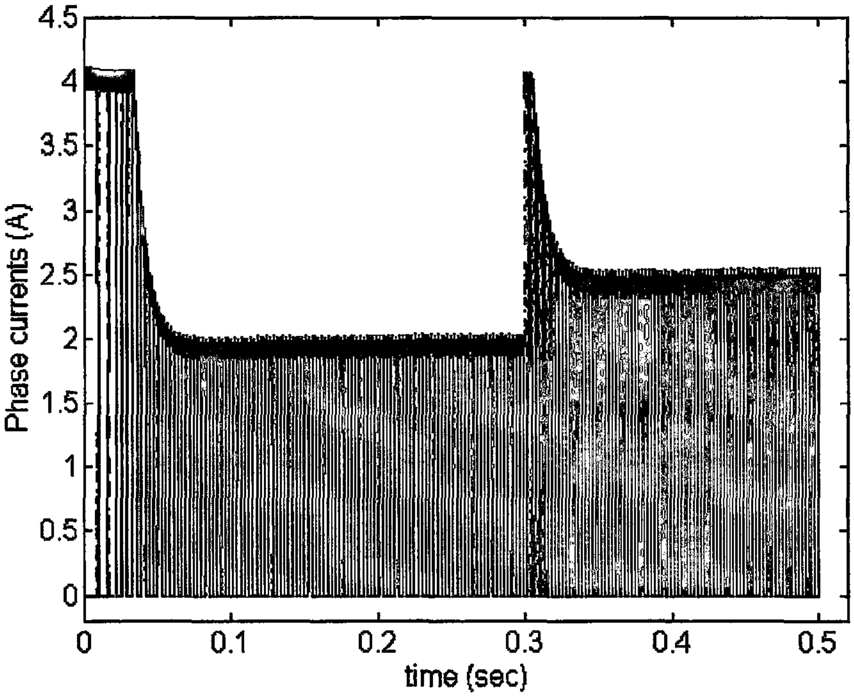

Figure 4.16-e) The stator currents

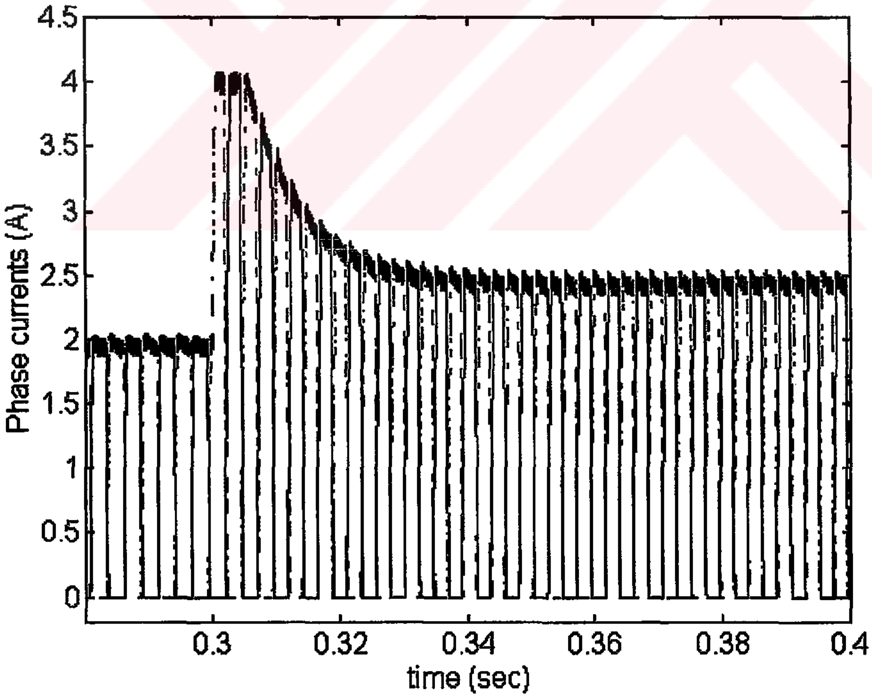

Figure 4.16-f) The extended stator currents

CHAPTER 5

CONCLUSION

5.1 General

In this study, a comprehensive computer aided parameter calculation and dynamic modeling approach have been presented for the prediction of two - phase performance of permanent magnet variable reluctance motor. The model, which uses the result of 2-dimension finite element method on machine parameter determination, has been developed for the simulation of a permanent magnet variable reluctance motor connected to a uni-directional chopper drive.

The finite element method has been used to compute permanent magnet variable reluctance motor parameters such as armature emf waveforms and armature inductance as a function of rotor position, which are key parameters in any permanent magnet variable reluctance motor drive simulation. In this thesis, self armature inductances have been calculated by using two different methods. The results from these have been compared to each other at rated load condition. Although the permanent magnets have been removed from the geometry of the machine in first method, the energy perturbation method which is second one is preferred especially at over load.

Prediction of machine winding inductances during the design and development stage, particularly in electronically commutated machines, where the high rates of current switching (high frequencies) are encountered is extremely important. This is because of the crucial role played by the inductive voltage drop terms (dλ/dt) in determining the overall performance of such machines. Such important role is also played in conventional machinery applications where accurate knowledge of values of winding inductance is key in successful and accurate performance and design calculations. This is to allow the determination of necessary design modifications in the magnetic circuits of such machines before final choices are made in the manufacturing process of such equipment, which would help avoid costly design changes at later stages.

A nonlinear model developed for the detailed analysis and simulation of the closed loop system , that includes the PI speed controller, hyteresis current controller and uni-directional chopper circuit, can reduce development and prototyping costs and time to manufacture. The performance prediction and dynamic simulation of a permanent magnet variable reluctance motor with its closed loop control are presented. The stator currents, electromagnetic torque, rotor speed and motor efficiency, have been directly obtained from the simulation program.

The detailed simulation of two - phase permanent magnet variable reluctance motor, which is firstly obtained in this study, is the key to optimal design using the analysis and simulation together with finite element analysis. A worthy estimation of design parameters of a permanent magnet reluctance motor requires the optimal control settings including the switching angles which can be performed through computer simulation. A comprehensive study here including voltage and current harmonics into the model enable a feasible alternative to the design of drive circuit in which the control parameters are obtained through extensive laboratory work .under the variable loads throughout the speed and torque ranges. The detailed simulation program employed in the design stage can increase the accuracy of performance prediction to meet the design specifications at minimum material cost and maximum efficiency.

5.2 Furtherwork

The following further studies are recommended for future investigation in detail.

1. As it is mentioned in section 3.2.2, design optimization is out of scope of this thesis. The motor dimensions are obtained through appropriate design equations and are confirmed through trail and error by using finite element analysis. In the performance analysis the motor efficiency is found to be around % 80-90 as being shown in figure 4.12. Optimum design studies on the motor dimensions can be carried out in order to maximize the motor efficiency.

2. In this study, the results of the analysis done with the help of pc have not been compared with the experiments done under in laboratory conditions. Another step to follow the study is the construction of the motor and drive circuit and also the experimental measurement of the motor parameters, backemfs, torques and efficiency.

3. In the thesis, the parameters of the PI controller which are used in speed controller have been obtained as appropriate values by means of trial and error. The optimum design of the controller can be carried out by using the modeling approach consisting of constant inductance matrix given in equation (4.46).

REFERENCES

Acarnley, P.P., Hill, R.J. & Hooper, C.W. (1985). Detection of Rotor Position in Stepping and Switched Motors by Monitoring of Current Waveforms. IEEE Tran.on Industrial Electronics, IE-32, 215-222

Acarnley, P.P. (1992). Stepping Motors: a Guide to Modern Theory and Practice (3 th ed.). London: Peter Peregrinus Ltd.

Ackermann, B., Janssen, J.H.H, Sottek, R. & Steen, R.I.V. (1992). New Technique for Reducing Cogging Torque in a Class of Brushless dc Motors. IEE Proceedings-B, 139,315-320

Akpınar E. & Pillay P. (1990). Modeling and Performance of Slip Energy Recovery Induction Drives. IEEE Tran. on Energy Conversion, 5, 203-210

Alhamadi, M.A. & Demerdash, N.A. (1991). Modeling of Effects of Skewing of Rotor Mounted Permanent Magnets on the Performance of Brushless DC Motors. IEEE Tran.on Energy Conversion, 6, 721-729

Alhamadi, M.A. & Demerdash, N.A. (1994). Three Dimensional Magnetic Field Computation by a Coupled Vector -Scalar Potential Method in Brushless DC Motors with Skewed Permanent Magnet Mounts-The No-Load and Load Results. IEEE Tran.on Energy Conversion, 9, 15-25

Alhamadi, M.A. & Demerdash, N.A. (1994). Modeling and Experimental Verification of the Performance of a Skew Mounted Permanent Magnet Brushless DC Motor Drive with Parameters Computed from 3D-FE Magnetic Field Solutions. IEEE Tran.on Energy Conversion, 9, 26-35

Ansys User Manual Vol:1 Procedure (1992)

Ansys Electromagnetics a Revision 5.0 Tutorial (1992).

Ansys Magnetic User's Guide for Revision 5.0, Vol:1, (1993).

Carlson, R., Mazenc, M.L. & Fagundes, C.D.S. (1992). Analysis of Torque Ripple Due4 to Phase Commutation in Brushless dc Machines. IEEE Tran. on Industry Appl., 28, 632-638

Chari, M.V.K., Bedrosian, G., D'Anglelo, J. & Konrad, A. (1993). Finite Element Applications in Electrical Enginnering. IEEE. Tran. on Magnetics, 29, 1306-1314

Chen, S., Binns, K.J., Liu, Z. & Shimmin, D.W. (1992). Finite Element Analysis of the Magnetic Field in Rare-Earth Permanent Magnet Systems with Consideration of Temperature Dependence. IEEE. Tran. on Magnetics, 28, 1303-1306

Clenet, S., Lefévre, Y., Sadowski, N., Astier, S. & Lajoie-Mazenc, M. (1993). Compensation of Permanent Magnet Motors Torque Ripple by Means of Current Supply Waveshapes Control Determined by Finite Element Method. IEEE Tran.on Magnetics, 29, 2019-2023

Craiu, O., Raduti, C. & Dan, N. (1995) Space-Time Analysii of the Induced Voltage in the Windings of Electrical Machines. ACEMP95 5-7 June Kuşadası Turkey, 1, 28-31

Craiu, O., Dan, N. & Badea, E.A. (1995). Numerical Analysis of Permanent Magnet DC Motor Performances. IEEE Tran.on Magnetics ,31, 3500-3502

Davey, K.R. (1995). Magnet Design Optimization Using Variable Metrics. IEEE Tran. on Magnetics, 31, 3566-3568

Demerdash, N.A., Fouad, F.A. & Nehl, T.W. (1982). Determination of Winding Inductances in Ferrite Type Permanent Magnet Electric Machinery by Finite Elements. IEEE Tran.on Magnetic, MAG-18, 1052-1054

Demerdash, N.A. & Nyamusa, T.A.(1985). Comparison of Effects of Overload on Parameters and Performance of Samarium-Cobalt and Strontium-Ferrite Radially Oriented Permanent Magnet Brushless DC Motors. IEEE Tran.on Power Apparatus and Systems, PAS-104, 2223-2231

Demerdash, N.A.O, Hijazi, T.M. & Arkadan, A.A. (1988). Computation of Winding Inductances of Permanent Magnet Brushless DC Motors with Damper Winding by Energy Perturbation. IEEE Tran.on Energy Conversion, 3, 705-713

Demerdash, N.A.O. & Alhamadi, M.A. (1996). Three Dimensional Finite Element Analysis of Permanent Magnet Brushless DC Motor Drives-Status of the State of the Art. IEEE Tran.on Industrial Electronics,43,268-275

Dexin, X., Baodong, B., Yingying, Y. & Fengxiang, W. (1995). Shape Design Optimization in Non-Linear magnetic Problems Using Simulated Annealing with Complex Strategy. IEEE. Tran. on Magnetics, 31, 3569-3571

Ermiş, M., Ertan, H.B., Akpınar,E. & Ülgüt, F. (1992). An Autonomous Wind Energy Conversion System with a Simple Controller for Maximum Power Transformer. IEE Proceedings-B, 139, 421-427

Fink D. G. & Beaty H.W. (1993). Standard Handbook for Electrical Engineers (13th ed.). McGraw Hill Inc.

Fitzgerald A. E., Kingsley C. & Umans S. D. (1992) Electrical Machinery 5th edition in SI units. Mc Graw-Hill Book Company

Gangla, V. & Ree, J.D.L. (1991). Electromechanical Forces and Torque in Brushless Permanent Magnet Machines. IEEE Tran.on Energy Conversion,6, 546-551

Hwang, M.S. & Lieu, D.K. (1994). Design Techniques for reduction of Reluctance Torque in Brushless Permanent Magnet Motors. IEEE Tran. on Magnetics, 30, 4287-4289

Hwang, M.S, & Lieu, D.K. (1995). Reduction of Torque Ripple in Brushless Dc Motors. IEEE Tran. on Magnetics, 31, 3737-3739

Ho, S.L., Fu, W.N. & Wong, H.C.(1995). Status of the Application of Finite Element Analysis in Induction Machines. ACEMP95 5-7 June Kuşadası Turkey, 1, 37,42

Hung, J.Y. & Ding, Z. (1993). Design of Currents to Reduce Torque Ripple in Brushless Permanent Magnet Motors. IEE Proceedings-B, 140, 260-266

Ishikawa, T. & Slemon, G.R. (1993) A Method of Reduction Ripple Troque in Permanent Magnet Motors without Skewing. IEEE Tran. on Magnetics, 29, 2028-2031

Kardestuncer, H. & Norrie, D.H. (1987). Finite Element Handbook. Mc Garw-Hill Book Company.

Kusko, A. & Peeran S. M. (1987) BLDC Motors Using Unsymmetrical Field Magnetization IEEE Tran.on Industry Applications, IA-3 , 319-326

Li, S.H-Y., Liang, F., Zhao, Y.& Lipo, T.A. (1995). A Doubly Salient Doubly Excited Variable Reluctance Motor. IEEE Tran.on Industry Applications, 31 ,99-106

Li, T. & Slemon, G. (1988). Reduction of Cogging Torque in Permanent Magnet Motors. IEEE Tran. on Magnetics, 24, 2901-2903

Lorenz, R. D. (1991). Performance and Design of Permanent Magnet AC Motor Drives. Sensors and Signal Converters in PM ac Motor Drives.

Low, T-S., Bi, C. & Chang, K-T. (1996). Motor "Identity"- a Motor Model for Torque Analysis and Control. IEEE Tran. on Industrial Electronics, 43, 285-291

Marinescu, M. & Marinescu, N. (1988). Numerical Computation of Torques in Permanent Magnet Motors by Maxwell Stresses and Energy Method. IEEE Tran.on Magnetics, 24, 463-466

Marinescu, M. & Marinescu, N. (1992). New Concept of permanent Magnet Excitation for Electrical Machines. Analytical and Numerical Computation. IEEE Tran. on Magnetics, 28, 1390-1393

Miller, T.J.E. (1989). Brushless Permanent-Magnet and Reluctance Motor Drives. New York: Oxford University Press.

Miller, T.J.E. & Rabinovici, R. (1994). Back-EMF Waveforms and Core Losses in Brushless DC Motors. IEE Proc. Electr. Power Appl., 141, 144-154

Miraoui, A., Fang, L.D., Li, K. & Charbonnier, S. (1992) Design and Optimization of a Small Brushless Dc Permanent Magnet Motor. ACEMP92 27-29 May Kuşadası Turkey, 2, 754- 757

Moallem, M. & Ong, C. M. (1990). Predicting the Torque of a Switched Reluctance Machine From its Finite Element Field Solution. IEEE Tran. on Energy Conversion ,5, 733-739

Neff, H. P. (1991). Introductory Electromagnetics. John Willey.

Nehl, T.W., Fouad, F.A., Demerdash, N.A. & Maslowski,E.A. (1982). Dynamic Simulation of Radially Oriented Permanent Magnet-Type Electronically Operated Synchronous Machines with Parameters Obtained from Finite Element Field Solutions. IEEE Tran.on Industry Applications,IA-18,172-182

Nehl, T.W., Fouad, F.A. & Demerdash, N.A. (1982). Determination of Saturated Values of Rotating Machinery Incremental and Apparent Inductances by an Energy Perturbation Method. IEEE Tran.on Power Apparatus and Systems , PAS-101, 4441-4451

Nehl, T.W., Demerdash, N.A. & Fouad, F.A. (1985). Impact of Winding Inductances and Other Parameters on the Design and Performance of Brushless Dc Motors. IEEE Tran. on Power Apparatures Systems, PAS-104, 2206-2213

Nehl, T. W. & Demerdash, N. A. O. (1992). Direct Current Permanent Magnet Motors in Adjustable Speed Drives. IEEE Tutorial on Adjustable Speed Drives, 86-108

Nehl, T. W. & Demerdash, N. A. O. (1992). Finite Element - State Space Modeling Environments for Electrical Motor Drives. IEEE Tutorial on Adjustable Speed Drives, 109-126

Petkovska, L. & Cundev, M. (1992). Numerical Calculation of Torques in the Electronically Operated Permanent Magnet Synchronous Motor with Quantities Obtained from 3D-FEM's Field Computation. ACEMP92 27-29 May Kuşadası Turkey, 1, 372-377

Petkovska, L., Cundev, M. & Cvetkovski, G. (1995). FEM Concept of Torque Optimisation in a DC Permanent Magnet Motor.ICEMP95 5-7 June Kuşadası Turkey, 1, 22-27

Plonsey, R. & Collin, E.R. (1961). Principles and Applications of Electromagnetic Fields. Mc Graw-Hill Book Company

Rahman, M.A. & Zhou, P. (1991). Determination of Saturated Parameters of PM Motors Using Loading Magnetic Fields. IEEE Tran. on Magnetics ,5, 3947-3950

Richard, G. & Pillay, P. (1994). Large Process Industry Motor Drive Performance and Power Quality Analysis. Research Raport EPRI RP3245-03 University of New Orleans

Rizzo, M., Savani, A. & Turowski, J. (1991). Influence of Number of Poles on the Torque of dc Brushless Motor with Auxilary Salient Poles. IEEE Tran. on Magnetics, 27, 5420-5422

Rizzo, M., Savini, A. & Turowski, J. (1992). Comparison of Performances of Brushless Electronically Controlled Small DC Motors with Various Magnetic Circuits. ACEMP92 27-29 May Kuşadası Turkey, 2, 614-617

Rizzo, M. (1992). Comparative Study of Two Permanent Magnet Brushless DC Micromotors on the Basis of Magnetic Field Analysis. ACEMP92 27-29 May Kuşadası Turkey, 1, 166- 170

Rizzo, M., Savani, A., Turowski, J. & Wiak, S. (1994) Optimization of Magnwtic Circuits of Dc Brushless Motors. NATO-Modern Electrical Drives Proceedings, 91-95

Salon, S., Bhatia S. & Burow D. (1997) Some Aspects of Torque Calculation in Electrical Machines. IEEE Tran .on Magnetics, 33, 2018-2021

Sadowski, N., Lefévre, Y., Lajoie-Mazenc, M. & Cros, J. (1992). Finite Element Torque Calculation in Electrical Machines While Considering the Mouvement. IEEE Tran .on Magnetics, 28, 1410-1413

Slemon G. R. (1994). Electrical Machines for Variable - Frequence Drives. IEEE Proceeding, 8, 1123-1138

Slemon G. R. (1991). Design of Permanent Magnet AC Motors for Variable Speed Drives. Performance and Design of PM Ac Motor Drives IEEE Tutorial , 3-1 - 3-25

Slemon G. R. (1994). On the Design of High -Performance Surface- Mounted PM Motors. IEEE Tran .on Industry Applications, 30, 134-140

Slemon G. R. & Liu X. (1992). Modeling and Design Optimization of PM Machines. Electrical Machines Power System, 2, 71-92

Sokira, T. J. & Jaffe, W. (1990). Brushless dc Motors Electronics Commutation and Controls Tab Book Inc.

Strnat, K. J. (1991). Magnet Materials and Properties. Performance and Design of Permanent Magnet Ac Motor Drives IEEE Tutorial, 2-1 - 2- 34

Turowski, J., Komeza, K., Pelikant, A., Wiak, S., Rizzo, M. & Savini, A.(1992). Electromagnetic Field Problems in Small Electronic Controlled Motors. ACEMP92 27-29 May Kuşadası Turkey, 2, 430-437

United State Steel (1980). Nonoriaented Sheet Steel for Magnetic Applications California

Wing, M. & Gieras, J.F. (1992). Calculation of the Steady State Performance for Small Commutator Permanent Magnet DC Motors:Classical and Finite Element Approaches. IEEE Tran.on Magnetics, 28, 2067-2071

APPENDIX A

```
      REAL XO(7), YDOT(7), XEND(7), VLT(2), VOLT(4)
      REAL TO, H, PI, PIN, POUT, PRES
      REAL RD1, RD2, RD3, RD4
      REAL TE, TE1, TE2, TE3, TE4, KLM1, KLM2
      REAL IREF, WREF, KT, KP, F
      INTEGER I, N, BR, JK
c*
      DO 10 I=1, 7
      XO(I)=0.0
10    CONTINUE
c*
      TO=0.0
      H=1.E-5
      BR=0.0
      KP=1.95
      KT=75
      WREF=600.
c*
      PI = 2*ASIN(1)
      RD1 = 0.0
      RD2 = PI*(45.0/180.0)
      RD3 = PI*(135.0/180.0)
      RD4 = PI
c*
      OPEN(20,FILE=’result1.plo’STATUS=’old’)
      OPEN(25,FILE=’result2.plo’STATUS=’old’)
      OPEN(30,FILE=’result3.plo’STATUS=’old’)
      OPEN(35,FILE=’result4.plo’STATUS=’old’)
c*
      DO 20 I=1,50000
      JK=0.0
c*
            CALL HYSCC (IREF,JK,XO,VLT,BR)
c*
            CALL RKSYST(JK,BR,VLT,TO,XO,XEND,YDOT,H,N,VOLT)
c*
             CALL ETORK (XO,TE,TE1,TE2,TE3,TE4,KLM1,KLM2)
c*
      F = KP*(WREF-XO(2)) + XO(7)
```

```
       IREF=F/KT
       IF(IREF.GT.4.0) THEN
            IREF=4.0
       ENDIF
       POUT=TE*XO(2)
c*
       IF (BR.EQ.2.AND.XO(3).EQ.0) THEN
            PIN=(VLT(1)*XO(3)+VLT(2)*XO(4)+VLT(1)*XO(5)+VLT(2)*XO(6))
            VOLT(1)=VLT(1)
            VOLT(2)=VLT(2)
       ENDIF
       IF (BR.EQ.2.AND.XO(3).NE.0) THEN
            PIN=(VOLT(1)*XO(3)+VOLT(2)*XO(4)+VOLT(1)*XO(5)
            +VOLT(2)*XO(6))
       ENDIF
       IF (BR.EQ.3.AND.XO(4).EQ.0) THEN
            PIN=(VLT(1)*XO(3)+VLT(2)*XO(4)+VLT(1)*XO(5)
            +VLT(2)*XO(6))
            VOLT(1)=VLT(1)
            VOLT(2)=VLT(2)
       ENDIF
       IF (BR.EQ.3.AND.XO(4).NE.0) THEN
            PIN=(VOLT(1)*XO(3)+VOLT(2)*XO(4)+VOLT(1)*XO(5)
            +VOLT(2)*XO(6))
       ENDIF
c*
      PRES=0.892*(XO(3)*XO(3)+XO(4)*XO(4)+XO(5)*XO(5)+XO(6)*XO(6))
c*
       WRITE(20,*) XO(1), XO(2)
       WRITE(25,*) XO(3), XO(4)
       WRITE(30,*) TO, TE
       WRITE(35,*) PIN, POUT
c*
20     CONTINUE
     STOP
     END
c*
c* ************************************************************
c*
       SUBROUTINE HYSCC (IREF,JK,XO,VLT,BR)
c*
       REAL RD1, RD2, RD3, RD4
       REAL ACI, XO(7), CUR(2),VLT(2), PI, PY
       REAL IREF, DELTA, DELPO, DELNE
       INTEGER I, V, BR, JK
c*
       ACI=XO(1)
      CUR(1)=XO(3)
      CUR(2)=XO(4)
c*
      PI=2*ASIN(1)
      RD1 = 0.
      RD2 = PI*(45.0/180.0)
      RD3 = PI*(135.0/180.0)
      RD4 = PI
c*
      DELTA=IREF/100
      DELPO=IREF+DELTA
      DELNE=IREF-DELTA
c*
      IF( ACI.GT.PI) THEN
            DO 10  I=1, 5000
            PY=I*PI
            IF( ACI.GT.PY.AND.ACI.LE.(PY+PI)) THEN
                  ACI = ACI - PY
            ENDIF
10          CONTINUE
      ENDIF
c*
      IF(ACI.GE.RD1.AND.ACI.LT.RD2) THEN
            BR=3.
      ELSE
            IF(ACI.GE.RD2.AND.ACI.LT.RD3) THEN
                  BR=2.
            ELSE
                  IF(ACI.GE.RD3.AND.ACI.LT.RD4) THEN
                        BR=3.
                  ENDIF
            ENDIF
      ENDIF
c*
c*   ******************************
c*      Hysteresis Current Control
c*   ******************************
c*
      IF(ACI.GE.RD1.AND.ACI.LT.RD2) THEN
      GO TO 35
      ELSE
      IF(ACI.GE.RD2.AND.ACI.LT.RD3) THEN
      GO TO 45
      ELSE
      IF(ACI.GE.RD3.AND.ACI.LT.RD4) THEN
      GO TO 35
      ENDIF
```

```
        ENDIF
        ENDIF
        GO TO 55
35      IF (CUR(1).GE.DELPO) THEN
              VLT(1)=0.0
              VLT(2)=0.0
              V=555.
        ENDIF
        IF (CUR(1).GE.DELNE.AND.CUR(1).LT.DELPO) THEN
                 IF (V.NE.555) THEN
                          VLT(1)=50.0
                          VLT(2)=0.0
                 ELSE
                          VLT(1)=0.0
                          VLT(2)=0.0
                 ENDIF
        ENDIF
        IF (CUR(1).LT.DELNE) THEN
                 VLT(1)=50.0
                 VLT(2)=0.0
                 V=0.
        ENDIF
        IF(CUR(2).GT.0.05) JK=11.
        GO TO 55
45      IF (CUR(2).GE.DELPO) THEN
                 VLT(1)=0.0
                 VLT(2)=0.0
                 V=555.
        ENDIF
        IF (CUR(2).GE.DELNE.AND.CUR(2).LT.DELPO) THEN
                 IF (V.NE.555) THEN
                          VLT(1)=0.0
                          VLT(2)=50.0
                 ELSE
                          VLT(1)=0.0
                          VLT(2)=0.0
                 ENDIF
        ENDIF
        IF (CUR(2).LT.DELNE) THEN
                 VLT(1)=0.0
                 VLT(2)=50.0
                 V=0.
        ENDIF
        IF (CUR(1).GT.0.05) JK=22.
55      CONTINUE
        RETURN
        END
```

```
c* **************************************************************
        SUBROUTINE RKSYST (JK,BR,VLT,TO,XO,XEND,YDOT,H,N,VOLT)
c*
        REAL VLT(2), XO(7), XEND(7), YDOT(7), XWRK(4,7)
        REAL H, TO
        INTEGER I, N, BR
        CALL DERIVS (JK,BR,VLT,XO,TO,YDOT,N,VOLT)
c*
        DO 10 I=1, 7
        XWRK(1,I)= H * YDOT(I)
        XEND(I)=XO(I) + XWRK(1,I)/2.0
10      CONTINUE
c*
         CALL DERIVS (JK,BR,VLT,XEND,TO+H/2.0,YDOT,N,VOLT)
c*
        DO 20 I=1, 7
        XWRK(2,I)= H * YDOT(I)
        XEND(I)=XO(I) + XWRK(2,I)/2.0
20      CONTINUE
c*
        CALL DERIVS (JK,BR,VLT,XEND,TO+H/2.0,YDOT,N,VOLT)
c*
        DO 30 I=1, 7
        XWRK(3,I)= H * YDOT(I)
        XEND(I)=XO(I) + XWRK(3,I)
30      CONTINUE
c*
        CALL DERIVS (JK,BR,VLT,XEND,TO+H,YDOT,N,VOLT)
c*
        DO 40 I=1, 7
        XWRK(4,I)= H * YDOT(I)
40      CONTINUE
c*
        DO 50 I=1, 7
        XEND(I)=XO(I)+(XWRK(1,I)+2.0*(XWRK(2,I)+
        XWRK(3,I))+XWRK(4,I))/6.0
50      CONTINUE
c*
         DO 60 I=1, 7
        XO(I)=XEND(I)
60      CONTINUE
        TO = TO + H
        RETURN
        END
```

```
c*  ****************************************************
        SUBROUTINE DERIVS (JK,BR,VLT,XO,TO,YDOT,N,VOLT)
c*
        REAL XO(7), YDOT(7), VLT(2)
        INTEGER BR, JK
c*
c*
        IF(BR.EQ.2) THEN
             IF (XO(3).LT.0.05) THEN
                   XO(3)=0.0
                   XO(5)=0.0
                   CALL STATE2 (VLT,XO,TO,YDOT,N)
             ELSE
                    CALL STATE3 (JK,VLT,XO,TO,YDOT,N,VOLT)
             ENDIF
        ENDIF
c*
        IF(BR.EQ.3) THEN
             IF (XO(4).LT.0.05) THEN
                     XO(4)=0.0
                     XO(6)=0.0
                     CALL STATE1 (VLT,XO,TO,YDOT,N)
              ELSE
                     CALL STATE3 (JK,VLT,XO,TO,YDOT,N,VOLT)
              ENDIF
        ENDIF
c*
        RETURN
        END
c*
c*  ***************************************************
c*
      SUBROUTINE STATE1 (VLT,XO,TO,YDOT,N)
c*
        REAL CRT(2), VLT(2), VOLT(2), FS(2), K(2)
        REAL XO(7), YDOT(7), C(2), U(2)
        REAL AA(92), BB(92), CC(92), DD(92)
        REAL AA1(92), BB1(92), CC1(92), DD1(92)
        REAL X(92), T(92), Y(92), S(92)
        REAL P(2,2), SQ(2,2), A(92,4)
        REAL FAZA(2,2), FAZADT(2,2), G(2,2)
        REAL AB, A1, B1, E1, F1, R, TL, W, WREF
        REAL PI, RDN, TO, PY, PYA, MOI, KLMA, KI
        REAL TETHA, TE, TE1, TE2, TE3, TE4, TTH
        INTEGER I, J, N
c*
```

```
      OPEN(33,FILE='aircog.in', STATUS='old')
      OPEN(44,FILE='backemfa.in', STATUS='old')
c*
      TETHA=XO(1)
      W=XO(2)
      CRT(1)=XO(3)
      CRT(2)=XO(5)
      VOLT(1)=VLT(1)
      VOLT(2)=VLT(1)
      TL=(2.5E-4*XO(2))
      TO=TO
      WREF=600
      KI=8.5
      MOI=18.7289E-6
      PI=2*ASIN(1)
      RDN = PI*(2.0/180.0)
      N=91
c*
      IF( TETHA.GT.PI) THEN
         DO 10  J=1, 5000
            PY=J*PI
            PYA=PY+PI
            IF( TETHA.GT.PY.AND.TETHA.LE.PYA) THEN
                  TETHA = TETHA - PY
            ENDIF
10       CONTINUE
      ENDIF
c*
      YDOT(1)=W
c*
      A1=5.434172E-3
      B1=6.521691E-5
      E1=4.177232E-4
      F1=3.375929E-5
      AB = 2*TETHA - PI
      FAZA(1,1) = A1 + B1 * COS(AB)
      FAZADT(1,1) = -2 * B1 * SIN(AB)
      FAZA(2,2) = FAZA(1,1)
      FAZADT(2,2) = FAZADT(1,1)
      FAZA(1,2) = E1 + F1 * COS(AB)
      FAZADT(1,2) = -2 * F1 * SIN(AB)
      FAZA(2,1) = FAZA(1,2)
      FAZADT(2,1) = FAZADT(1,2)
c*
      TE1=0.5*(CRT(1)*CRT(1)*FAZADT(1,1) +
      CRT(2)*CRT(2)*FAZADT(2,2))
c*
```

```
        DO 15 I=0,90
        X(I+1)=I * RDN
15      CONTINUE
c*
        READ(33,*) (T(I),I=1,91)
        IEND=3
        CALL CUBSPL(X,T,S,N,IEND,A)
c*
        DO 20 I=1,90
                AA(I)=(S(I+1) - S(I))/(6*RDN)
                BB(I)=S(I)/2.0
                CC(I)=(T(I+1)-T(I))/RDN - RDN*(2*S(I)+S(I+1))/6.0
                DD(I)=T(I)
20      CONTINUE
c*
        DO 30 I=1,90
        IF(TETHA.EQ.X(I)) THEN
                TE2=T(I)
        ENDIF
        IF(TETHA.GT.X(I).AND.TETHA.LT.X(I+1)) THEN
                TTH=TETHA - X(I)
                TE2 = AA(I)*TTH*TTH*TTH+BB(I)*TTH*TTH
                +CC(I)*TTH+DD(I)
        ENDIF
        IF (TETHA.EQ.X(I+1)) THEN
                TE2=T(I+1)
        ENDIF
30      CONTINUE
c*
        TE3 = CRT(1)*CRT(2)*FAZADT(1,2)
c*
        READ(44,*) (Y(I),I=1,91)
        IEND=3
        CALL CUBSPL(X,Y,S,N,IEND,A)
c*
        DO 40 I=1,90
                AA1(I)= (S(I+1) - S(I))/(6*RDN)
                 BB1(I)=S(I)/2.0
                 CC1(I)=(Y(I+1)-Y(I))/RDN - RDN*(2*S(I)+S(I+1))/6.0
                 DD1(I)=Y(I)
40      CONTINUE
c*
        DO 50 I=1,90
        IF (TETHA.EQ.X(I)) THEN
                KLMA=Y(I)
        ENDIF
        IF(TETHA.GT.X(I).AND.TETHA.LT.X(I+1)) THEN
```

```
                    TTH=TETHA - X(I)
                    KLMA=AA1(I)*TTH*TTH*TTH + BB1(I)*TTH*TTH +
                     CC1(I)*TTH + DD1(I)
          ENDIF
          IF (TETHA.EQ.X(I+1)) THEN
                    KLMA=Y(I+1)
          ENDIF
50        CONTINUE
c*
      U(1) = VOLT(1) - (KLMA * W)
      U(2) = VOLT(2) - (KLMA * W)
      TE4 = CRT(1)*KLMA +  CRT(2)*KLMA
      TE= TE1 + TE2 + TE3 + TE4
      YDOT(2)= (TE - TL)/MOI
c*
          CALL MATINV(FAZA,2)
          DO 60 I=1,2
          DO 60 J=1,2
                 G(J,I)=FAZA(I,J)
60         CONTINUE
c*
          R=0.892
          DO 70 I=1,2
          DO 70 J=1,2
                 IF(I.EQ.J) THEN
                             P(I,J)=R + W * FAZADT(I,J)
                 ELSE
                             P(I,J)=W * FAZADT(I,J)
                 ENDIF
70      CONTINUE
          DO 80 L=1,2
                DO 90 I=1,2
                    DO 100 J=1,2
                                 K(J)=G(L,J)*P(J,I)
100                  CONTINUE
                SQ(L,I)=K(1)+K(2)
90              CONTINUE
80        CONTINUE
          DO 110 I=1,2
          DO 120 J=1,2
          K(J)=G(I,J)*U(J)
120       C(I)=K(1) + K(2)
110       CONTINUE
          DO 130 I=1,2
          DO 140 J=1,2
                K(J) = SQ(I,J) * CRT(J)
140       FS(I) = K(1) + K(2)
```

```
130       CONTINUE
c*
          YDOT(3) = C(1)-FS(1)
          YDOT(4) = 0.
          YDOT(5) = C(2)-FS(2)
          YDOT(6) = 0.
           YDOT(7) = KI*(WREF-XO(2))
          RETURN
          END
c*
c*  *********************************************
c*
      SUBROUTINE STATE2 (VLT,XO,TO,YDOT,N)
c*
      REAL CRT(2), VLT(2), VOLT(2), FS(2), K(2)
      REAL XO(7), YDOT(7), C(2), U(2)
      REAL AA(92), BB(92), CC(92), DD(92)
      REAL AA2(92), BB2(92), CC2(92), DD2(92)
      REAL X(92), T(92), Z(92), S(92)
      REAL P(2,2), SQ(2,2), A(92,4)
      REAL FAZB(2,2), FAZBDT(2,2), G(2,2)
      REAL EF, A1, B1, E1, F1, R, KLMB, W,WREF
      REAL PI, RDN, TO, PY, PYA, TTH, MOI, KI
      REAL TETHA, TE, TE1, TE2, TE3, TE4, TL
      INTEGER I, J, N
c*
          OPEN(33,FILE='aircog.in', STATUS='old')
          OPEN(55,FILE='backemfb.in', STATUS='old')
c*
          TETHA=XO(1)
          W=XO(2)
           CRT(1)=XO(4)
           CRT(2)=XO(6)
           VOLT(1)=VLT(2)
           VOLT(2)=VLT(2)
          TO=TO
          TL=(2.5E-4*XO(2))
          WREF=600.
          KI=8.5
          MOI=18.7289E-6
          PI=2*ASIN(1)
          RDN = PI*(2.0/180.0)
          N=91
c*
          IF( TETHA.GT.PI) THEN
             DO 10  J=1, 5000
                    PY=J*PI
```

```
                 PYA=PY+PI
                 IF( TETHA.GT.PY.AND.TETHA.LE.PYA) THEN
                    TETHA = TETHA - PY
                 ENDIF
10            CONTINUE
           ENDIF
c*
           YDOT(1)=W
c*
           A1=5.4447510E-3
           B1=5.487284E-5
           E1=4.136995E-4
           F1=3.094121E-5
           EF = 2*TETHA
c*
           FAZB(1,1) = A1 + B1 * COS(EF)
           FAZBDT(1,1) = -2 * B1 * SIN(EF)
           FAZB(2,2) = FAZB (1,1)
           FAZBDT(2,2) = FAZBDT(1,1)
           FAZB(1,2) = E1 + F1 * COS(EF)
           FAZBDT(1,2) = -2 * F1 * SIN(EF)
           FAZB(2,1) = FAZB(1,2)
           FAZBDT(2,1) = FAZBDT(1,2)
c*
           TE1=0.5*(CRT(1)*CRT(1)*FAZBDT(1,1) +
           CRT(2)*CRT(2)*FAZBDT(2,2))
c*
           DO 15 I=0,90
           X(I+1)=I * RDN
15         CONTINUE
c
           READ(33,*) (T(I),I= 1,91)
           IEND=3
           CALL CUBSPL(X,T,S,N,IEND,A)
c*
           DO 20 I=1,90
                 AA(I)= (S(I+1) - S(I))/(6*RDN)
                 BB(I)=S(I)/2.0
                 CC(I)=(T(I+1)-T(I))/RDN - RDN*(2*S(I)+S(I+1))/6.0
                 DD(I)=T(I)
20         CONTINUE
           DO 30 I=1,90
           IF (TETHA.EQ.X(I)) THEN
                TE2 = T(I)
           ENDIF
           IF(TETHA.GT.X(I).AND.TETHA.LT.X(I+1)) THEN
                 TTH=TETHA - X(I)
                TE2 = AA(I)*TTH*TTH*TTH+BB(I)*TTH*TTH
                +CC(I)*TTH+DD(I)
        ENDIF
        IF (TETHA.EQ.X(I+1)) THEN
                TE2 = T(I+1)
        ENDIF
30      CONTINUE
c*
        TE3 = CRT(1)*CRT(2)*FAZBDT(1,2)
        READ(55,*) (Z(I),I= 1,91)
        IEND=3
        CALL CUBSPL(X,Z,S,N,IEND,A)
c*
        DO 40 I=1,90
                AA2(I)= (S(I+1) - S(I))/(6*RDN)
                 BB2(I)=S(I)/2.0
                CC2(I)=(Z(I+1)-Z(I))/RDN - RDN*(2*S(I)+S(I+1))/6.0
                DD2(I)=Z(I)
40      CONTINUE
c*
        DO 50 I=1,90
        IF (TETHA.EQ.X(I)) THEN
                KLMB=Z(I)
        ENDIF
        IF(TETHA.GT.X(I).AND.TETHA.LT.X(I+1)) THEN
                TTH=TETHA - X(I)
                KLMB=AA2(I)*TTH*TTH*TTH + BB2(I)*TTH*TTH +
                CC2(I)*TTH + DD2(I)
        ENDIF
        IF (TETHA.EQ.X(I+1)) THEN
                KLMB=Z(I+1)
        ENDIF
50      CONTINUE
        U(1) = VOLT(1) - (KLMB * W)
        U(2) = VOLT(2) - (KLMB * W)
        TE4 = CRT(1)*KLMB + CRT(2)*KLMB
        TE= TE1 + TE2 + TE3 + TE4
        YDOT(2)= (TE - TL)/MOI
                CALL MATINV(FAZB,2)
        DO 60 I=1,2
         DO 60 J=1,2
              G(J,I)=FAZB(I,J)
60      CONTINUE
c*
        R=0.892
        DO 70 I=1,2
         DO 70 J=1,2
```

```
          IF(I.EQ.J) THEN
                 P(I,J)=R + W * FAZBDT(I,J)
          ELSE
                 P(I,J)=W * FAZBDT(I,J)
           ENDIF
70         CONTINUE
          DO 80 L=1,2
            DO 90 I=1,2
              DO 100 J=1,2
                       K(J)=G(L,J)*P(J,I)
100                CONTINUE
            SQ(L,I)=K(1)+K(2)
90          CONTINUE
80        CONTINUE
        DO 110 I=1,2
        DO 120 J=1,2
              K(J)=G(I,J)*U(J)
120     C(I)=K(1) + K(2)
110     CONTINUE
        DO 130 I=1,2
        DO 140 J=1,2
              K(J) = SQ(I,J) * CRT(J)
140     FS(I) = K(1) + K(2)
130     CONTINUE
        YDOT(3) = 0.
        YDOT(4) = C(1)-FS(1)
        YDOT(5) = 0.
        YDOT(6) = C(2)-FS(2)
        YDOT(7) = KI*(WREF-XO(2))
        RETURN
        END
c*
c*  ************************************************
c*
        SUBROUTINE STATE3 (JK,VLT,XO,TO,YDOT,N,VOLT)
c*
        REAL CRT(4), VLT(2),VOLT(4), FS(4), K(4)
        REAL XO(7), YDOT(7), C(4), U(4), SS(4), ST(4)
        REAL AA(92), BB(92), CC(92), DD(92)
        REAL AA1(92), BB1(92), CC1(92), DD1(92)
        REAL AA2(92), BB2(92), CC2(92), DD2(92)
        REAL X(92), T(92), Y(92), Z(92), S(92)
        REAL END(4,4), ENDOT(4,4), G(4,4), P(4,4), SQ(4,4), A(92,4)
        REAL AD, AB, AC, R, A1, B1, C1, D1, E1, F1
        REAL A11, B11, E11, F11, PY, PYA, WREF, KI
        REAL TETHA, TE, TE1, TE2, TE3, TE4, TTH
        REAL PI, RDN, TO, TL, KLM1, KLM2, W, MOI
```

```
      INTEGER I, J, N, JK
c*
      OPEN(33,FILE='aircog.in', STATUS='old')
      OPEN(44,FILE='backemfa.in', STATUS='old')
      OPEN(55,FILE='backemfb.in', STATUS='old')
c*
      TETHA=XO(1)
      W=XO(2)
      CRT(1)=XO(3)
      CRT(2)=XO(4)
      CRT(3)=XO(5)
      CRT(4)=XO(6)
c*
      IF (JK.EQ.11.) THEN
            VOLT(1)=VLT(1)
            VOLT(2)=-50.0
            VOLT(3)=VLT(1)
            VOLT(4)=-50.0
      ELSE
            IF (JK.EQ.22.) THEN
                  VOLT(1)=-50.0
                  VOLT(2)=VLT(2)
                  VOLT(3)=-50.0
                  VOLT(4)=VLT(2)
            ELSE
                  VOLT(1)=VLT(1)
                  VOLT(2)=VLT(2)
                  VOLT(3)=VLT(1)
                  VOLT(4)=VLT(2)
            ENDIF
       ENDIF
c*
          TO=TO
          TL=(2.5E-4*XO(2))
          MOI=18.7289E-6
          WREF=600.
          KI=8.5
          PI = 2*ASIN(1)
          RDN = PI*(2.0/180.0)
          N=91
c*
          IF( TETHA.GT.PI) THEN
            DO 10  J=1, 5000
                  PY=J*PI
                  PYA=PY+PI
                  IF( TETHA.GT.PY.AND.TETHA.LE.PYA) THEN
                        TETHA = TETHA - PY
```

```
                    ENDIF
10             CONTINUE
         ENDIF
c*
         YDOT(1)=W
c*
         A1=5.434172E-3
         B1=6.521691E-5
         E1=4.177232E-4
         F1=3.375929E-5
         A11=5.4447510E-3
         B11=5.487284E-5
         E11=4.136995E-4
         F11=3.094121E-5
         C1=4.0099903E-4
         D1=6.624186E-6
         AD = 2*TETHA
         AB = 2*TETHA - PI
         AC = 4*TETHA - PI
c*
         END(1,1)= A1 + B1 * COS(AB)
         ENDOT(1,1)=-2 * B1* SIN(AB)
         END(3,3)=END(1,1)
         ENDOT(3,3)=ENDOT(1,1)
         END(2,2)= A11 + B11 * COS(AD)
         ENDOT(2,2)= -2 * B11 * SIN(AD)
         END(4,4)=END(2,2)
         ENDOT(4,4)=ENDOT(2,2)
         END(1,3)= E1 + F1 * COS(AB)
         ENDOT(1,3)=-2 * F1 * SIN(AB)
         END(3,1)=END(1,3)
         ENDOT(3,1)=ENDOT(1,3)
         END(2,4)= E11 + F11 * COS(AD)
         ENDOT(2,4)=-2 * F11 * SIN(AD)
         END(4,2)=END(2,4)
         ENDOT(4,2)=ENDOT(2,4)
         END(1,2)= C1 + D1 * COS(AC)
         ENDOT(1,2)=-4 * D1 * SIN(AC)
         END(2,1)=END(1,2)
         ENDOT(2,1)=ENDOT(1,2)
         END(1,4)=END(1,2)
         ENDOT(1,4)=ENDOT(1,2)
         END(4,1)=END(1,2)
         ENDOT(4,1)=ENDOT(1,2)
         END(2,3)=END(1,2)
         ENDOT(2,3)=ENDOT(1,2)
         END(3,2)=END(1,2)
```

```
      ENDOT(3,2)=ENDOT(1,2)
      END(3,4)=END(1,2)
      ENDOT(3,4)=ENDOT(1,2)
      END(4,3)=END(1,2)
      ENDOT(4,3)=ENDOT(1,2)
c*
      DO 15 I=1,4
      SS(I)=0.5 * CRT(I) * CRT(I) * ENDOT(I,I)
15    TE1=SS(1) + SS(2) + SS(3) + SS(4)
      DO 20 I=0,90
      X(I+1)=I * RDN
20    CONTINUE
c*
      READ(33,*) (T(I), I=1,91)
      IEND=3
      CALL CUBSPL(X,T,S,N,IEND,A)
c*
      DO 30 I=1,90
      AA(I)= (S(I+1) - S(I))/(6*RDN)
      BB(I)=S(I)/2.0
      CC(I)=(T(I+1)-T(I))/RDN - RDN*(2*S(I)+S(I+1))/6.0
      DD(I)=T(I)
30    CONTINUE
      DO 40 I=1,90
      IF (TETHA.EQ.X(I)) THEN
            TE2 = T(I)
      ENDIF
      IF(TETHA.GT.X(I).AND.TETHA.LT.X(I+1)) THEN
            TTH=TETHA - X(I)
            TE2 = AA(I)*TTH*TTH*TTH+BB(I)*TTH*TTH
            +CC(I)*TTH+DD(I)
      ENDIF
      IF (TETHA.EQ.X(I+1)) THEN
            TE2=T(I+1)
      ENDIF
40    CONTINUE
      DO 50 I=1,4
      DO 60 J=1,4
      IF (I.NE.J) THEN
            SS(J)= 0.5 * CRT(I) * CRT(J) * ENDOT(I,J)
      ELSE
            SS(J)=0.0
      ENDIF
60    CONTINUE
            ST(I)= SS(1) + SS(2) + SS(3) + SS(4)
50    CONTINUE
      TE3= ST(1) + ST(2) + ST(3) + ST(4)
      READ(44,*) (Y(I), I=1,91)
      IEND=3
      CALL CUBSPL(X,Y,S,N,IEND,A)
c*
      DO 70 I=1,90
      AA1(I)=(S(I+1) - S(I))/(6*RDN)
      BB1(I)=S(I)/2.0
      CC1(I)=(Y(I+1)-Y(I))/RDN - RDN*(2*S(I)+S(I+1))/6.0
      DD1(I)=Y(I)
70    CONTINUE
c*
      READ(55,*) (Z(I), I=1,91)
      IEND=3
      CALL CUBSPL(X,Z,S,N,IEND,A)
c*
      DO 80 I=1,90
            AA2(I)= (S(I+1) - S(I))/(6*RDN)
            BB2(I)=S(I)/2.0
            CC2(I)=(Z(I+1)-Z(I))/RDN - RDN*(2*S(I)+S(I+1))/6.0
            DD2(I)=Z(I)
80    CONTINUE
c*
      DO 90 I=1,90
      IF (TETHA.EQ.X(I)) THEN
            KLM1=Y(I)
            KLM2=Z(I)
      ENDIF
      IF(TETHA.GT.X(I).AND.TETHA.LT.X(I+1)) THEN
            TTH=TETHA - X(I)
            KLM1= AA1(I)*TTH*TTH*TTH + BB1(I)*TTH*TTH
             + CC1(I)*TTH + DD1(I)
            KLM2= AA2(I)*TTH*TTH*TTH + BB2(I)*TTH*TTH
            + CC2(I)*TTH + DD2(I)
      ENDIF
      IF (TETHA.EQ.X(I+1)) THEN
            KLM1=Y(I+1)
            KLM2=Z(I+1)
      ENDIF
90    CONTINUE
c*
      DO 100 J=1,4
      IF (J.EQ.1.OR.J.EQ.3) THEN
            U(J) = VOLT(J) - (KLM1*W)
            SS(J)= CRT(J) * KLM1
      ELSE
            U(J) = VOLT(J) - (KLM2*W)
            SS(J)= CRT(J) * KLM2
      ENDIF
100   CONTINUE
c*
      TE4= SS(1) + SS(2) + SS(3) + SS(4)
      TE= TE1 + TE2 + TE3 + TE4
      YDOT(2)= (TE - TL)/MOI
c*
      CALL MATINV(END,4)
c*
      DO 110 I=1,4
         DO 110 J=1,4
            G(J,I)=END(I,J)
110   CONTINUE
      R=0.892
      DO 120 I=1,4
        DO 120 J=1,4
            IF(I.EQ.J) THEN
                P(I,J)=R + W * ENDOT(I,J)
            ELSE
                P(I,J)=W * ENDOT(I,J)
            ENDIF
120   CONTINUE
      DO 130 L=1,4
          DO 140 I=1,4
             DO 150 J=1,4
                         K(J)=G(L,J)*P(J,I)
150                CONTINUE
          SQ(L,I)=K(1)+K(2)+K(3)+K(4)
140       CONTINUE
130  CONTINUE
      DO 160 I=1,4
      DO 170 J=1,4
             K(J)=G(I,J)*U(J)
170          C(I)=K(1) + K(2) + K(3) + K(4)
160    CONTINUE
c*
      DO 180 I=1,4
      DO 190 J=1,4
             K(J)=SQ(I,J)*CRT(J)
190          FS(I)=K(1) + K(2) + K(3) + K(4)
180   CONTINUE
      DO 200 J=1,4
             YDOT(J+2)=C(J)-FS(J)
200   CONTINUE
      YDOT(7)=KI*(WREF-XO(2))
      RETURN
      END
```

```
c*  ************************************************
c*
        SUBROUTINE ETORK (XO,TE,TE1,TE2,TE3,TE4,KLM1,KLM2)
c*
        REAL CUR(4), XO(7), SS(4), ST(4)
        REAL AA(92), BB(92), CC(92), DD(92)
        REAL AA1(92), BB1(92), CC1(92), DD1(92)
        REAL AA2(92), BB2(92), CC2(92), DD2(92)
        REAL X(92), T(92), Y(92), Z(92), S(92)
        REAL END(4,4), ENDOT(4,4), A(92,4)
        REAL AD, AB, AC, A1, B1, C1, D1
        REAL A11, B11, E11, F11, E1, F1
        REAL TETHA, TE, TE1, TE2, TE3, TE4, TTH
        REAL PI, RDN, KLM1, KLM2, W, PY, PYA
        INTEGER I, J, N
c*
        TETHA=XO(1)
        W=XO(2)
        CUR(1)=XO(3)
        CUR(2)=XO(4)
        CUR(3)=XO(5)
        CUR(4)=XO(6)
        PI = 2*ASIN(1)
        RDN = PI*(2.0/180.0)
        N=91
c*
        IF( TETHA.GT.PI) THEN
          DO 10  J=1, 5000
                PY=J*PI
                PYA=PY+PI
                IF( TETHA.GT.PY.AND.TETHA.LE.PYA) THEN
                   TETHA = TETHA - PY
                ENDIF
10        CONTINUE
        ENDIF
c*
        A1=5.434172E-3
        B1=6.521691E-5
        E1=4.177232E-4
        F1=3.375929E-5
        A11=5.4447510E-3
        B11=5.487284E-5
        E11=4.136995E-4
        F11=3.094121E-5
        C1=4.0099903E-4
        D1=6.624186E-6
        AD = 2*TETHA
```

```
            AB = 2*TETHA - PI
            AC = 4*TETHA - PI
            END(1,1)= A1 + B1 * COS(AB)
            ENDOT(1,1)=-2 * B1* SIN(AB)
            END(3,3)=END(1,1)
            ENDOT(3,3)=ENDOT(1,1)
            END(2,2)= A11 + B11 * COS(AD)
            ENDOT(2,2)= -2 * B11 * SIN(AD)
            END(4,4)=END(2,2)
            ENDOT(4,4)=ENDOT(2,2)
            END(1,3)= E1 + F1 * COS(AB)
            ENDOT(1,3)=-2 * F1 * SIN(AB)
            END(3,1)=END(1,3)
            ENDOT(3,1)=ENDOT(1,3)
            END(2,4)= E11 + F11 * COS(AD)
            ENDOT(2,4)=-2 * F11 * SIN(AD)
            END(4,2)=END(2,4)
            ENDOT(4,2)=ENDOT(2,4)
            END(1,2)= C1 + D1 * COS(AC)
            ENDOT(1,2)=-4 * D1 * SIN(AC)
            END(2,1)=END(1,2)
            ENDOT(2,1)=ENDOT(1,2)
            END(1,4)=END(1,2)
            ENDOT(1,4)=ENDOT(1,2)
            END(4,1)=END(1,2)
            ENDOT(4,1)=ENDOT(1,2)
            END(2,3)=END(1,2)
            ENDOT(2,3)=ENDOT(1,2)
            END(3,2)=END(1,2)
            ENDOT(3,2)=ENDOT(1,2)
            END(3,4)=END(1,2)
            ENDOT(3,4)=ENDOT(1,2)
            END(4,3)=END(1,2)
            ENDOT(4,3)=ENDOT(1,2)
c*
            DO 15 I=1,4
               SS(I)=0.5 * CUR(I) * CUR(I) * ENDOT(I,I)
15          TE1=SS(1) + SS(2) + SS(3) + SS(4)
c*
        DO 20 I=0,90
        X(I+1)=I * RDN
20      CONTINUE
c*
        READ(33,*) (T(I), I=1,91)
        IEND=3
        CALL CUBSPL(X,T,S,N,IEND,A)
c*
```

```
        DO 30 I=1,90
                  AA(I)= (S(I+1) - S(I))/(6*RDN)
                  BB(I)=S(I)/2.0
                  CC(I)= (T(I+1)-T(I))/RDN - RDN*(2*S(I)+S(I+1))/6.0
                  DD(I)=T(I)
30      CONTINUE
        DO 40 I=1,90
        IF (TETHA.EQ.X(I)) THEN
                  TE2 = T(I)
        ENDIF
        IF(TETHA.GT.X(I).AND.TETHA.LT.X(I+1)) THEN
                  TTH=TETHA - X(I)
                  TE2=AA(I)*TTH*TTH*TTH+BB(I)*TTH*TTH
                  +CC(I)*TTH+DD(I)
        ENDIF
        IF (TETHA.EQ.X(I+1)) THEN
                  TE2=T(I+1)
        ENDIF
40      CONTINUE
        DO 50 I=1,4
        DO 60 J=1,4
        IF (I.NE.J) THEN
                  SS(J)= 0.5 * CUR(I) * CUR(J) * ENDOT(I,J)
        ELSE
                  SS(J)=0.0
        ENDIF
60      CONTINUE
        ST(I)= SS(1) + SS(2) + SS(3) + SS(4)
50      CONTINUE
        TE3= ST(1) + ST(2) + ST(3) + ST(4)
c*
        READ(44,*) (Y(I), I=1,91)
        IEND=3
        CALL CUBSPL(X,Y,S,N,IEND,A)
c*
        DO 70 I=1,90
        AA1(I)=(S(I+1) - S(I))/(6*RDN)
        BB1(I)=S(I)/2.0
        CC1(I)=(Y(I+1)-Y(I))/RDN - RDN*(2*S(I)+S(I+1))/6.0
        DD1(I)=Y(I)
70      CONTINUE
c*
        READ(55,*) (z(I), I=1,91)
        IEND=3
        CALL CUBSPL(X,Z,S,N,IEND,A)
c*
        DO 80 I=1,90
```

```
                AA2(I)= (S(I+1) - S(I))/(6*RDN)
                BB2(I)=S(I)/2.0
                CC2(I)=(Z(I+1)-Z(I))/RDN - RDN*(2*S(I)+S(I+1))/6.0
                DD2(I)=Z(I)
80      CONTINUE
c*
        DO 90 I=1,90
        IF (TETHA.EQ.X(I)) THEN
                KLM1=Y(I)
                KLM2=Z(I)
        ENDIF
        IF(TETHA.GT.X(I).AND.TETHA.LT.X(I+1)) THEN
                TTH=TETHA - X(I)
                KLM1= AA1(I)*TTH*TTH*TTH + BB1(I)*TTH*TTH +
                CC1(I)*TTH + DD1(I)
                KLM2= AA2(I)*TTH*TTH*TTH + BB2(I)*TTH*TTH +
                CC2(I)*TTH + DD2(I)
        ENDIF
        IF (TETHA.EQ.X(I+1)) THEN
                KLM1=Y(I+1)
                KLM2=Z(I+1)
        ENDIF
90      CONTINUE
        DO 100 J=1,4
        IF (J.EQ.1.OR.J.EQ.3) THEN
                SS(J)= CUR(J) * KLM1
        ELSE
                SS(J)= CUR(J) * KLM2
        ENDIF
100             CONTINUE
        TE4= SS(1) + SS(2) + SS(3) + SS(4)
        TE= TE1 + TE2 + TE3 + TE4
        RETURN
        END
c*
c************************************************
        SUBROUTINE MATINV(A,N1)
        DIMENSION  A(4,4), B(4,1),INDEX(4,4)
        EQUIVALENCE (IROW,JROW),(ICOLUM,JCOLUM),(AMAX,T,SWAP)
c*
        N1=4
        M=1
        N=N1
10      DETERM=1.0
15      DO 20 J=1,N
20          INDEX (J,3)=0
30       DO 550 I=1,N
```

```
40                  AMAX=0.0
45                  DO 105 J=1,N
                        IF (INDEX(J,3)-1) 60,105,60
60                         DO 100 K=1,N
                                IF (INDEX(K,3)-1) 80,100,715
80                              IF (AMAX-ABS(A(J,K))) 85,100,100
85                              IROW=J
90                              ICOLUM=K
                                AMAX=ABS(A(J,K))
100                        CONTINUE
105                 CONTINUE
                    INDEX (ICOLUM,3)=INDEX (ICOLUM,3)+1
260              INDEX (I,1)=IROW
270              INDEX (I,2)=ICOLUM
c*
c*
130                 IF (IROW-ICOLUM) 140,310,140
140              DETERM=-DETERM
150              DO 200 L=1,N
160                           SWAP=A(IROW,L)
170                           A(IROW,L)=A(ICOLUM,L)
200                           A(ICOLUM,L)=SWAP
                              IF (M) 310,310,210
210                                DO 250 L=1,M
220                                     SWAP=B(IROW,L)
230                                     B(IROW,L)=B(ICOLUM,L)
250                                     B(ICOLUM,L)=SWAP
c*
c*
310
      PIVOT=A(ICOLUM,ICOLUM)
                                        DETERM=DETERM*PIVOT
330                                     A(ICOLUM,ICOLUM)=1.0
340                                     DO 350 L=1,N
350   A(ICOLUM,L)=A(ICOLUM,L)/PIVOT
355   IF (M) 380,380,360
360   DO 370 L=1,M
370   B(ICOLUM,L)=B(ICOLUM,L)/PIVOT
c*
c*
380   DO 550 L1=1,N
390   IF (L1-ICOLUM) 400,550,400
400   T=A(L1,ICOLUM)
420   A(L1,ICOLUM)=0.0
430   DO 450 L=1,N
450   A(L1,L)=A(L1,L)-A(ICOLUM,L)*T
455   IF (M) 550,550,460
```

```
460     DO 500 L=1,M
500     B(L1,L)=B(L1,L)-B(ICOLUM,L)*T
550     CONTINUE
c*
600     DO 710 I=1,N
610     L=N+1-I
620     IF (INDEX(L,1)-INDEX(L,2)) 630,710,630
630     JROW=INDEX(L,1)
640     JCOLUM=INDEX(L,2)
650     DO 705 K=1,N
660     SWAP=A(K,JROW)
670     A(K,JROW)=A(K,JCOLUM)
700     A(K,JCOLUM)=SWAP
705     CONTINUE
710     CONTINUE
        DO 730 K=1,N
        IF (INDEX(K,3)-1) 715,720,715
715     ID=2
        GO TO 740
720     CONTINUE
730     CONTINUE
        ID=1
740     RETURN
      END
c*
c********************************************
        SUBROUTINE CUBSPL (X,Y,S,N,IEND,A)
c*
        REAL X(92), Y(92), S(92), A(92,4), DX1, DY1, DX2,
        REAL DY2, DXN1, DXN2
        INTEGER N,IEND,NM1,NM2,I,J
c*
        NM2=N-2
        NM1=N-1
        DX1=X(2) - X(1)
        DY1=(Y(2) - Y(1))/DX1*6.0
        DO 10 I=1, NM2
                DX2=X(I+2) - X(I+1)
                DY2=(Y(I+2) - Y(I+1))/DX2*6.0
                A(I,1)=DX1
                A(I,2)=2.0*(DX1 + DX2)
                A(I,3)=DX2
                A(I,4)=DY2 - DY1
                DX1 = DX2
                DY1 = DY2
10      CONTINUE
        GO TO (20,50,80), IEND
```

```
20      GO TO 100
50      A(1,2)=A(1,2) + X(2) -X(1)
        A(NM2,2)=A(NM2,2) + X(N) -X(NM1)
        GO TO 100
80      DX1=X(2) - X(1)
        DX2=X(3) - X(2)
        A(1,2)=(DX1 + DX2) * (DX1 + 2.0*DX2)/DX2
        A(1,3)=(DX2*DX2 - DX1*DX1)/DX2
        DXN2=X(NM1) - X(NM2)
        DXN1=X(N) - X(NM1)
        A(NM2,1)=(DXN2*DXN2 - DXN1*DXN1)/DXN2
        A(NM2,2)=(DXN1 + DXN2)*(DXN1 + 2.0*DXN2)/DXN2
        GO TO 100
100     DO 110 I=2, NM2
              A(I,2)=A(I,2) - A(I,1)/A(I-1,2)*A(I-1,3)
              A(I,4)=A(I,4) - A(I,1)/A(I-1,2)*A(I-1,4)
110     CONTINUE
        A(NM2,4)=A(NM2,4)/A(NM2,2)
        DO 120 I=2,NM2
              J=NM1-I
              A(J,4)=( A(J,4) - A(J,3)*A(J+1,4))/A(J,2)
120     CONTINUE
        DO 130 I=1, NM2
              S(I+1)=A(I,4)
130     CONTINUE
        GO TO (150,160,170), IEND
150     S(1)=0.0
        S(N)=0.0
        RETURN
160     S(1)=S(2)
        S(N)=S(N-1)
        RETURN
170     S(1)=((DX1 + DX2)*S(2) - DX1*S(3))/DX2
        S(N)=((DXN2 + DXN1)*S(NM1) - DXN1*S(NM2))/DXN2
        RETURN
        END
```

T.C.
DOKÜMA... ...SYON MERKEZİ